INVESTIGATION OF THERMAL COMFORT PERFORMANCE OF RADIANT HEATING SYSTEMS: COMPARISONS OF DIFFERENT HEATING SURFACE CONFIGURATIONS

A Thesis

By

Ruşen Can Acet

Submitted to the
Graduate School of Sciences and Engineering
In Partial Fulfillment of the Requirements for
the Degree of

Master of Science

in the
Department of Mechanical Engineering

Özyeğin University

February 2018

INVESTIGATION OF THERMAL COMFORT PERFORMANCE OF RADIANT HEATING SYSTEMS: COMPARISONS OF DIFFERENT HEATING SURFACE CONFIGURATIONS

Approved by:

Professor M. Pınar Mengüç, Advisor,
Department of Mechanical Engineering
Özyeğin University

Professor Ş. Özgür Atayılmaz,
Department of Mechanical Engineering
Yıldız Technical University

Assistant Professor Altuğ Başol,
Department of Mechanical Engineering
Özyeğin University

Date Approved: 27 February 2018

To my family

ABSTRACT

This thesis is an experimental-numerical study for the thermal comfort assessment of radiant heating system for different heating configuration such as from a wall, ceiling and combination of both that is installed in a test room with dimensions of 4m x 4m x 3m. Comfort evaluation was done by using the PMV (The Predicted Mean Vote) - PPD (Predicted Percentage of Dissatisfaction) index developed by Fanger [1]. In addition, for each heating scenario, human body exergy balance was calculated and the effect of exergy consumption rate on thermal comfort was evaluated.

The data generated during the tests are used in numerical model for the validation of it. Numerical model is used to investigate the air temperature distribution, velocity fields for different cases. Three different heating configurations were evaluated in numerical model as same as experimental study. Wall heating, ceiling heating wall and ceiling heating scenarios were explored in terms of PMV thermal comfort index and human body exergy balance approach.

All the numerical analysis studies were conducted using the Academic version of ANSYS 17.1, which is a commercial package program for numerical modelling. It contains special modules for different stages of the modelling process. After the three-dimensional room geometry was created in the Design Modeler module, the meshing module was subjected to decomposition using the finite volume method. Numerical solutions were made in Fluent, a widely used computational fluid dynamics module. The temperature and velocity fields were visually inspected using CFD-Post software as the final processor program. The natural convection was modelled using the Boussinesq approach, and the standard k-ε model which is a common numerical solution was picked to model turbulence. A Discrete Ordinates model with no scattering was

used for radiative heat transfer. Numerical solution results were compared with different mesh numbers and mesh independence was observed.

Radiant panels have been investigated to provide and maintain thermal comfort at different surface set temperatures. In the given set values, temperature distribution in the vertical and horizontal direction, mean radiant temperature and air velocity values in the room were examined. It has been observed that the exergy consumption values in the radiant heating system are close to the lowest values stated in the literature. Also, the temperature distribution in the room is considerably lower than all conventional systems. This demonstrates that radiant systems using low quality energy sources provide efficient, environmentally-friendly comfort solutions. It should be stated that it is a preliminary study for the location-based heating technologies and this method can be an innovative solution for heating / cooling industry. Therefore, it can be further evaluated in future research studies.

ÖZETÇE

Bu tez çalışmasında boyutları 4m x 4m x 3m olan bir odanın duvar ve tavan radyant panellerle ısıtması ve ikisinin bir arada olduğu ısıtma konfigurasyonları için deneysel ve sayısal konfor değerlendirmesi yapılmıştır. Bu tezde Fanger [1] tarafından geliştirilen standart termal konfor değerlendirme ölçeği olarak kabul edilen Tahmini Ortalama Konfor Oylaması (PMV- The Predicted Mean Vote) ve Tahmini Memnuniyetsizlik Oranı (PPD- Predicted Percentage of Dissatisfaction) değerleri her bir durum için hesaplanmıştır. Ayrıca her senaryo için insan vücudunun ekserji dengesi hesaplanarak, vücudun tükettiği ekserji değerinin konfora olan etkisi araştırılmıştır.

Sayısal model, test odasında oluşturulan deneysel veriler ile doğrulanmıştır. Belirlenen senaryolar, PMV-PPD termal konfor indeksi ve insan vücudu ekserji dengesi yaklaşımı kullanılarak değerlendirilmiştir. Sayısal model yardımıyla oda içerisinde farklı durumlar için hava sıcaklık dağılımı ve hava hızı dağılımı incelenmiştir.

Sayısal analiz çalışmaları, dünya genelinde yaygın olarak kullanılan bir ticari paket program olan ve arayüzünde farklı modelleme araçları bulunan ANSYS 17.1'in akademik versiyonu kullanılarak yapılmıştır. Odanın geometrisi Design Modeler modülünde tasarlanmıştır. Sonrasında yazılımın Meshing modülünde sonlu hacimler metodu kullanılarak ayrıklaştırma işlemi gerçekleştirilmiştir. Bir hesaplamalı akışkanlar dinamiği (HAD) yazılımı olan Fluent yazılımı kullanılarak sayısal çalışmalar gerçekleştirilmiştir. Gerçekleştirilen analizlerin sonuçları, CFD-Post yazılımında detaylı görseller ve hesap fonksiyonları ile birlikte incelenmiştir. Sıcaklık ve hız dağılımı, bu bölümde incelenmiştir. Doğal taşınımda Boussinesq yaklaşımı, türbülansın modellenmesinde standart k-ε modeli ve radyasyonla ısı transferi için Discrete Ordinates modeli saçılma dahil edilmeden kullanılmıştır. Sayısal çözüm sonuçları farklı mesh sayılarında kıyaslamıştır ve mesh bağımsızlığının olduğu gözlenmiştir.

Panellerin ayarlanan yüzey sıcaklıklarında termal konforu sağlayıp sağlamadıkları incelenmiştir. Verilen set değerlerinde oda içerisinde düşey ve yatay yöndeki sıcaklık dağılımı, ortalama ışınımsal sıcaklık ve hava hızı değerleri incelenmiştir. Radyant ısıtma sisteminde ekserji tüketim değerlerinin literatürde belirtilen en düşük değerlere yakın olduğu gözlemlenmiştir. Bu da radyant sistemlerin düşük kalitede (low-ex) enerji kaynaklarını kullanarak, klasik sistemlere göre daha çevreci ve ekonomik bir iklimlendirme çözümü olduğunu ortaya koymaktadır.

Bu tez içerisinde yer alan farklı konumlardan ışınım ile ısıtma yapılması hususu, gelecekte kullanıcıya sunulabilecek yenilikçi bir yöntemdir ve konum bazlı ısıtma-soğutma çözümleri için bir ön çalışma niteliğinde olduğu belirtilmelidir.

ACKNOWLEDGEMENTS

Firstly, I would like to express my sincere gratitude to my advisor Prof. M. Pınar Mengüç for the continuous support of my study, for his patience, motivation, and immense knowledge.

I acknowledge my gratitude to Mir Araştırma ve Geliştirme A.Ş. for the absolute support to the thesis in terms of facilities and time they have provided me for my academic career.

I have many people to thank for supporting and having to tolerate me over the past five years of study. I cannot begin to express my gratitude and appreciation for their friendship. I am very thankful to all these big-hearted people.

TABLE OF CONTENTS

LIST OF TABLES

LIST OF FIGURES

ABBREVIATIONS AND ACRONYMS

ESCO	Energy Service Company
ASHRAE	American Society of Heating, Refrigerating and Air-Conditioning Engineers.
EN	European Standard
TS	Turkish Standard
HVAC	Heating, Ventilation and Air Conditioning
DV	Displacement Ventilation
DOAS	Dedicated Outdoor Air System
MRT	Mean Radiant Temperature
PMV	The Predicted Mean Vote
PPD	Predicted Percentage of Dissatisfaction
PD	Percentage of Dissatisfaction (Local Comfort Parameter)
TSV	Thermal Sensation Vote
IEQ	Indoor Environmental Quality
LCA	Life Cycle Analysis
PEX	Cross-Linked Polyethylene Material
EPS	Expanded Polystyrene
DO	The Discrete Ordinates
DMCS	Data Monitoring and Control System
RTE	Radiative Transfer Equation
VBA	Visual Basic for Applications

NOMENCLATURE

A	Area [m^2]
c_p	Specific heat at constant pressure [J/kgK]
$F_{\varepsilon_{s-j}}$	Radiation interchange factor
F_{s-j}	View factor between radiant surface and j-surface
h_c	Total heat transfer coefficient [W/(m^2K)]
h_r	Radiation heat transfer coefficient [W/(m^2K)]
h_{tot}	Convective heat transfer coefficient [W/(m^2K)]
$\dot{m}$	Mass flow rate [kgm^{-3}]
M	Metabolic energy generation rate [W/m^2]
Q_{total}	Total heat transfer [W]
Q_{loss}	Backward heat transfer [W]
q_c	Convective heat flux [W/m^2]
q_{net}	Net heat flux [W/m^2]
q_r	Radiation heat flux [W/m^2]
T_a	Air temperature [°C]
T_j	j-surface temperature [°C]
T_{mrt}	Mean radiant temperature [°C]
T_{op}	Operative temperature [°C]
T_s	Surface temperature [°C]

T_w	Water temperature [°C]
U	Coefficient of thermal transmittance of surfaces [W/(m^{2}K)]
ε	Emissivity
σ	Stefan-Boltzmann constant [W/(m^{2}K)]
T_o	Outdoor air temperature as environmental temperature for exergy calculation [K]
T_{cr}	Body-core temperature [K]
t	Time [s] and is its infinitesimal increment *dt*
V_{in}	Volumetric rate of inhaled air [(m^3/s)/m^2]
c_{pa}	Specific heat capacity of dry air [J/(kgk)]
$\mathfrak{M}_a$	Molar mass of dry air [g/mol]
R	Gas constant [J/(mol K)]
T_{ra}	Room air temperature [K]
P	Atmospheric air pressure [Pa]
p_{vr}	Water-vapor pressure in the room space [Pa]
c_{pv}	Specific heat capacity of water vapor [J/(kgk)]
$\mathfrak{M}_w$	Molar mass of water molecules [g/mol]
p_{vo}	Water-vapor pressure of the outdoor air [Pa]
V_{w-core}	Volumetric rate of liquid water generated in the body core [(m^3/s)/m^2]
ρ_w	Density of liquid water [kg/m^3]
c_{pw}	Specific heat capacity of liquid water [J/(kgk)]
$p_{vs}(T_o)$	Saturated water-vapor pressure at outdoor air temperature [Pa]
$V_{w-shell}$	The volumetric rate of liquid water generated in the body shell as sweat [(m^3/s)/m^2]
T_{sk}	Skin temperature [K]

f_{eff}	The ratio of the effective area of human body for radiant-heat exchange to the surface area of the human body with clothing
f_{cl}	The ratio of human body area with clothing to the naked human body area
a_{pj}	Absorption coefficient between the human body surface
ε_{cl}	Emittance of clothing surface [dimensionless]
h_{rb}	Radiative heat-transfer coefficient of a black surface [W/(m^{2}k)]
T_j	Temperature of surface [K]
δS_g	Amount of entropy generation during the infinitesimal period [(Onnes/s)/m^2]
Q_{core}	Heat capacity of body core [J/(m^{2}k)]
dT_{cr}	Infinitesimal increment of body-core temperature [K]
Q_{shell}	Heat capacity of body shell [J/(m^{2}k)]
dT_{sk}	Infinitesimal increment of skin temperature [K]
V_{out}	Volumetric rate of exhaled air [(m^3/s)/m^2]
$p_{vs}(T_{cr})$	Saturated water-vapor pressure at body-core temperature [K]
T_{cl}	Clothing surface temperature [K]
h_{ccl}	Average convective heat transfer coefficient over clothed body-surface [W/(m^{2}k)]

1 INTRODUCTION

1.1 Motivation

Achieving energy efficiency in buildings where comfortable and economic living is desired can pose a significant challenge. This challenge, along with the increase in energy consumption and in turn the decrease in non-renewable energy sources around the globe need to be considered together. The environmental concerns, especially the increase in greenhouse gases have led scientist to focus on energy-efficient technologies to curtail the use of fossil energy and to promote renewable energy use in the building sector since buildings are major consumers of energy for heating, cooling, lighting, etc. Building sector has a considerable footprint on the consumption of natural resources. Currently, the portion of energy consumed in buildings accounts approximately 40% of the global energy demand. And the energy requirement for space heating, ventilation and air conditioning (HVAC) of a building is approximately 60% of the total energy consumed in buildings [2, 3]. Reducing the buildings' energy consumption could be the main objective in saving energy. Hence, people need to improve the efficiency of energy use in buildings through the implementation of more efficient systems and sustainable sources for heating and cooling operations.

Energy use reductions can be achieved through minimizing the energy demand, through the recovery of heat and cold and thereby using energy from the ambient air and from the ground [4]. Furthermore, human thermal conditions should be considered carefully in new buildings. Thermal comfort being one of the most important elements of living environment has a direct effect on people's quality of

life and health and also affects people's performance [5]. Now hydronic radiant heating or cooling panels have become a common solution in heating and cooling operations in buildings based on the advantages they offer for thermal comfort and high energy efficiency. Radiant systems have been a well-known HVAC solution in the provision of thermal comfort. They are divergent from conventional air conditioning systems that they condition surfaces instead of conditioning air and thus radiant systems have ability to consume less energy while delivering superior thermal comfort. It is a proven technology which carries out the requirements which are explained in related standards [6, 7]. There is enough motivation provided to work on energy efficiency and thermal comfort issues in building sector according to global needs afore mentioned. The research trends are also in this direction.

1.2 Scope of the Thesis

Thermal comfort is an important issue for people's life quality. Therefore many studies are being carried out on this topic. In this thesis, a coupled experimental-numerical study was conducted for thermal comfort evaluation of radiant heating system. The objective of the thesis is to evaluate the radiant heating configurations based on panel locations and surface temperatures.

Thermal comfort evaluation was made by using PMV-PPD method which was developed by Fanger [1]. As it is known that this model is based on the first law of thermodynamics. To go further level, exergy concept was taken into consideration to understand comfort exergy mechanism and numerical results were put into human body exergy balance model. Exergy metrics are calculated and compared with PMV-PPD values.

1.3 Literature Review

1.3.1 Radiant Systems

Heating and cooling systems provide conditioning via radiant and/or convective heat transfer for comfortable indoor environment. As a conditioning system, radiant system uses the surfaces to heat or cool the space via the main heat transfer phenomena, radiation and convection. The system is called “radiant” because of the heat transfer amount via radiation is more than %50 of the total heat transfer [8]. The more favorable radiation exchange among the inhabitants and the radiant surfaces permits the air temperature to be slightly lower whilst preserving thermal conditions, therefore better building thermal properties that reduce the heat loss are important [9]. Therefore, the radiant heating system can keep room air temperature lower than the convection-based systems, while ensuring the equal thermal comfort. As far as radiant cooling systems are concerned, the heat is extracted from inhabitants by radiation from cold surfaces allowing for the room temperature to be comparatively greater than convection-based systems.

Radiant systems have various types which can be categorized based on the location of radiant surfaces, thermal medium, integration with building structure, and others. The radiant systems can be constructed as radiant ceiling, floor or wall heating or cooling systems considering the location of radiation surfaces. Based on the integration of radiant systems with building’s architecture, when hydronic system is installed into the building elements, e.g. slab, then the radiant systems are called as thermally activated building components [10].

Radiant systems generally use water as heat transfer fluid, thus they have been also called as hydronic heating and cooling systems [11] or water-based

surface heating and cooling systems [12]. Furthermore, the radiant systems can be expressed as low temperature heating [12] or high temperature cooling systems [13] just because they can work with the water temperature that is near to the required room temperature, on account of comparatively extensive heat transfer areas.

Air conditioning systems exclusively rest on air-forced convection heat transfer for heating or cooling, and they condition the air, but not the surfaces. This causes to energy utilization and higher fan power capacities [14]. Besides, the air circulation on a large scale in a conditioned room may result in annoying noise and uncomfortable space due largely to cold draught. Focusing on all convective systems, radiant systems are more favorable due to use of water as thermal medium, meaning that less energy is required to heat or cool the climatized space.

In addition, radiant systems can be coupled with the renewable energy sources such as geothermal or solar energy and may supply water in convenient temperatures for low temperature heating or high temperature cooling approaches. The radiant systems do not affect the peak time energy consumption, but they reduce the variations of room air temperature due to utilization of building thermal mass. The radiant heat transfer may allow for advanced thermal comfort through inhibition of cold draught likely alleviating the noise carried by air from the system activity. Therefore, they contribute positively to the indoor environmental quality. The radiant cooling system may be more satisfactory than convection-based conditioned systems as the base for homogeneous vertical temperature gradient, lower air speed. In addition, the attenuated territorial discomfort for inhabitants in the course of long-time remains in cooled room environment is avoided [15]. For the sake of improved thermal comfort through individual controls, the radiant systems offer practical options because they facilitate an easy and effective zone

control [16]. The radiant systems are preferable in terms of space saving and eradication of noise than conventional system due to its energy transfer primarily by radiation [17]. Radiant heating systems improve the indoor environmental quality and spread less dust in comparison with conventional heating systems [18]. The radiant system has been gaining more importance over last several decades. A whole variety of researches have been done for improving the performance of the systems as well as these advantages of the radiant system. Besides the conventional radiant heating systems, e.g. Korean Ondol [19], Chinese Kang [20], and Roman Hypocaust [21], different radiant heating and cooling systems are currently performed to residential, office, school, museum and even airport terminal buildings [5]. The radiant systems are powerful alternative to HVAC systems for green buildings concept since they may conform with sustainable design strategies [22] and integrate with renewable energy and low exergy systems [23].

1.3.1.1 Research Trend and Historical Review of Radiant Systems

Radiant systems have a history up to thousands of years, and its foundations were validated through archaeology and historical researches [24]. Roman hypocaust system can be classified as the beginning of radiant system applications in Europe. Bansal [21] reviewed Roman hypocaust, which supplies hot gases through walls and floors. In this study, a numerical analysis is done to investigate the properties of hypocaust such as cavity width and storage capacity of hypocaust. There are some examples of radiant systems in Turkey. Architect Sinan had used floor heating system in 16th century. He adopted innovative technique in the Yunus Pasha Mosque (1517) and Suleymaniye Mosque (1550) to heat the prayer hall by using the floor heating system by digging water channels under the mosque to allow the warm water flow coming from the public bath (Hammam) [25].

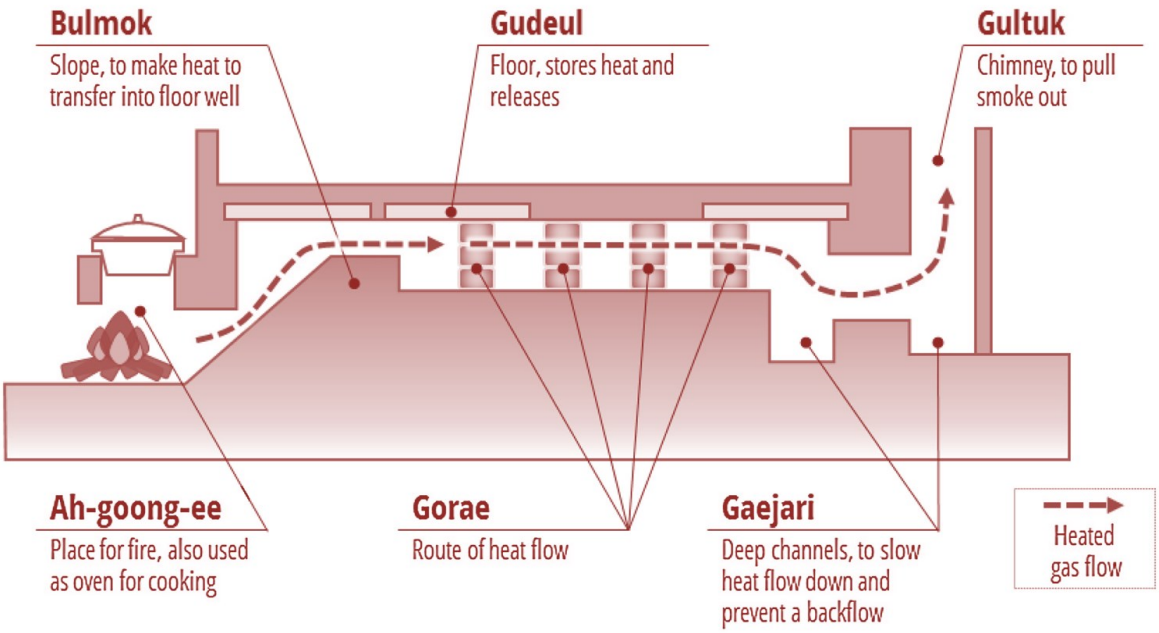

Figure 1: A Schematic of Korean Ondol [26].

Another example of radiant system was studied extensively in Asia; the well-known concept of Korean Ondol is shown in Fig. 1. It is one more ancient radiant heating system that employs the hot combustion gas to heat floor stones for heating. Korean people have been used that for more than two thousand years. This system was transformed to the hydronic floor heating system which provides better indoor environmental quality and energy efficiency in 1970s [27, 28].

In the last decade, a type of radiant systems which are floor heating systems were commonly applied in residential buildings in Korea, and it is also getting widespread throughout the world. In Europe, especially in Germany, Austria and Denmark, radiant heating systems are used in 30-50% of new houses. It is considered that floor heating system is an energy efficient and comfortable heating system in residential buildings. In addition to that, radiant systems are also commonly used in commercial and industrial buildings in Europe [18]. Because of

these, it has been a growing research interest for the assessment of radiant systems in terms of the heat transfer performances and the thermal comfort evaluation [29]. The paper by Rhee [30] outlines the number of research papers published on the Journal of Building and Environment related to radiant systems. Figure 2 shows the increasing trend of the subject area over the years.

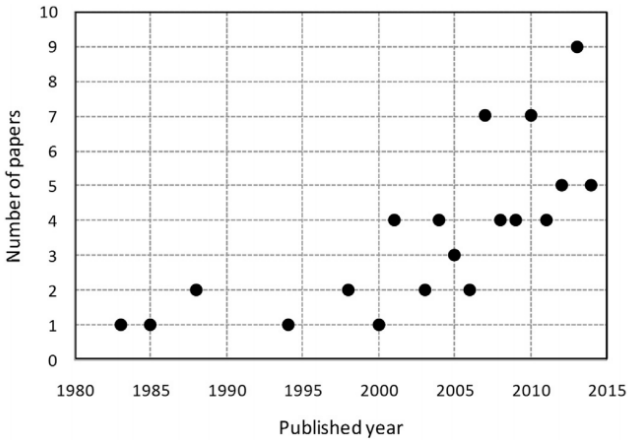

Figure 2: Number of articles published about radiant system [30].

1.3.1.2 Research Topics of Radiant Systems

In the literature there are several academic studies on thermal comfort evaluation of various HVAC systems. In parallel, radiant systems have been evaluated on different research topics. The main research subjects related to comfort and radiant systems are classified into three sub-types: (1) thermal comfort models, (2) general comfort (3) local discomfort [30]. Apart from thermal comfort evaluation studies, radiant systems are evaluated in this thesis in terms of human exergetic balance equations. The exergy concept is used to evaluate the radiant systems from a different point of view that is described in following chapters.

Furthermore, a special attention is given to the assessment of thermal performances of different radiant systems in the literature. Because the operation of radiant systems is generally associated with three heat transfer modes, i.e. (i)

conductive heat transfer between embedded pipe and the surface, (ii) convective heat transfer between cooled/heated surfaces and room air, and (iii) radiant heat transfer between radiant surfaces and inhabitants. Building suitable and detailed numerical models becomes necessary for analyzing a system with sensible accuracy. These subjects concentrating on thermal performance assessment were classified as follows: (1) heat transfer analysis, (2) heating/cooling capacity, (3) CFD analysis, and in the literature [30] (4) energy simulation.

In addition, many studies put forward system integration and/or control scenarios for the effective utilization of radiant systems. Similar systems such as DV (Displacement ventilation) and DOAS (Dedicated Outdoor Air System) were considered, for ensuring fresh outdoor air and/or taking the latent load away from the field covered by the radiant system. Moreover, diverse studies focusing on the control strategies of the radiant systems for the condensation risk, reducing overheating concerns, decreasing energy consumption etc. These topics could be classified as: (1) system integration and (2) control scenarios for the application of the radiant systems [30].

In Chapter 2 of this thesis, thermal comfort assessment parameters and methods are reviewed. Evaluation metrics are going to be specified and described according to the general thermal comfort concept and calculation procedure which is discussed in related standards. Furthermore, the local factors to provide better indoor environment are presented and a review of thermal comfort evaluation concepts are going to be given.

In Chapter 3 of this thesis, the experimental methodology of the thermal comfort analysis of radiant systems is described. In this Chapter detailed explanations are given

on constructive and the thermal properties of the test chamber. In addition to that the application of the sensors and hydraulic circuit of radiant panels are contained therein.

In Chapter 4, a detailed numerical methodology is explained, and validation of the test results is shown. In addition to that the validation of radiation model and mesh independence study is carried out.

In Chapter 5, results and discussions take place. Experimental and numerical results are evaluated in terms of human thermal comfort.

In Chapter 6, the conclusion part covers all studies that have been done during the thesis. In addition to that the future research suggestions are given in this Chapter.

2 THERMAL COMFORT

2.1 Heat Transfer Mechanism of Human Body

Human body is known to have its own thermal regulation system [31]. It continuously generates heat by metabolic processes and exchanges heat with the environment. The metabolic heat generated in the body is dissipated through radiation, convection, conduction and evaporation. Lungs and skin are the main heat exchange equipment for the transfer of sensible heat. The latent heat is transferred by evaporation to the environment. Latent heat represents the heat of vaporization of water as it evaporates in the lungs and on the skin by absorbing body heat. The total rate of heat loss from the body can be expressed as:

$$\dot{Q}_{body} = \dot{Q}_{skin} + \dot{Q}_{lungs} = \left(\dot{Q}_{sensible} + \dot{Q}_{latent}\right)_{skin} + \left(\dot{Q}_{sensible} + \dot{Q}_{latent}\right)_{lungs}$$

The total rate of heat transfer from the body is equal to the rate of metabolic heat generation in terms of steady conditions. Metabolic rate can vary from 100 W to 1000 W according to a person's activity level.

Sensible heat loss from the skin depends on the skin temperature, the temperature of surrounding surfaces and the environment. The latent heat exchange works depend on the skin wettedness and the relative humidity of the environment. The insulation layer of the body which is clothing effects on heat transfer and reduces both the sensible and latent heat loss from the body. The heat transfer from the lungs through respiration depends on the breathing and the volume of the lungs. The convection and radiation heat losses from the outer surface of a clothed body can be expressed as a general form in Watts [31]:

$$\dot{Q}_{conv} = h_{conv} A_{clothing} (T_{clothing} - T_{ambient})$$

$$\dot{Q}_{rad} = h_{rad} A_{clothing} (T_{clothing} - T_{surr})$$

2.2 Thermal Comfort

Thermal comfort assessment parameters and methods need to be able to design a human-centered system. Evaluation metrics are specified and described according to the general thermal comfort concept and calculation procedure which is discussed in related standards [6, 7]. Furthermore, the local factors to provide better indoor environment are presented.

In ASHRAE 55 [7] and EN7730 standards [6], thermal comfort is defined as "that condition of mind which expresses satisfaction with the thermal environment". This description raises a question concerning which metrics can be used to evaluate thermal comfort. The comfort metrics which have been used in radiant system assessment are going to be described in this part of the thesis.

Assessment of thermal comfort is possible with a range of options, but the most common method is via the measurement of air temperature, mean radiant temperature (MRT) (can be calculated from globe temperature), and operative temperature (which includes convective and radiative effects). The predicted mean vote (PMV) is another comfort parameter developed to assess thermal feeling from "cold" to "hot" [1]. This objective metric was evolved using human votes about their sensations in a test chamber and is dependent on an energy balance equation implemented to the human body. Fanger [1] test the models of thermal comfort based on the energy balance of the human body. These models deal with heat exchange between the human body and its surroundings. Through laboratory

practice, it was discovered that thermal circumstances where the energy input corresponds with the energy output, the feeling becomes considerably comfortable. The result is the predicted mean vote (PMV) approach revealing the prediction of the mean vote of a larger group on a basis of the indoor air temperature, radiant temperature, humidity, air velocity, together with the metabolic rate and the level of clothing insulation of a person. It ranges from −3 (cold) to +3 (hot) with the value of 0 set as neutral. This 7-point thermal sensation scale is shown in the Table 1. This metric has been translated into a predicted percentage of dissatisfaction (PPD) rate which establishes a quantitative prediction of the percentage of thermally dissatisfied people. Most comfortable number of thermal comfort index (lowest PPD = %5 and PMV=0) is associated with a neutral body sensation.

Table 1: Seven-point thermal sensation scale [6].

+3	Hot
+2	Warm
+1	Slightly warm
0	Neutral
-1	Slightly cool
-2	Cool
-3	Cold

In PMV approach, Fanger has combined psychological theory with statistical data and has developed a mathematical model that predicts thermal sensation. According to Fanger, PMV indicator, which is used to determine comfort conditions for six comfort variables such as clothing, ambient air temperature, average radiant temperature, air velocity, the metabolic activity rate and relative humidity. These

metrics are classified as personal parameters which are clothing and metabolic rate and environmental parameters which are air temperature, mean radiant temperature, relative humidity and air velocity.

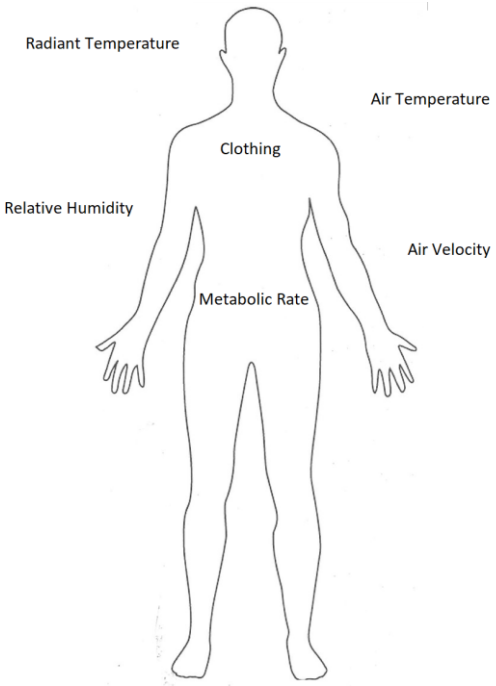

Figure 3: Thermal comfort evaluation parameters in PMV approach.

By using these parameters, PMV calculation can be done using Equations (1) to (5) given in the EN 7730 Standard [6]:

$$PMV = \left(0.303 \cdot e^{-0{,}036 \cdot M} + 0.028\right) \begin{bmatrix} (M-W) - 3.05 \cdot 10^{-3} \cdot \{5733 - 6.99 \cdot (M-W) - p_a\} \\ -0.42 \cdot \{(M-W) - 58.15\} - 1.7 \cdot 10^{-5} \cdot M \cdot (5867 - p_a) \\ -0.0014M\,(34 - T_a) - 3.96 \cdot 10^{-8} f_{cl} \left\{(T_{cl} + 273)^4 - (T_r + 273)^4\right\} \\ -f_{cl} \cdot h \cdot (T_{cl} - T_a) \end{bmatrix} \quad (1)$$

Here, the terms T_{cl}, h and f_{cl} are calculated by equations 2, 3 and 4, respectively. The equations 2 and 3 are solved by iteration [6]:

$$T_{cl} = 35.7 - 0.028 \cdot (M - W) - I_{cl} \cdot \begin{bmatrix} 3.96 \cdot 10^{-8} \cdot f_{cl} \cdot \left\{ (T_{cl} + 273)^4 - (T_r + 273)^4 \right\} \\ + f_{cl} \cdot h_c \cdot (T_{cl} - T_a) \end{bmatrix} \quad (2)$$

$$h = \begin{Bmatrix} 2.38 \cdot |T_{cl} - T_a|^{0.25} \Leftarrow 2.38 \cdot |T_{cl} - T_a|^{0.25} > 12.1 \cdot \sqrt{V_{ar}} \\ 12.1 \cdot \sqrt{V_{ar}} \Leftarrow 2.38 \cdot |T_{cl} - T_a|^{0.25} < 12.1 \cdot \sqrt{V_{ar}} \end{Bmatrix} \quad (3)$$

$$f_{cl} = \begin{Bmatrix} 1 + 1.29 \cdot I_{cl} \Leftarrow I_{cl} \le 0.078 m^2 \cdot K / W \\ 1.05 + 0.645 \cdot I_{cl} \Leftarrow I_{cl} > 0.078 m^2 \cdot K / W \end{Bmatrix} \quad (4)$$

The PPD forecasts the percentage of thermally uncomfortable people in a considerable number of people. The rest of the group will sense thermally neutral, slightly warm or slightly cool. PPD value can be calculated with the Equation 5 given below [6]:

$$PPD = 100 - 95 \cdot \exp(-0.03353 \cdot PMV^4 - 0.2179 \cdot PMV^2) \quad (5)$$

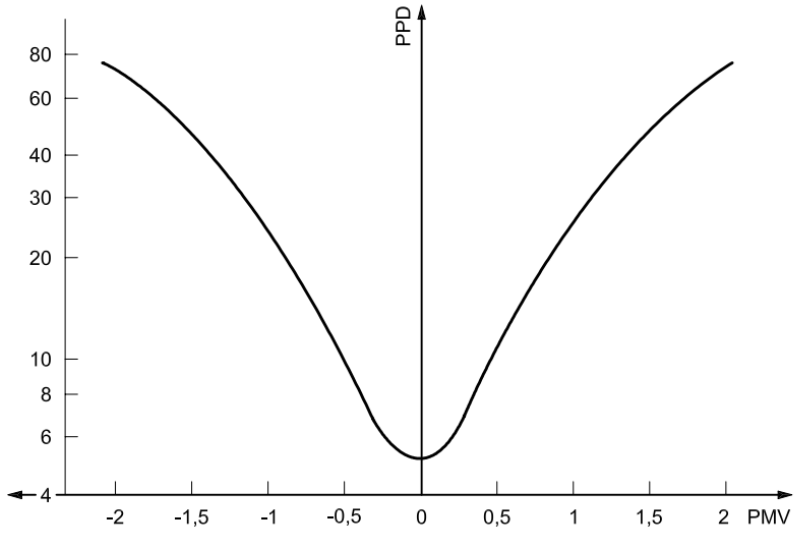

Figure 4: PPD and PMV graph [6].

Indoor comfort requirement can vary based on the indoor conditions. EN ISO 7730 [6] and EN 15251 [32] set three categories of thermal requirements for mechanically conditioned spaces: category I (or class A) (PPD < 6%, i.e. −0.2 < PMV < +0.2), category II (or class B) (PPD < 10%, i.e. −0.5 < PMV < +0.5) and

category III (or class C) (PPD < 15%, i.e. −0.7 < PMV < +0.7). To be able to be classified as one of these types, the standard puts some requirements that should be met. Several research studies show that the tightly air-temperature-controlled space which means that very precisely conditioned place (class A) did not supply greater conditions for occupants than non-tightly air-temperature-controlled spaces (class B and C) [33, 34]. According to these arguments ASHRAE 55 [7] did not include the classification of building categories.

The temperature felt by the human body is not equal to the ambient air temperature. The temperature of the objects and surfaces in the environment also affects the temperature that is felt. And they exchange heat by radiation transfer. The indoor parameters such as air temperature, air velocity and relative humidity affect the thermal sensation relatively. In these studies, environmental parameters are needed, which can be defined as follows:

- Air temperature is a variable that determines the amount of heat exchange made by convection between human body and its environment. Heat transfer with convection between the person and the environment occurs until the body surface temperature and air temperature are balanced. For this reason, air temperature is one of the important environmental variables that affect the thermal comfort of a person.
- Mean radiant temperature expresses the combined effect of the temperatures of the surrounding surfaces to determine the heat transfer between the person and the surrounding surfaces through radiation heat transfer. It depends on the position of the person in the space, the shape of the posture and the temperature of the surrounding surfaces.

- Humidity of the air is another variable that affects the amount of heat transferred from the body through water vapor diffusion and breathing through the skin of a person.
- Air velocity; is also an important variable that affects the amount of convective heat transfer between the human and its surroundings, since it affects the heat transport coefficient between any surface and air.

Personal variables affecting thermal comfort are the activity level and the clothing type [1, 6].

- The level of activity is a variable that affects the amount of energy produced by the body. The activity rate is directly related to the kind of action that a person makes, and it is one of the important variables affecting thermal comfort. Depending on the muscle-related activities, human body generates energy. This activity rate is measured in "met" (1 met = 58.15 W/m^2). For normal adults, the body surface is defined as $1.7m^2$. A thermally comfortable person sitting in an environment has a heat loss of 100 W. Some activity rate values are given in Table 2 in W/m^2 and met [6].
- Clothing rate is one of the personal variables that should be known when the thermal comfort conditions are determined. Because it determines the thermal insulation resistance of the clothes and therefore affects the amount of heat transfer between the human and its surroundings. Heat insulation resistance of clothes is usually expressed in terms of clo unit. (1 clo = 0.155 $m^2 \cdot K/W$) Thermal insulation resistances for different types of clothing are shown in Table 3 according to the EN 7730 Standard [6].

Table 2: Activity rates according to the standard EN 7730 [6].

Type of Activity	Activity Rates	
	W/m^2	met
Reclining	46	0.8
Seated, relaxed	58	1
Sedentary activity (office, dwelling, school, laboratory)	70	1.2
Standing, light activity (shopping, laboratory, light industry)	93	1.6
Walking at 2 km/h	110	1.9
Standing, medium activity (shop assistant, domestic work, machine work)	116	2
Walking at km/h	200	3.4

Table 3: Thermal Insulation properties of some clothes [6].

Clothes	I_{cl} (clo)	I_{cl} (m^{2}K/W)
Underwear		
Panties	0.03	0.005
Underpants with long legs	0.10	0.016
Singlet	0.04	0.006
T-shirt	0.09	0.014
Shirt with long sleeves	0.12	0.019
Panties and bra	0.0	0.005
Shirts/Blouses		
Short sleeves	0.15	0.023
Light-weight. long sleeves	0.20	0.031
Normal. long sleeves	0.25	0.039
Flannel shirt. long sleeves	0.30	0.047
Light-weight blouse. long sleeves	0.15	0.023
Trousers		
Shorts	0.06	0.009
Light-weight	0.20	0.031
Normal	0.25	0.039
Flannel	0.28	0.043
Dresses/Skirts		
Light skirts (summer)	0.15	0.023
Heavy skirt (winter)	0.25	0.039
Light dress. short sleeves	0.20	0.031
Winter dress. long sleeves	0.40	0.062
Boiler suit	0.55	0.085
Outdoor clothing		
Coat	0.60	0.093
Down jacket	0.55	0.085
Parka	0.70	0.109
Fibre-pelt overalls	0.55	0.085

In Tables 2 and 3, a general outline of the comfort evaluation parameters are given. Local comfort parameters are also very important factors that are particularly relevant for the evaluation of comfort. The local comfort is related with the radiant asymmetry, airflow-draught rate, vertical air temperature difference, and contact with hot and cold surfaces. These parameters related to some well-established standards are discussed below:

(1) Radiant asymmetry (ΔT_{pr}): EN ISO 7730 [6] and ASHRAE 55 [7] define limits of radiant asymmetry when using radiant walls, floors and ceilings. According to the standards, Figure 5 shows the percentage of dissatisfaction as a function of the radiant temperature asymmetry caused by a warm ceiling, a cool wall, a cool ceiling or by a warm wall. For horizontal radiant asymmetry, Figure 5 applies from side-to-side (left/right or right/left) asymmetry, the curves providing a conservative estimate of the discomfort: no other positions of the body in relation to the surfaces (e.g. front/back) cause higher asymmetry discomfort. Determine the *PD* using Equations (6-9), as applicable.

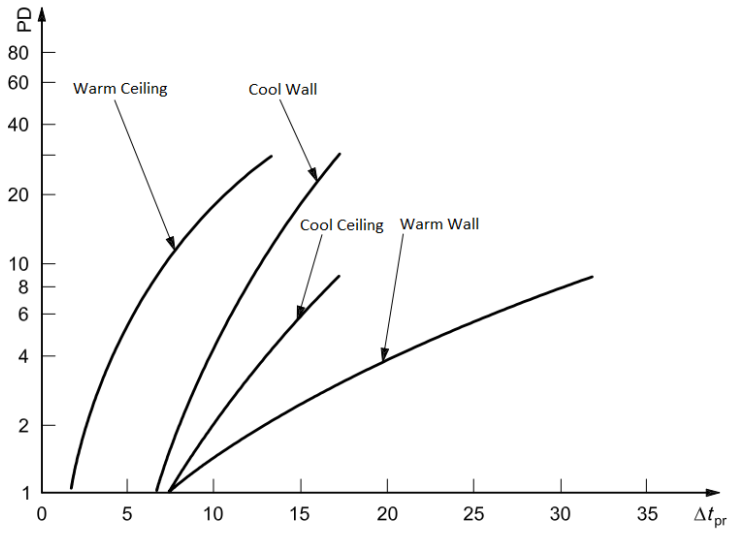

Figure 5: Local thermal discomfort caused by radiant temperature asymmetry [6].

a) Warm ceiling effect:

$$PD = \frac{100}{1+\exp(2.84-0.174\cdot\Delta T_{pr})} - 5.5 \Leftarrow \Delta T_{pr} < 23°C \quad (6)$$

b) Cool wall effect:

$$PD = \frac{100}{1+\exp(6.61-0.345\cdot\Delta T_{pr})} \Leftarrow \Delta T_{pr} < 15°C \quad (7)$$

c) Cool ceiling effect:

$$PD = \frac{100}{1+\exp(9.93-0.5\cdot\Delta T_{pr})} \Leftarrow \Delta T_{pr} < 15°C \quad (8)$$

d) Warm wall effect:

$$PD = \frac{100}{1+\exp(3.72-0.052\cdot\Delta T_{pr})} - 3.5 \Leftarrow \Delta T_{pr} < 35°C \quad (9)$$

(2) Floor temperature is important to provide comfort. If it has too low or too high temperature, it can cause discomfort. EN ISO 7730 [6] and ASHRAE 55 [7] specify limits for rooms occupied by sedentary or/and standing people wearing shoes. Both standards recommend floor surface temperatures within the occupied zone to be kept between 19°C and 29°C. Figure 6 shows the percentage of dissatisfaction as a function of the floor temperature, based on studies with standing and/or sedentary people.

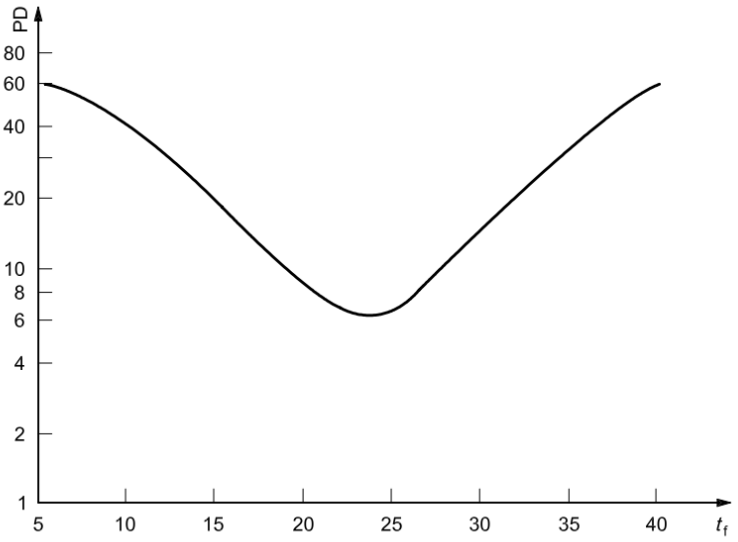

Figure 6: Local thermal discomfort caused by warm or cold floors [6].

(3) Vertical air temperature difference (ΔT_{av}) between head and ankles can cause discomfort [35]. Discomfort rate (*PD*) is defined in EN ISO 7730 [6] and ASHRAE 55 [7]. This metric only applies for head temperature being higher than feet temperatures (people are less sensitive under opposite conditions). *PD* can be calculated using Equation (10):

$$PD = \frac{100}{1+\exp(5.76-0.856\cdot\Delta T_{av})} \Leftarrow \Delta T_{av} < 8°\text{C} \qquad (10)$$

Figure 7 shows the percentage of dissatisfaction (*PD*) as a function of the vertical air temperature difference between head and ankles.

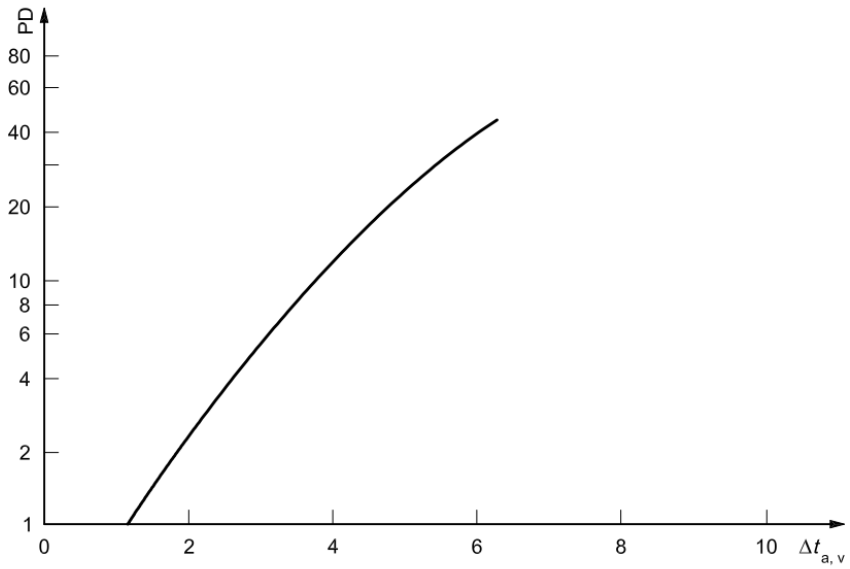

Figure 7: Local discomfort caused by vertical air temperature difference [6].

(4) Draught is defined as an undesired local cooling of the body caused by air movement. Fanger and his research team [36] developed a draught model using three variables (air temperature, mean air velocity, and turbulence intensity). Based on human subject testing this model was converted into percentage of dissatisfaction for draft (PD_{draft}). This index is further defined within the EN ISO 7730 [6] but it was removed from ASHRAE 55 because it was found to overestimate the draught risk [37].

$$DR = (34 - T_{al}) \cdot (V_{al} - 0.05)^{0.62} \cdot (0.37 \cdot V_{al} \cdot Tu + 3.14) \qquad (11)$$

T_{al}: is the local air temperature, in degrees Celsius, 20 °C to 26 °C;

V_{al}: is the local mean air velocity, in metres per second, < 0.5 m/s;

T_u: is the local turbulence intensity, in percent, 10 % to 60 % (if unknown, 40 % may be used)

For $v_{a,l} < 0.05$ m/s: use $v_{a,l} = 0.05$ m/s For $DR > 100$ %: use $DR = 100$ %

Another discomfort metric related to non-steady-state thermal environments is the ‘temperature drift’. This metric is defined as a steady, non-cyclic change in operative temperature of an enclosed space. Temperature drift is associated with discomfort and is reported in [K/h]. Standard EN ISO 7730 [6] allows a maximum drift of 2 K/h. ASHRAE Standard 55 [7] allows for 2.2 K/h for drift duration of 1h, but not more than 2.6 K/h during any 0.25h period within that 1h period. ASHRAE 55 also requires drift lasting 4h to be reduced to 0.8 K/h.

Thermal sensation vote (TSV) is another index to evaluate comfort in addition to the metrics described before. This scale focuses on thermal sensation from “cold” to “hot” via collecting votes from occupants for a specific thermal environment at a specified time. This metric was used to develop the PMV index and is sometimes referred to as ‘actual mean vote’. TSV can be conducted for whole body (global) sensation as well as for local sensation. The latter allows a comparison with the physiological measurements of local body parts.

Thermal comfort vote (TCV) is a scale to rate thermal comfort from “uncomfortable” to “comfortable”. This scale also uses human votes to asset comfort. ISO-defined 4-point scale (“uncomfortable”, “slightly uncomfortable”, “slightly comfortable”, “comfortable”) is used for TCV; however, in this vote, there is no “0” condition for neutral feeling [38]. T. Imanari et al. later used a 5-point scale that includes a “neutral” comfort vote [39].

Occupant satisfaction votes are often used for indoor environmental quality (IEQ) surveys in buildings. These surveys usually use 5- or 7-point scales ranging from “(very) dissatisfied” to “(very) satisfied” and with the value of 0 set as neutral (e.g., CBE Occupant IEQ Survey [40].

2.3 Exergy Concept

Thermal comfort assessment methods are based on the first law of thermodynamics for many years. In such an analysis of thermal comfort, the heat transfer between the body and the environment is calculated using the energy balance of the human body. On the other hand, the second law of thermodynamics reveals the concept of exergy as a suitable method for comfort evaluation. Exergy consumption in the human body depends on the quality of energy transfer between a body and its environment. Human body indeed consumes exergy (available energy) to reach to a desired thermal comfort level. A similar situation can be seen when the first law of thermodynamics is considered for comfort evaluation. The situation in which the body reaches the thermal equilibrium with the environment indicates that the condition is thermally satisfied. In contrast, when the exergy consumption is minimum it means that human body is thermally satisfied. It is shown that in the literature when the room temperature is lowered into a neutral temperature, the exergy consumption rate decreases and reaches a minimum at a certain temperature. When the temperature is set to a lower value than neutral conditions, body generates energy by shivering to keep the body temperature at a desirable level. At that point exergy (available energy) input and output increase. When skin temperature also goes down, body consumes more exergy because of the temperature difference between the core and the skin.

Similarly, when a air condition system is blowing very hot or cold air, the rate of exergy consumption increases, although there is a smaller temperature difference between the body and the environment. In this case, the neutral state and the current skin / core temperature difference trigger the body to sweat. The evaporation via

sweating cools the body but at the same time it increases the exergy consumption rate [41, 42].

The reason why we have used exergy concept in thermal comfort evaluation is because exergy analysis shows how exergy consumption of human body depends on the environmental conditions. In addition, under steady-state conditions, the literature research show that there is a relation among the exergy consumption of human body and the expected level of thermal comfort [41].

2.3.1 Introduction to Exergy Concept for Comfort

The quality of the supplied energy is considered by the exergy concept besides the quantity [43], as shown in Figure 8. The exergy (available energy) contained by a system is the "maximum available work that can be extracted from the energy contained by that system" into its environment. Exergy concept analyses the degree of waste within a system or a variety of systems work in harmony across the energy transformation. This concept can allow optimization of HVAC systems by the aim of sustainable building design and operation.

The usage of exergy approach into the design and operation of air conditioning systems is set up in a relative fashion. However, the usage for human being's thermal sensation in conditioned fashion is not well-established. Exergy concept is being used more often in building energy assessment. It can be seen in various studies in the literature [44, 45, 46, 47]. The highest level of energy wasted in buildings is due to the climatization of spaces by controlling room temperature, lighting, relative humidity and domestic hot water. The needed amount of exergy to provide comfortable indoor environment which can be achieved mostly between 20°C and 26°C [48], is not high, mainly in heating and cooling applications. Despite that, high quality sources such as fossil fuels or electricity are being used to meet

the requirement. A general schematic is given in Figure 8 that gives a quality-based orientation of sources and uses [44].

Energy balance-based analysis alone is not able to account for the latter problem. Exergy analysis makes it possible to provide information on the correlation between the requirement and the supply to evaluate in which part of the energy flow for the whole chain of building systems may allow the biggest savings [44,46,47,49].

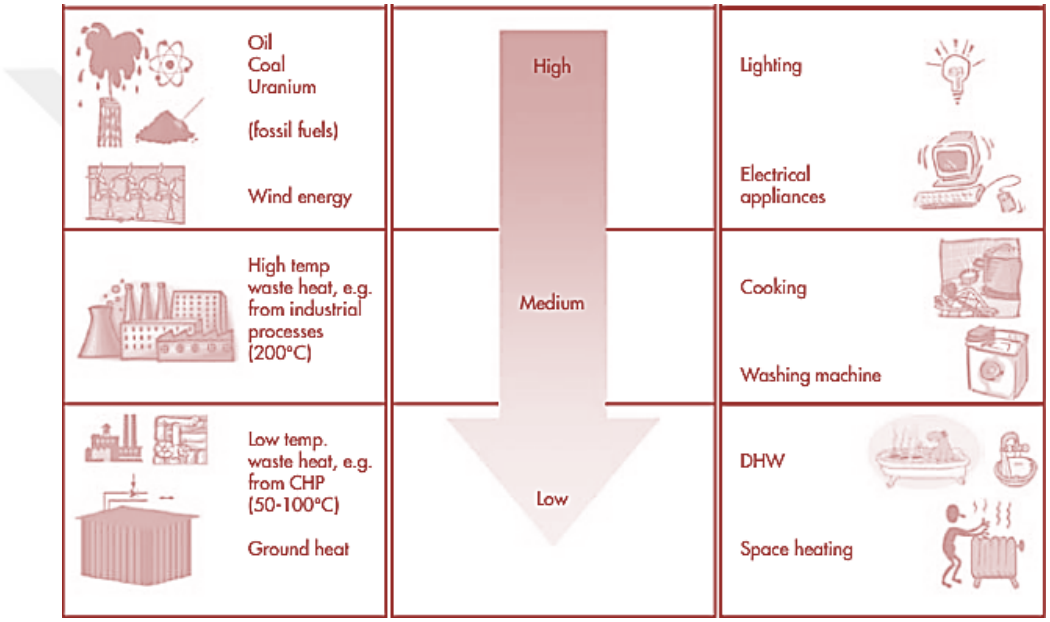

Figure 8: Quality based classification sources and uses [49]

Achieving thermal comfort and energy savings is possible using the exergy concept that combines various parameters such as outdoor thermal conditions, living space thermal parameters and occupant's objective preferences that ensures climate conditioning systems provide thermal comfort with the lowest possible human-body exergy consumption rate. The results suggest the use of low exergy sources (radiant heating/cooling, natural ventilation, etc.).

Currently, there are not many studies available that focus on the relation between the exergy consumption rate of the human body and thermal sensation. A

recent study [48] suggests that human body exergy balance analysis could give more accurate indication of thermal comfort. Another study by Prek [42] compared calculated human-body exergy consumption rate to the results obtained from PMV/PPD model, which predicts the average thermal sensation of a large group of people.

This thesis evaluates radiant systems in terms of the human-body exergy model and PMV/PPD model by using the data generated from different combinations of the indoor climate parameters temperature, humidity, air velocity, and others by experimental and CFD analysis.

2.3.2 Background of Human-body Exergy Balance Model

Shukuya and Saito developed human-body exergy theory in the middle of 1990s [49]. Prof. Dr. I. Oshida, from Japan, who was one of the first scientists in the field of solar exergy utilization, brought up the correspondence between the input and output exergy of human body and thermal sensation [50]; around 15 years prior to Shukuya and Saito initiated their research. However, Oshida was not the one who developed the theory of human-body exergy balance.

Combining the energy balance and entropy balance equations for human body, Saito and Shukuya developed the earliest version of human-body exergy balance model (Figure 9). Assuming that the environmental temperature equals to the ambient air temperature and mean radiant temperature, they calculated human-body exergy balance under a thermally steady state.

They discovered that the exergy-consumption rate within the human body is the minimum at the state that outgoing heat is equal to the metabolic heat-generation, It indicates that lowest exergy consumption rate within human body resulted as thermally neutral condition [46].

In the early 2000, Isawa, Komizo and Shukuya developed another version of human-body exergy calculation model. For sensible thermal exergy transfer, they considered convective exergy and radiant exergy separately. They also provided a better mathematical expression for sweat secretion and its evaporation which makes possible the calculation for situations where indoor relative humidity is different than the outdoor relative humidity. A few theoretical re-examinations on the derivation of liquid-water exergy and moist-air exergy were made after these revisions until 2006 [49].

There is an optimum range of mean radiant temperature and room air temperature providing the human body with the lowest exergy consumption rate. [41, 42, 45] show that this is possible for the mean radiant temperature from 23 to 26°C and the room air temperature from 17 to 19°C, that corresponds to human-body exergy balance calculation made for winter condition suggests.

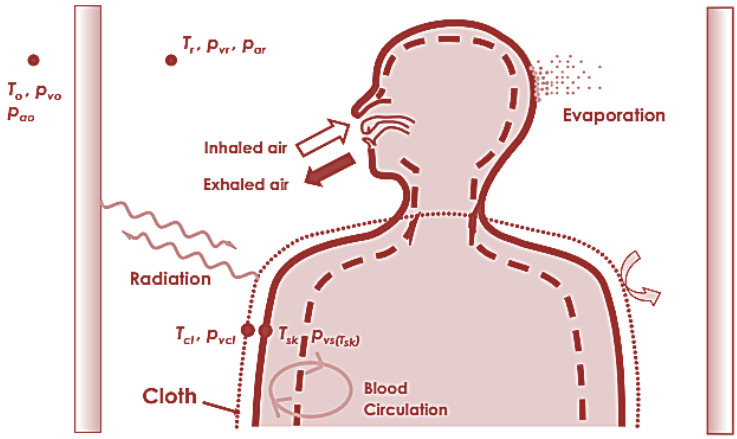

Figure 9: Human body system [49]

Experienced architects and engineers suggest indoor thermal environment in this condition is generally in harmony with a convenient level of thermal comfort [46, 52]. On the other hand, for summer conditions, it was found that a combination

of mean radiant temperature ranging from 28°C to 29°C and air current of exceeding 0.2 m/s with a higher air temperature and humidity (30°C; 65%) provides the lowest exergy consumption rate. With a high-temperature radiant cooling system combined with natural ventilation and a good quality of solar control together with interior-heat-generation control, it is possible to obtain such an indoor thermal environment [51]. The modality of verifying the outcome of the efficiency of the low-exergy heating process was combined with cooling systems.

A current research centering behavior of occupants and their thermal background connected to human-body exergy balance [52] suggests that the human-body exergy consumption rate of the occupant tend to become higher towards the time of closing windows and become lower afterwards, in spite of the fact this is based on the field measurement done in fall equinox.

Takunaga et al. [53] have also studied the distinction of human-body exergy consumption rate in each occupant's thermal background. They conducted an experimental research on sweat secretion and its relation to human-body exergy balance in hot and humid setting. The subjects who were not much exposed to air-conditioned space at houses and other locations could feel pleasant with a smaller rate of sweat secretion and a lower exergy-consumption rate within human body in contrast to those stayed much in air-conditioned space.

2.3.3 Calculation of Human Body Exergy Balance

Consumption of exergy comprised nutrients by people within their body resulted that they can sense, think and perform any physical work flexing their muscles. Eventually, entropy is produced by human being unavoidably and it is a necessity that it should be disposed into the built habitat. Regardless of the fact that they are active or passive, climate control systems for buildings also function as

exergy-entropy process. “Exergy” is the idea to express what is used within a system and “entropy” is what is discarded as unusable from the system. In a different way of expression, exergy is the notion that calibrates the potential of energy and material to scatter, and entropy is the notion that calibrates the amount of scattered energy and matter [46]. Exergy-entropy processes exist in any organic or inorganic processes can be exampled as biochemical or technological processes. Production of exergy, use of exergy, entropy production and entropy dispensing are their essential attributes. Exergy balance equation for the human body as a system is indicated below in its standard form [49];

[Exergy input] – [Exergy consumption] = [Exergy stored] + [Exergy output].

A detailed form of exergy balance equation can be defined firstly with an energy balance equation is defined using the 1st law of thermodynamics and then the complementary entropy balance equality formula can be driven using second law of thermodynamics [49]. The output of the entropy balance equation and outdoor temperature value coming from the energy balance are used for exergy balance equation. The comprehensive explanation of a heating system as a sample can be found in [49]. Stored exergy amount is another issue that should be discussed. Esentially, it can be defined as the difference among the energy change and the output of the entropy change and the outdoor temperature.

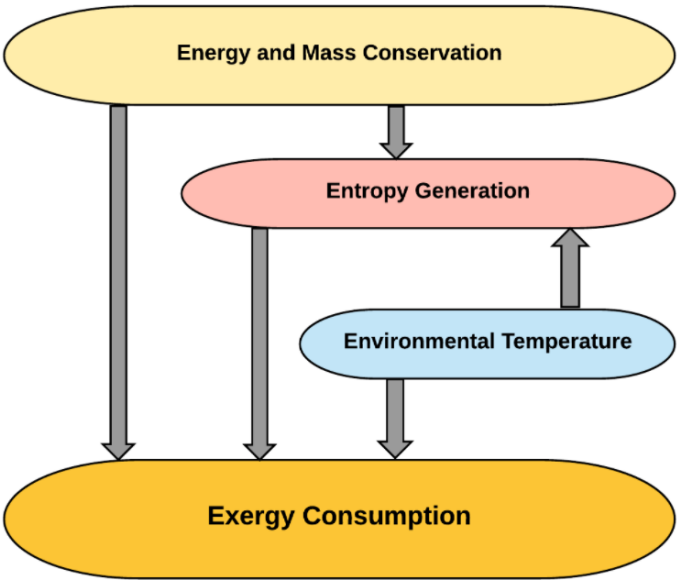

Figure 10: Exergy consumption equation: $\delta X_c = \delta S_g \cdot T_c$.

It is crucial to note that use of exergy and stored exergy at optimal values are needed with a rational combination of exergy input and output to carry on comfort and healthy conditions.

In [48], the exergy balance of human body is was developed according to the two-node model that has nodes called core and shell. A general formula of exergy balance for this concept is given in Table 4. The detailed calculation procedure is given in Appendix A. That calculation precedure was used in this thesis.

Table 4: Input Variables of Human Body Exergy Balance

Input Variables-Outdoor	
Outdoor Air Temperature	T_o (ºC)
Relative Humidity of Outdoor Air	ϕ_{out} (%)
Input Variables-Indoor	
Room Air Temperature	T_{ra} (ºC)
Mean Radiant Temperature	T_{mr} (ºC)
Relative Humidity of Room Air	ϕ_{air} (%)
Air Speed	v_{rair} (m/s)
Human Body	
Clothing	clo
Activity	M (met) (1met=58.2 W/m^2)

Table 5: Exergy Balance Equation [49]

[Warm exergy generated by metabolism] + [Warm/cool and wet/dry exergies of the inhaled humid air] + [Warm and wet exergies of the liquid water generated in the core by metabolism] + [Warm/cool and wet/dry exergies of the sum of liquid water generated in the shell by metabolism and dry air to let the liquid water disperse] + [Warm/cool radiant exergy absorbed by the whole of skin and clothing surfaces] - [Exergy consumption] = [Warm exergy stored in the core and the shell] + [Warm and wet exergies of the exhaled humid air] + [Warm/cool exergy of the water vapor originating from the sweat and wet/dry exergy of the humid air containing the evaporated water from the sweat] + [Warm/cool radiant exergy discharged from the whole of skin and clothing surfaces] + [Warm/cool exergy transferred by convection from the whole of skin and clothing surfaces into the surrounding air]

According to equations given in Appendix A, a calculation algorithm was introduced by Asada et al. [54] in the form of VBA macros written for an excel-sheet, available for download at web site of [49]. In order to process multiple lines at once, the macros were rewritten to be usable for the R statistical software [55]. The tool needs eight input parameters which are shown is Table 4 to calculate human body exergy balance. These parameters and calculation formulae are given in Appendix A. The exergy balance calculations in this thesis are done by using R statistical code. The comfort research library called “comf v0.1.7” is used for the calculations. Input parameters are taken from the experimental measurements.

3 EXPERIMENTAL METHODOLOGY

In this part of the thesis, the experimental methodology for the thermal comfort analysis of radiant systems is described. In the following sections, detailed explanations are given on construction of the test chamber and related parameters. In addition to that the application of the sensors and hydraulic circuit of radiant panels are discussed.

Experiments carried out for the case of wall heating, ceiling heating and heating from both surfaces in the test volume which simulates a room in winter conditions. In these experiments, for wall heating and ceiling heating cases 5 different water supply temperatures were given for the system. For the scenario that wall and ceiling surfaces both selected as heating surfaces, tests were done at 3 different water supply temperatures.

In the wall tests, 5 panels were used in dimensions of 0.6m x 2m. For ceiling, 12 ceiling panels were used in dimensions of 1m x 1.2m. In all cases the water runs in surface basis; therefore each panel was not separately conditioned.,Indoor air temperature and wall surface temperatures measured at the required points during the tests are described in detail below. During all experiments, the relative humidity of the test chamber was set to be constant at 50%.

Thermal comfort calculations have been done for the measured test results. Mean radiant temperature, air temperature and relative humidity values were taken from the test results. Air velocity, clothing factor and metabolic activity values (clothing and metabolic activity are personal parameters for thermal comfort evaluation which are defined in Chapter 2) were chosen as clo=1, met=1.2 and v=0.1 m/s.

3.1 Description of test chamber

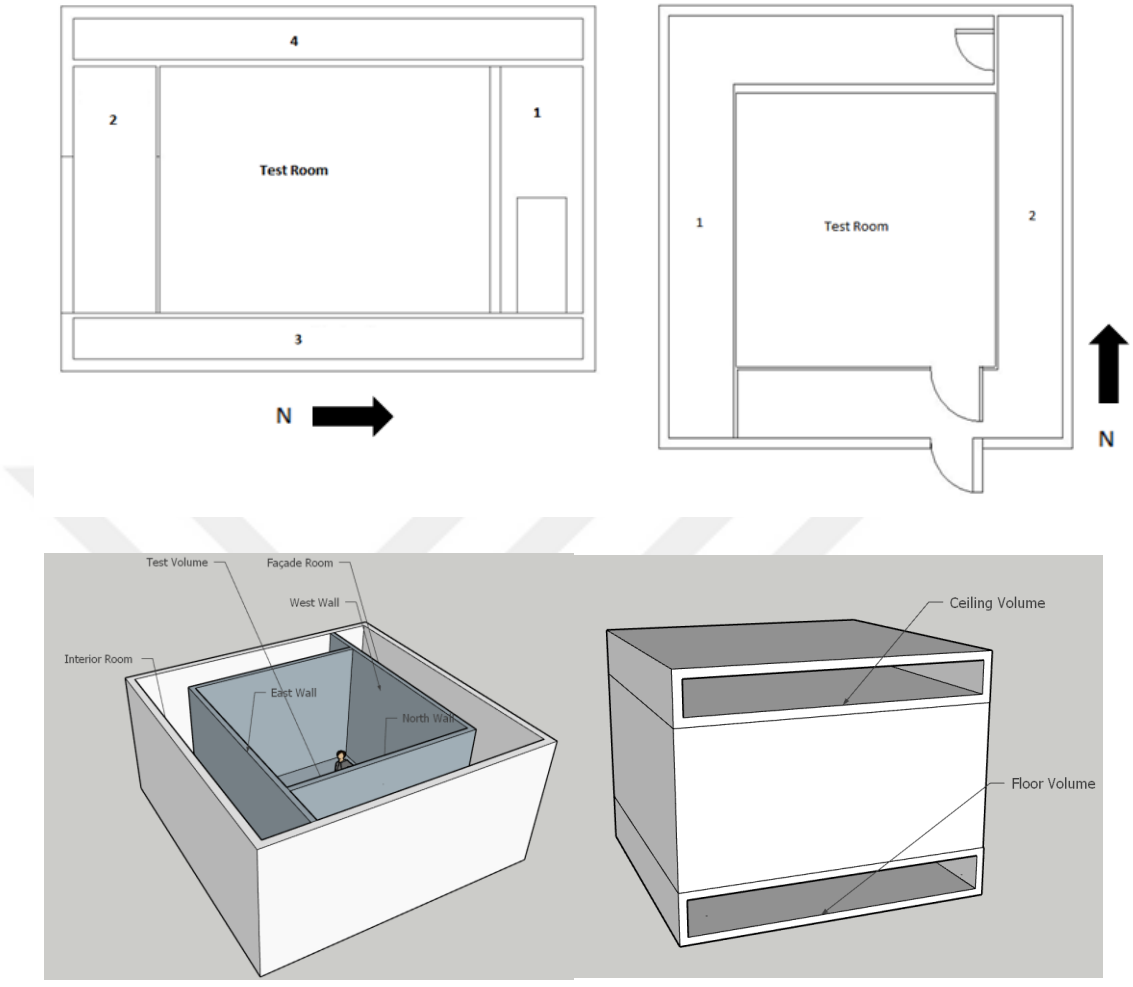

Figure 11: General view of the climatic test room in 2D and 3D.

The test chamber was constructed to test different heating applications under multi-climate conditions which are listed in Table 6. It is illustrated in Fig. 11. The chamber consists of 5 zones including façade volume, inner zone volume, floor volume, ceiling volume and test volume. The test volume has a footprint area of 16m^2 (4m × 4m) and an internal height of 3m. The thermal transmittance coefficients of the wall and ceiling constructions (made out of sheet metal with polyurethane insulation) are presented in Table 7. Sandwich type wall panels were used in the construction of the room. The sandwich panel consists of a polyurethane

insulation between two sheet metal layers which have locking mechanism for durability. Thermal properties of the wall were characterized according to the Turkish Standard TS 825 [56] (thermal insulation requirements for buildings). Mechanical air conditioner system was installed in test chamber to supply the desired boundary conditions to the test volume.

This test chamber has been developed by Mir Research and Development Inc. located in Istanbul and used in various research activities related with radiant systems [57, 58]. As it was defined in previous researches, the emissivity of the unheated indoor surfaces and radiant wall/ceiling surfaces were taken from previous works [59].

Table 6: Controlled parameters in zones.

	Ceiling	**Floor**	**Façade Room**	**Interior Room**
Temperature Range	-10˚C / +40˚C	+0˚C / +30˚C	-10˚C / +40˚C	+0˚C / +30˚C
Temperature Tolerance	± 0.5 ˚C	± 0.5 ˚C	± 0.5 ˚C	± 0.5 ˚C
Humidity Range	n/a	n/a	%35 / %85 RH	n/a
Humidity Control Steps	n/a	n/a	%1	n/a
Humidity Tolerance	n/a	n/a	± % 0.5 RH	n/a
Air Velocity	n/a	n/a	0.5 – 5 m/s	n/a

The test chamber is constructed to supply general requirements that defined by the ASHRAE Standard 138 [60] and there is a minor difference with the standard that is the ensuring climatic conditions in all volumes of test chamber conditioned by the enclosed volumes are provided by air handling units.

Table 7: Thermal properties of walls.

Surfaces	*U* (W/m²K)	*L* (m)	*k* (W/mK)	Description
Ceiling	0.3	0.08	0.024	Radiant Ceiling panels are applied. The ceiling volume behind the surface is conditioned as outdoor space.
Floor	0.4	0.06	0.024	The volume below the floor surface conditioned as indoor space
North Wall	0.4	0.13	0.052	The Surface is unheated. The volume behind the surface conditioned as outdoor space.
West Wall	0.4	0.04	0.016	The volume behind the surface conditioned as outdoor space. Radiant wall panels are applied on this wall.
East Wall	0.8	0.04	0.032	The Surface is unheated. The volume behind the surface conditioned as indoor space.
South Wall	0.8	0.04	0.032	The Surface is unheated. The volume behind the surface conditioned as indoor space.

3.2 Hydraulic circuit and radiant panels

The temperature of the water filled in the radiant panels depends on the heating season for varying climatic circumstances. For each case study, a water conditioning system was used in the test room to circulate the water in all panels. The hydraulic system was amplified to the test system to provide proper inlet water temperature and flow rate to the radiant panels. As it can be seen in Fig.12, the hydraulic line is supplied with; a storage tank that heats the water to required temperature by an electric heater, a four-way valve used to mix the supply and return lines, a three-way valve used to keep the demanded mass-flow rate, an ultrasonic flow meter to evaluate the mass- flow rate and to provide input to the flow control system.

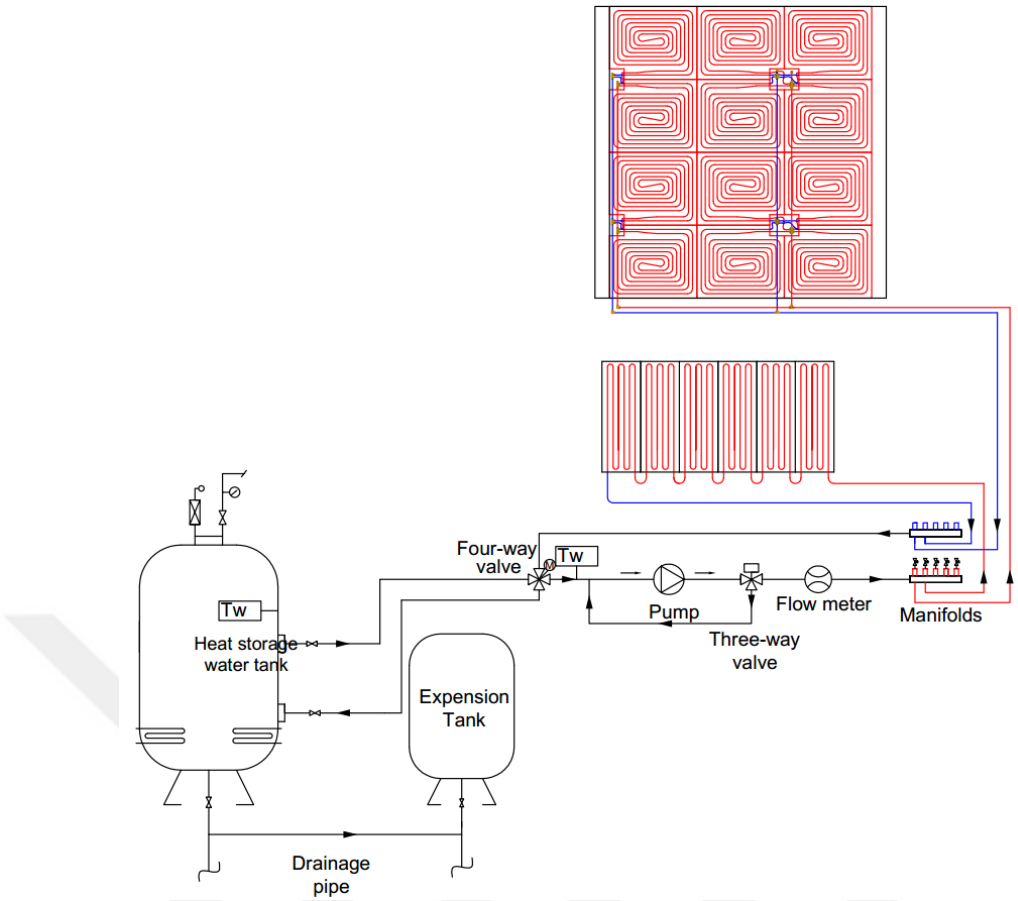

Figure 12: Hydraulic System.

As it can be seen in Fig. 12, the inlet water, which accesses the system through the tank primarily comes to a four-way valve. Here, the valve mixes it with the return pipeline. The mixture water temperature exits the four-way valve being equal to the water inlet temperature and enters the pump to supply the necessary pressure. After the pump, the water comes to a three-way valve. The purpose of the three-way valve is to return surplus of the fluid back to be equal to secure the flow rate when the water which comes from the pump has a higher flow rate than required. Then, the fluid passes through the flow meter, where the volumetric flow rate was calculated. The data for the flow rate control is delivered from electromagnetic flow meter. Following, the water goes to manifolds and then the panel facility to activate the heat transfer mechanism. After finishing the cycle in

the panels, the water comes to the four-way valve again through the return line and it is blended with the water that comes from the tank in case it is necessary (to alter the required temperature of the fluid).

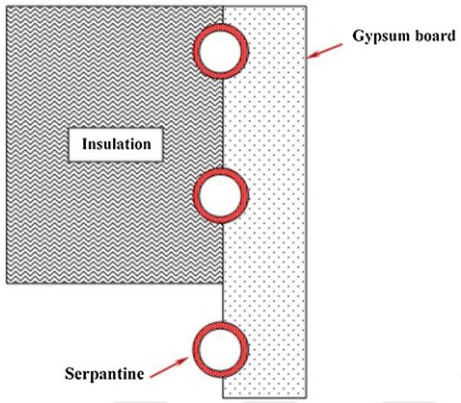

Figure 13: Radiant panel details.

Radiant wall/ceiling panels are made of three layers: drywall, heating pipe and insulation; from inner to outer layers. The thickness of the drywall layer is 15 mm while the insulation panel's thickness is 30 mm. The plastic pipes (PEX) has a 10.1 mm external diameter and 55 mm of modulation. Expanded polystyrene (EPS) is used as an insulation material which has a coefficient of thermal transmittance value of 0.035 W/mK (at 10˚C). The material properties were taken from the previous work done in the same test chamber [57].

Table 8: Components of radiant panel.

Specification	
Radiant Ceiling Panel	1 m × 1.2 m, 12 panels
Radiant Wall Panel	0.6 m × 2 m, 5 panels
Pipe	Polyethylene pipes, inside diameter: 9 mm outer diameter: 10.1 mm Modulation: 55 mm
Insulation	Expanded polystyrene (EPS), 20 mm
Surface material	Gypsum board, 15 mm

3.3 The Measurement Equipment

Basic working principle of the test chamber was already explained above. The given water mass-flow rate was 0.04 kg/s for each case. The measurements were done by following the EN 14240 [61] under stable conditions. In order to alter the temperature of the outer volumes to simulate a winter day conditions, the zones were adjusted at designated temperatures until desired temperature ranges (±0.5 °C) were guaranteed. The water conditioning system was turned-on to provide heat to the radiant panels for each heating case and the steady-state initial and boundary conditions were acquired before collecting the measurement data. Based on the studied cases and the boundary conditions, steady-state requirements were reached within 5–6 h in terms of stability of supply water temperature and water flow rates, surface temperature of the panels and unheated surfaces. Before performing the heat transfer measurements, conditioned water was provided to the radiant system to keep the radiant surfaces at the chosen temperature, while the unheated surface temperatures and the air temperature of interior were varied subject to the heat output of the panels.

During the tests, inlet-outlet water temperatures (T_w) were measured. T_{op} was used which was acquired experimentally directly by the thermal comfort device. The operative temperature was determined according to ASHRAE 55 [7] which is the weighted average value between the mean radiant temperature and the dry-bulb air temperature. Air temperature transducer (T_a) was located at the middle of the test volume. Moreover, air temperatures of indoor and enclosed zones, surface temperatures of and unheated surfaces, mass-flow rate of water, supply and return water temperatures were evaluated, controlled and accumulated for each measuring time-interval (1 min). Time span of the experiments was determined as around 16 h

so that all important variables achieved and steady-state conditions, to store adequate data as well. Outcomes associated to standard values were measured during the periods of 30 minutes in which stable conditions were guaranteed. Tests were performed by the alteration of radiant surface temperatures according to inlet water temperatures for radiant heating (wall/ceiling). As the heated surface and indoor air temperatures became stable within the band of 0.1 K/min, evaluations were started.

The mass-flow rate of the provided water was approximated using the ultrasonic flow meter with the uncertainty of ±1%. T_o monitor and preciously control the water temperature in the line, additional water temperature sensors were positioned at the buffer tank. The control system of the test room includes two separate systems which are Data Monitoring and Control System (DMCS) for the enclosed zones and NI LabVIEW© system for the studied volume.

Table 9: Measurement Equipment

Measured Parameter		**Equipment**	**Range**	**Accuracy**
Air Temperature (°C)	T_a	K-Type Thermocouple	10-50	±0.1°C
Surface Temperature (°C)	T_s	K-Type Thermocouple	10-50	±0.1°C
Water Temperature (°C)	T_w	PT100	10-50	±0.1°C
Operative Temperature (°C)	T_{op}	Operative Temperature Sensor	10-50	±0.1°C

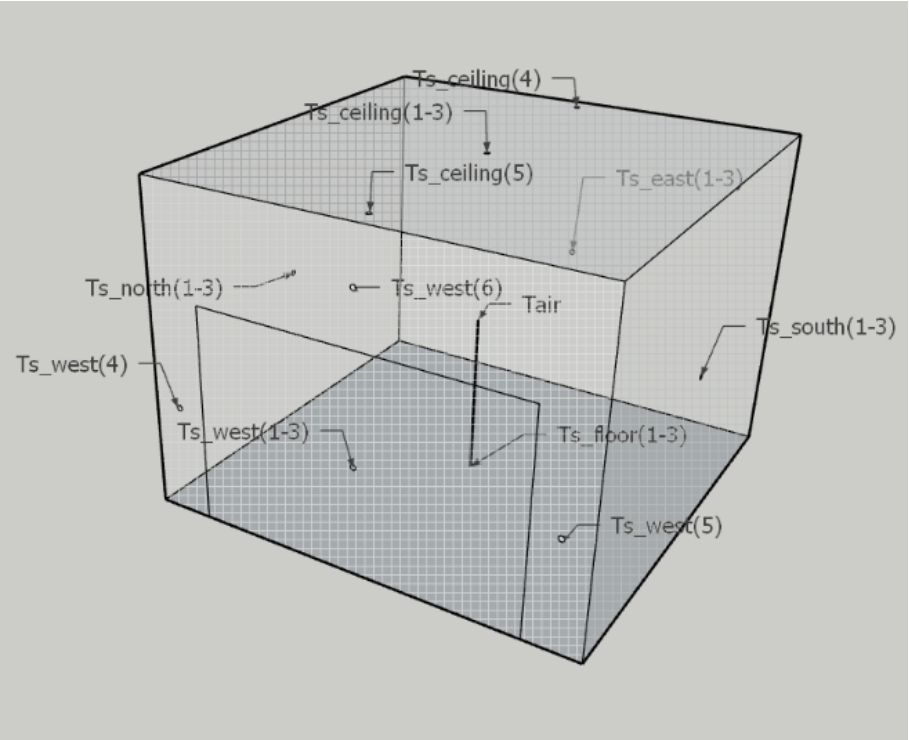

Figure 14: Arrangement of the temperature transducers in the room.

Surface temperatures were taken from the midpoint of heated or unheated surfaces with three thermocouples. The average value of the measurements is used in the calculations. Detailed arrangement of the sensors is shown in Figure 14.

4 NUMERICAL METHODOLOGY

4.1 Problem Definition

Computational Fluid Dynamics (CFD) methodology allows the analyze of various thermo-fluid and heat transfer cases of heating, cooling, ventilation and air conditioning systems and can be compared against the experimental data [62]. In this chapter, a detailed numerical methodology is explained, and validation of the test results are shown. In addition, mesh independence study is carried out.

All numerical analyses were conducted using the Academic version of ANSYS 17.1, a commercial package program. It contains special modules for different stages of the modelling process. After the three-dimensional room geometry was created in the Design Modeler module, the meshing module was applied to decomposition using the finite volume method. Numerical solutions were made in Fluent, a widely used computational fluid dynamics module. The temperature and velocity fields were visually inspected using CFD-Post software as the final processor program. The natural convection was modelled using the Boussinesq approach, and the standard k-ε model which is a common numerical solution and gives good results in the flow near the wall was picked to model turbulence. The Discrete Ordinates model was used for radiative heat transfer, although no scattering is considered numerical solution results were compared with different mesh numbers and mesh independence was observed.

4.2 Numerical Solution Method

4.2.1 Governing Equations

The behavior of fluids in a volume is defined mathematically based on the following three laws of conservation equations governed. The total mass flow through the surfaces of a very small control volume of the fluid is equal to the change in mass within that volume over time. This law is known as conservation of mass. For the same control volume; the total momentum flow across the surfaces equals the change in momentum in volume over time. This also equals to the net force applied to the volume, and it is called as the conservation of momentum. The change in the total energy of the control volume element is equal to the sum of the heat transfer amount and the work exchange on the volume element. This is the law of conservation of energy. In this study, it is assumed that the flow is three-dimensional, stable and the physical values such as flow density, viscosity and heat transfer coefficient are constant. Accordingly, the conservation equations are obtained as [63]:

The continuity equation is expressed as:

$$\frac{\partial u}{\partial x}+\frac{\partial v}{\partial y}+\frac{\partial w}{\partial z}=0 \tag{12}$$

Conservation of Momentum at *x, y, z:*

$$u\frac{\partial u}{\partial x}+v\frac{\partial u}{\partial y}+w\frac{\partial u}{\partial z}=-\frac{1}{\rho}\frac{\partial p}{\partial x}+\nu\left(\frac{\partial^2 u}{\partial x^2}+\frac{\partial^2 u}{\partial y^2}+\frac{\partial^2 u}{\partial z^2}\right) \tag{13-a}$$

$$u\frac{\partial v}{\partial x}+v\frac{\partial v}{\partial y}+w\frac{\partial v}{\partial z}=-\frac{1}{\rho}\frac{\partial p}{\partial y}+\nu\left(\frac{\partial^2 v}{\partial x^2}+\frac{\partial^2 v}{\partial y^2}+\frac{\partial^2 v}{\partial z^2}\right)-g \tag{13-b}$$

$$u\frac{\partial w}{\partial x}+v\frac{\partial w}{\partial y}+w\frac{\partial w}{\partial z}=-\frac{1}{\rho}\frac{\partial p}{\partial z}+\nu(\frac{\partial^2 w}{\partial x^2}+\frac{\partial^2 w}{\partial y^2}+\frac{\partial^2 w}{\partial z^2}) \quad (13\text{-c})$$

Conservation of Energy:

$$u\frac{\partial T}{\partial x}+v\frac{\partial T}{\partial y}+w\frac{\partial T}{\partial z}=\alpha\left(\frac{\partial^2 T}{\partial x^2}+\frac{\partial^2 T}{\partial y^2}+\frac{\partial^2 T}{\partial z^2}\right) \quad (14)$$

4.2.2 Modelling of Natural Convection

In natural convection, flow motion is affected by gravity and density. The increase of density can depend on several reasons, but the most common cause is the temperature change. The change of the pressure inside and outside of the boundary layer should be equal.

Inside the test chamber, natural convection occurs between air and panel surfaces. The *y*-pressure gradient at any point in the boundary layer due to natural convection on the panel must be equal to the pressure gradient in the stationary region outside the boundary layer. However, $v = 0$ in this region, so the Eq. 13-b becomes [64]:

$$\frac{\partial p}{\partial y}=-\rho_0 g \quad (15)$$

If the Eq. 15 is substituted in Eq. 13-b, Equation 16 which is valid for every point in the natural convection boundary layer, is obtained [64]. The first term on the right side of Eq. 16 is the buoyancy force term.

$$u\frac{\partial v}{\partial x}+v\frac{\partial v}{\partial y}+w\frac{\partial v}{\partial z}=\frac{g}{\rho}(\rho_0-\rho)+\nu(\frac{\partial^2 v}{\partial^2 x}+\frac{\partial^2 v}{\partial^2 y}+\frac{\partial^2 v}{\partial^2 z}) \quad (16)$$

4.2.2.1 The Boussinesq Model

In Eq. 15, natural convection can be modelled by taking the density constant if a relationship can be established between the density change in the term of buoyancy force and the temperature change. The Boussinesq model is constructed by taking advantage of this relational volumetric thermal expansion coefficient (β) depending on the temperature and density [64]:

$$\beta = -\frac{1}{\rho}(\frac{\partial \rho}{\partial T})_P \tag{17}$$

In this equation, the partial derivative is converted to the difference expression by moving from a reference density and temperature point:

$$\beta \approx -\frac{1}{\rho}\frac{\Delta \rho}{\Delta T} = -\frac{1}{\rho}\frac{\rho_0 - \rho}{T_0 - T} \tag{18}$$

Here the density difference in equation 15 is converted to the temperature difference:

$$\rho_0 - \rho \approx \rho\beta(T - T_0) \tag{19}$$

The equation 15, which is based on the Boussinesq approach, follows [64]:

$$u\frac{\partial v}{\partial x} + v\frac{\partial v}{\partial y} + w\frac{\partial v}{\partial z} = g\beta(T - T_0) + \nu(\frac{\partial^2 v}{\partial^2 x} + \frac{\partial^2 v}{\partial^2 y} + \frac{\partial^2 v}{\partial^2 z}) \tag{20}$$

Using the Boussinesq model, faster convergence can be achieved in the numerical solution since the density is fixed. This approach can be used as long as the variations in air density and temperature are small such as: $\beta\ (T\text{-}T_0) < 1$. The parameters have to be defined for Boussinesq model during the numerical analysis are as follows:

- T_0, operating temperature
- ρ_0, constant density values that correspond to the T_0
- β, volumetric thermal expansion coefficient

By making ideal gas acceptance, the thermal expansion coefficient can be calculated from the following equation:

$$\beta = -\frac{1}{\rho}\left(\frac{\partial \rho}{\partial T}\right)_p = \frac{1}{\rho}\frac{p}{RT^2} = \frac{1}{T} \tag{21}$$

Here, the constant temperature T_0 is taken as the T temperature.

4.2.2.2 Natural Convection

The flow regime for natural convection is determined by Grashof number. The Grashof number takes on the role of Reynolds number in forced convection in natural convection. The Reynolds number indicates the ratio of inertial forces acting on a fluid particle to the frictional forces. In contrast, the Grashof number is an indication of the ratio of the buoyancy forces acting on the fluid to the frictional forces [64]:

$$Gr_L = \frac{g\beta(T_s - T_\infty)L^3}{\nu^2} \tag{22}$$

The Prandtl number is the ratio of the frictional forces to the thermal forces:

$$Pr = \frac{\nu}{\alpha} \tag{23}$$

The transition region in a natural convection boundary layer depends on the relative magnitude of the lift and friction forces in the fluid. This is usually expressed in Rayleigh number. The Rayleigh number is equal to Grashof and Prandtl numbers. The critical Rayleigh number for vertical plates is 10^9, whereas

for horizontal plates it is 10^7. Above and below these values the flow is laminar or turbulent [64]:

$$Ra_{x,c} = Gr_{x,c}\, Pr = \frac{g\beta(T_s - T_\infty)x^3}{\nu\alpha} \approx 10^9 \text{ for vertical plates} \quad (24\text{-a})$$

$$Ra_{x,c} = Gr_{x,c}\, Pr = \frac{g\beta(T_s - T_\infty)x^3}{\nu\alpha} \approx 10^7 \text{ for horizontal plates} \quad (24\text{-b})$$

4.2.3 Modelling of Turbulence

The characteristic feature of turbulent flow is that the velocity field is fluctuating. This character plays an important role in the efficient transport of quantities such as momentum and energy. Because these fluctuations can be small-scale and high-frequency, the numerical modelling of the flows in this feature requires high processing capacity. Therefore, to require less processing capacity, the conservation equations are written in terms of instantaneous variables which can be time-averaged or modelled in small-scale structures [65]. However, these equations modified for turbulent flow do not form a closed system of equations. The addition of a turbulent flow requires additional variables to enter the equations, so that the number of unknown variables becomes greater than the number of equations. For this reason, turbulence models have been developed. Even though turbulence may play a small role in natural convection, it is considered here for the sake of completeness.

Some of common turbulence models are listed below [65]:

- Spalart-Allmaras model
- *k*-ε models
    - Standart *k*-ε model
    - Renormalization-group (RNG) *k*-ε model

    - Realizable k-ε model
- k-ω models
    - Standart k- ω model
    - Shear-stress transport (SST) k- ω model
- Reynolds stress model (RSM)
    - Linear pressure-strain RSM model
    - Quadratic pressure-strain RSM model
    - Low-Re stress-omega RSM model
- Detached eddy simulation (DES) model
- Large eddy simulation (LES) model

In this thesis, the turbulence is modelled with the k-ε model that is one of the two-equation models in which the solution of two separate transport equations allows the turbulent velocity and length scales to be independently determined. The standard k-ε model in ANSYS FLUENT falls within this class of models and has become the workhorse of practical engineering flow calculations in the time since it was proposed by Launder and Spalding [66]. Robustness, economy, and reasonable accuracy for a wide range of turbulent flows explain its popularity in industrial flow and heat transfer simulations. It is a semi-empirical model, and the derivation of the model equations relies on phenomenological considerations and empiricism.

The standard k-ε model [66] is a semi-empirical model based on model transport equations for the turbulence kinetic energy (k) and its dissipation rate (ε). The model transport equation for k is derived from the exact equation, while the model transport equation for ε was obtained using physical reasoning and bears little resemblance to its mathematically exact counterpart.

In the derivation of the *k*-*ε* model, the assumption is that the flow is fully turbulent, and the effects of molecular viscosity are negligible. The standard *k*-*ε* model is therefore valid only for fully turbulent flows. The turbulence kinetic energy, *k*, and its rate of dissipation, *ε*, are obtained from the following transport equations [65]:

$$\frac{\partial}{\partial t}(\rho k)+\frac{\partial}{\partial x_i}(\rho k u_i)=\frac{\partial}{\partial x_j}\left[\left(\mu+\frac{\mu_t}{\sigma_k}\right)\frac{\partial k}{\partial x_j}\right]+G_k+G_b-\rho\varepsilon-Y_M \qquad (25\text{-a})$$

$$\frac{\partial}{\partial t}(\rho \varepsilon)+\frac{\partial}{\partial x_i}(\rho \varepsilon u_i)=\frac{\partial}{\partial x_j}\left[\left(\mu+\frac{\mu_t}{\sigma_\varepsilon}\right)\frac{\partial \varepsilon}{\partial x_j}\right]+C_{1\varepsilon}\frac{\varepsilon}{k}(G_k+C_{3\varepsilon}G_b)-C_{2\varepsilon}\rho\frac{\varepsilon^2}{k} \qquad (25\text{-b})$$

In these equations G_k represents the generation of turbulence kinetic energy due to the mean velocity gradients, G_b is the generation of turbulence kinetic energy due to buoyancy, Y_M represents the contribution of the fluctuating dilatation in compressible turbulence to the overall dissipation rate, $C_{1\varepsilon}$, $C_{2\varepsilon}$, $C_{3\varepsilon}$ are constants, σ_k and σ_ε are the turbulent Prandtl numbers for *k* and *ε*, respectively.

The turbulent (or Eddy) viscosity μ_t is computed by combining *k* and *ε* as follows:

$$\mu_t=\rho C_\mu\frac{k^2}{\varepsilon} \qquad (26)$$

where C_μ is a constant. The model constants and $C_{1\varepsilon}$, $C_{2\varepsilon}$, C_μ, σ_k and σ_ε have the following values [65] $C_{1\varepsilon}=1.44$, $C_{2\varepsilon}=1.92$, $C_\mu=0.09$, $\sigma_k=1.0$, $\sigma_\varepsilon=1.3$ These default values have been determined from experiments with air and water for fundamental turbulent shear flows including homogeneous shear flows and decaying isotropic grid turbulence. They have been found to work well for a wide range of wall-bounded and free shear flows.

We note that for the majority; if cases studied in this thesis, turbulence makes very small input. These equations are added only for the sake of complete analyses.

4.2.4 Modelling of Radiation

The effect of radiation must be considered in a room conditioned by radiative heaters. When radiant heating systems applied in a space, the heat transfer ratio via radiation becomes equal to %50 or greater.

Below, governing equations for radiative transfer in absorption, scattering and medium is given. Note that in the system considered there are no scattering particles; therefore, scattering is not accounted for. Nevertheless, we provide a detailed analysis first, which is simplified subsequently. The net heat flow through the radiation is obtained by solving an integro-differential equation called the Radiative Transfer Equation (RTE). RTE refers to the variation along the path of the intensity of spectral radiation in an environment [65]. The radiative transfer equation (RTE) for an absorbing, emitting, and scattering medium at position $\vec{r}$ in the direction $\vec{s}$ is:

$$\frac{dI\left(\vec{r},\vec{s}\right)}{ds} + \underbrace{(a+\sigma_s)I(\vec{r},\vec{s})}_{Absorbing} = \underbrace{an^2\frac{\sigma T^4}{\pi}}_{Emitting} + \underbrace{\frac{\sigma_s}{4\pi}\int_{4\pi} I(\vec{r},\vec{s}')\Phi(\vec{s}',\vec{s})d\Omega}_{Scattering} \quad (27)$$

Here, $\vec{r}$ is the position vector, $\vec{s}$ is the direction vector, $\vec{s'}$ is the propagation direction vector, s is the path taken, a is the absorption coefficient, n is the refractive index, σ_s is the propagation coefficient, σ is the Stefan-Boltzmann constant, T is the temperature, Φ is the phase function, and Ω is the solid angle [67].

Since no scattering is present we can use a simplified discrete ordinates (DO) radiation model, which is reduced to discrete transfer radiative model. In this study DO model is used in ANSYS Fluent.

4.2.4.1 Discrete Ordinates Method:

The discrete ordinates (DO) radiation model solves the radiant heat transfer equation for discrete solid particle angles in finite number, each related to the $\vec{s}$ vector direction specified in the global cartesian system. The DO model transforms the RTE into a transport equation written for radiation intensity and solves this equation for all directions. This model incorporates scattering, semi-transparent media, reflecting surfaces and dependence on wavelength, and is a conservative method that can provide heat balance for coarse splitting. In addition to this, sensitivity can be increased by fine discretization [65].

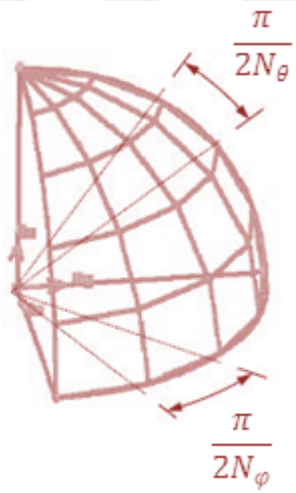

Figure 15: Discretization of angular space [65].

Angular discretization is controlled by the parameters Theta Division (N_θ) and Phi Division (N_φ). These parameters specify the number of control angles used to separate each 1/8 of the angular space that is shown in Fig. 15. Each discrete ordinate is in the same direction as the radiation in a solid angle. The angles θ and φ are the polar and azimuthal angles respectively. These angles are measured with respect to the global cartesian system (x,y,z) and is presented in Figure 1. Azimuth angle is $0 < \varphi < 2\pi$ and the polar angle is $0 < \theta < \pi / 2$.

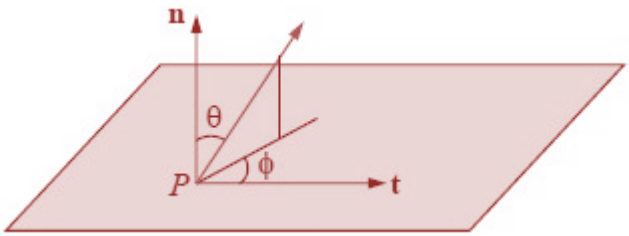

Figure 16: Presentation of φ and θ angles on coordinate system [65].

The Discrete Ordinate radiation model can solve the problem of fluid or solid media on both sides of non-transparent walls. Some of the radiation energy that comes to the non-transparent wall surface is reflected to the surrounding wall, and some of it is absorbed by the wall, and this energy balance can be expressed as [65]:

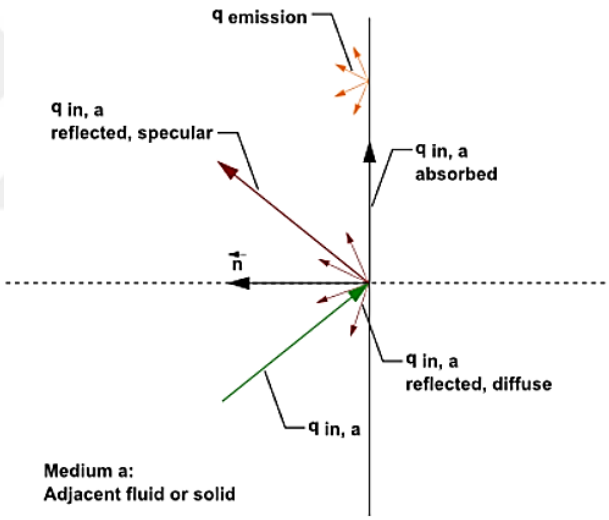

Figure 17: Schematic of radiation on an opaque wall in ANSYS Fluent [65].

The schematic in Figure 17 shows incident radiation $q_{in,a}$ on side "a" of an opaque wall. Some of the radiant energy is reflected diffusely and specularly, depending on the diffuse fraction f_d for side "a" of the wall that you specify as a boundary condition. Some of the incident radiation is absorbed at the surface of the wall and some radiation is emitted from the wall surface. The amount of incident radiation absorbed at

the wall surface and the amount emitted back depends on the emissivity of that surface and the diffuse fraction. Radiation is not transmitted through an opaque wall [65].

Radiant incident energy that impacts an opaque wall can be reflected to the surrounding medium and absorbed by the wall. The radiation that is reflected can be diffusely reflected and/or specularly reflected, depending on the diffuse fraction f_d. If q_{in} is the amount of radiative energy incident on the opaque wall, then the following general quantities are computed by ANSYS Fluent for opaque walls [65]:

Emission from the wall surface $$q_{emission} = n^2 \varepsilon_w \sigma T_w^4 \quad (28\text{-a})$$

Diffusely reflected energy $$q_{absorbed} = f_d (1-\varepsilon_w) q_{in} \quad (28\text{-b})$$

Specularly reflected energy $$q_{diffusely,reflected} = (1-f_d)(1-\varepsilon_w) q_{in} \quad (28\text{-c})$$

Absorption at the wall surface $$q_{specularly,reflected} = \varepsilon_w q_{in} \quad (28\text{-d})$$

Where f_d is the diffuse fraction, n is the refractive index of the adjacent medium, ε_w is the wall emissivity, σ is the Stefan-Boltzmann Constant, and T_w is the wall temperature.

4.2.4.2 Validation of Discrete Ordinates Method:

In this part, the discrete ordinates model, which is used to model radiation in numerical solutions, and the analytical calculation method are compared on a simple example problem. Here, a simple cube-shaped room with a heating surface of at a high temperature was considered. The radiation heat transfer amount from the heating surface to other cold surfaces was taken into consideration.

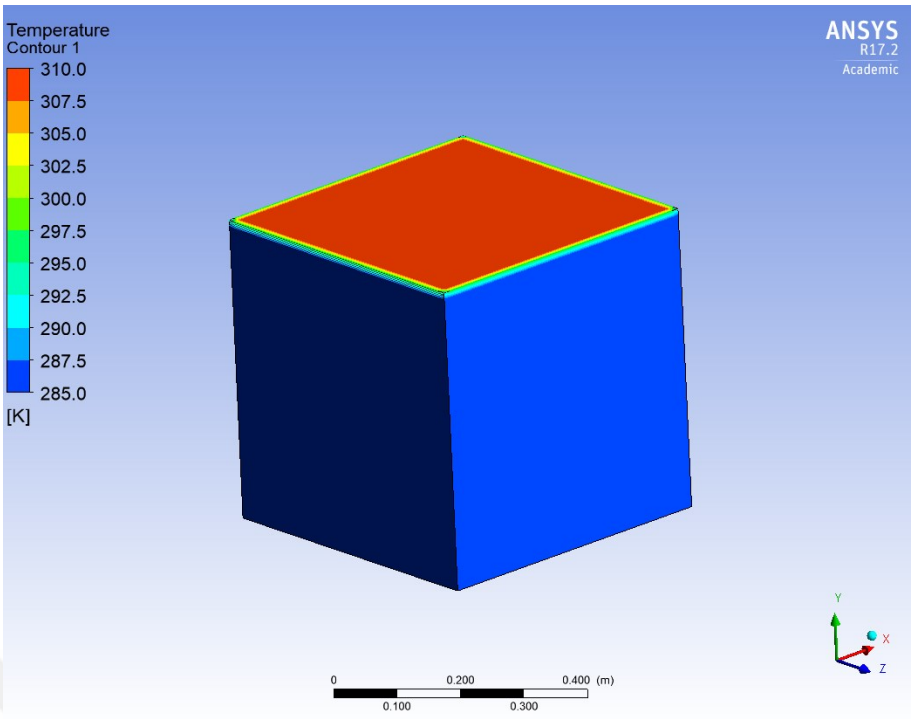

Figure 18: Minimized room model.

The analytical calculations were made for the room shown in Figure 19 with dimensions of 0.5m x 0.5m x 0.5m. The wall surface material was taken as gypsum and the hot surface was accepted at 310 *K* and the cold surfaces at 285 *K* temperature. Since the room is a closed volume, the net heat transfer with cold surface radiation from the hot surface is calculated by Equation 29 [64].

$$q_{rad} = \frac{E_{b1} - E_{b2}}{\frac{1-\varepsilon_1}{A_1\varepsilon_1} + \frac{1}{A_1 F_{12}} + \frac{1-\varepsilon_2}{A_2\varepsilon_2}} \tag{29}$$

Here, the emissivity values of wall surfaces are determined as $\varepsilon_1 = \varepsilon_2 = 0.85$. If the temperatures of the cold surfaces are equal, the shape factor is $F_{1,2} = 1$. The hot surface area $A_1 = 0.25$ m^2 and the sum of the cold surface areas $A_2 = 1.25$ m^2. E_b, radiation power of the surface is calculated by Equation 30.

$$E_b = \sigma T^4 \tag{30}$$

Total resistance in the thermal circuit is calculated as follows:

$$\sum R_t = \frac{1\text{-}0.8}{0.25 \cdot 0.8} + \frac{1}{0.25 \cdot 1} + \frac{1\text{-}0.8}{1.25 \cdot 0.8} = 5.2\ m^2 \cdot K/W$$

Heat transfer amount from heating surface to cold surfaces found with the analytical calculations:

$$q_{rad} = \frac{5.67 \cdot 10^{-8} \cdot (310^4 - 285^4)}{5.2} = 28.76\ W$$

For the comparison of analytical and numerical results. Minimized room geometry is modelled in ANSYS Fluent Software and the same boundary conditions were defined. As mentioned above discrete ordinates model was selected as the radiation model.

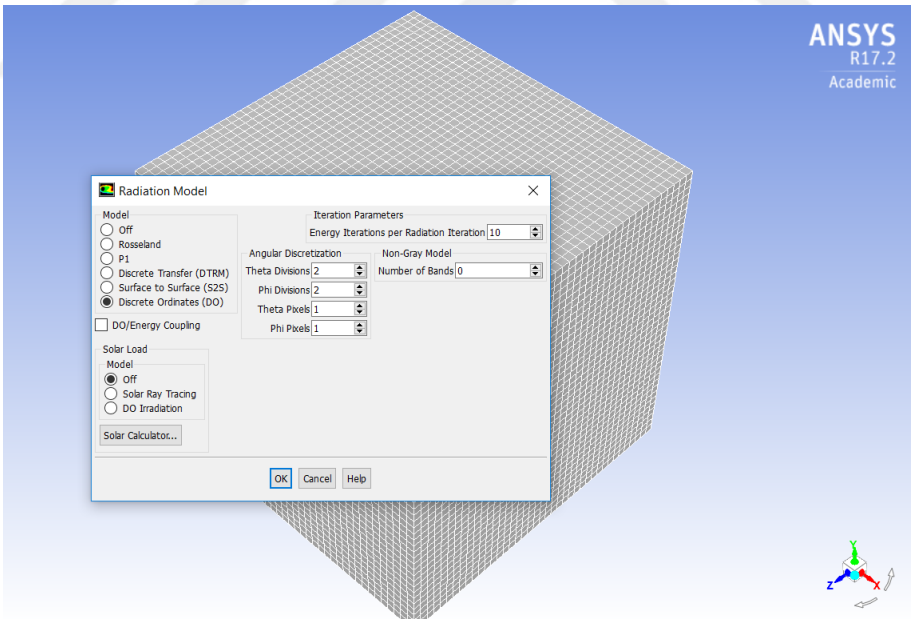

Figure 19: Parameters of DO radiation model.

The angular separation parameters Theta Divisions (N_θ) and Phi Divisions (N_φ) were selected as default values that are acceptable values for many engineering problems [65] shown in Figure 20.

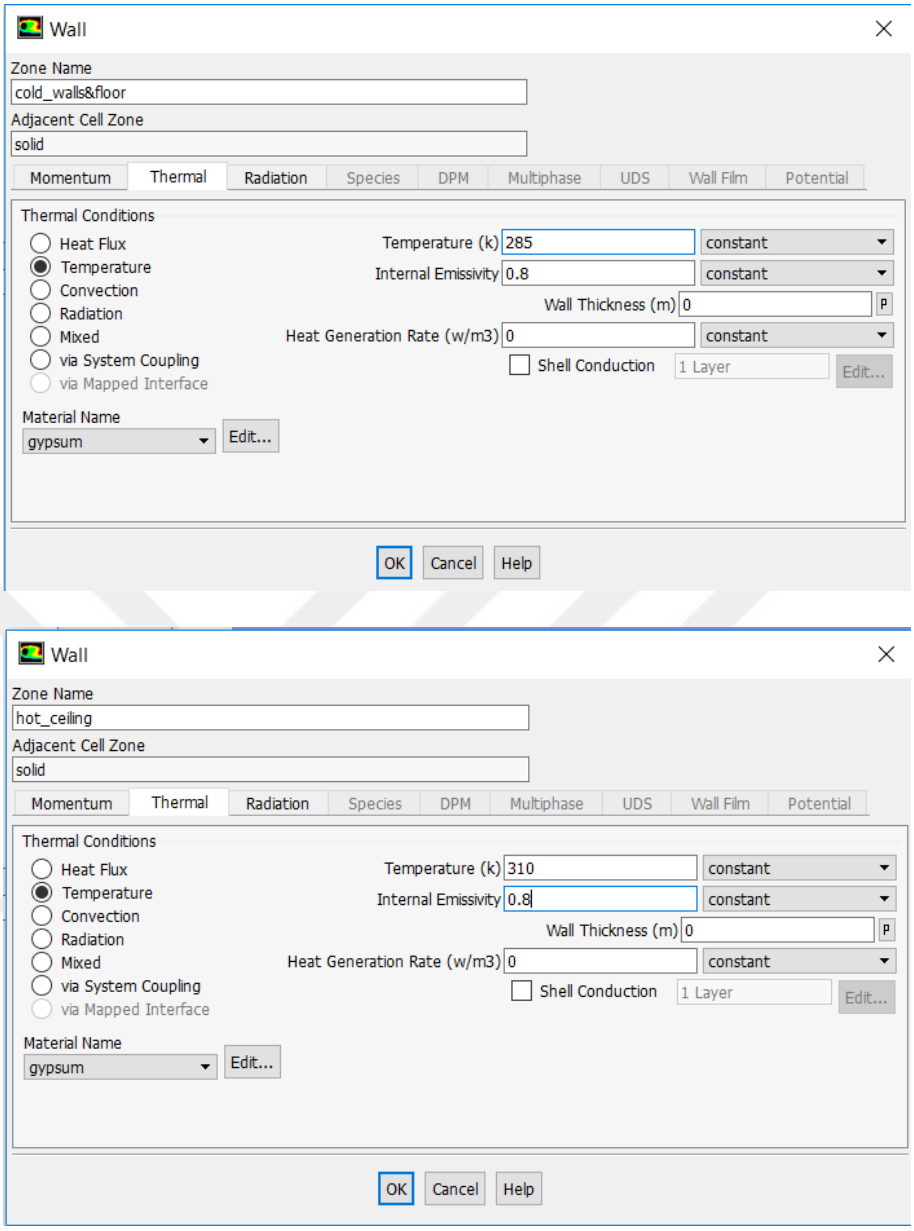

Figure 20: Wall boundary conditions.

Figure 21 shows the temperature and emissivity values of the wall surfaces defined as the boundary condition in the program. Walls are provided with a constant surface temperature boundary condition.

The amount of heat transfer with radiation in the numerical analysis results was found to be 28.41 W. Numerical solution and analytical solution have less than 1%

difference between them. Since this difference is quite small, the decision to use DO model is validated.

4.3 Modelling of Test Chamber

All numerical work has been done by using the academic edition of ANSYS Fluent 17.2. Numerical modelling steps are given in Figure 23.

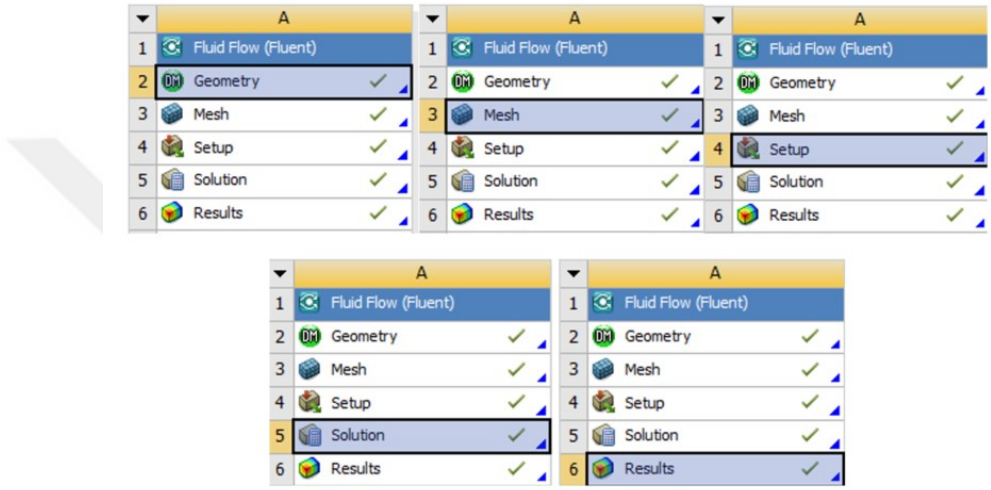

Figure 21: Numerical Study Solution Schematic.

4.3.1 Geometry

First, Design Modeller is used as the design tool of the software and it is used to create geometry of test chamber. The test volume is modelled by a floor area of 16 m2 (4.00 m × 4.00 m) and an internal height of 3.00 m. Modelled geometry is shown in Figure 22.

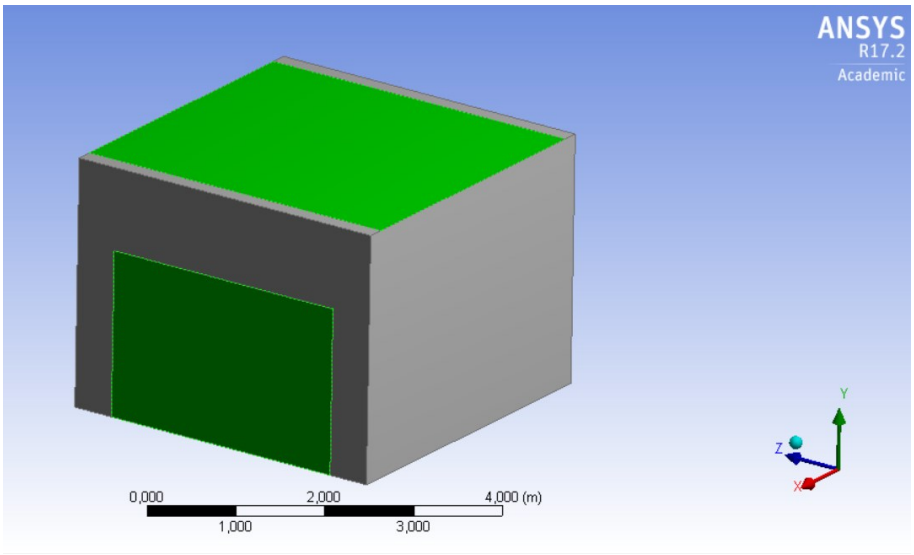

Figure 22: 3D Model of Test Chamber.

4.3.2 Mesh

In the meshing module, discretization was performed using the finite volume method. Numerical solutions were made in Fluent, a widely used computational fluid dynamics software. The temperature and velocity fields were visually inspected using CFD-Post software as a final step.

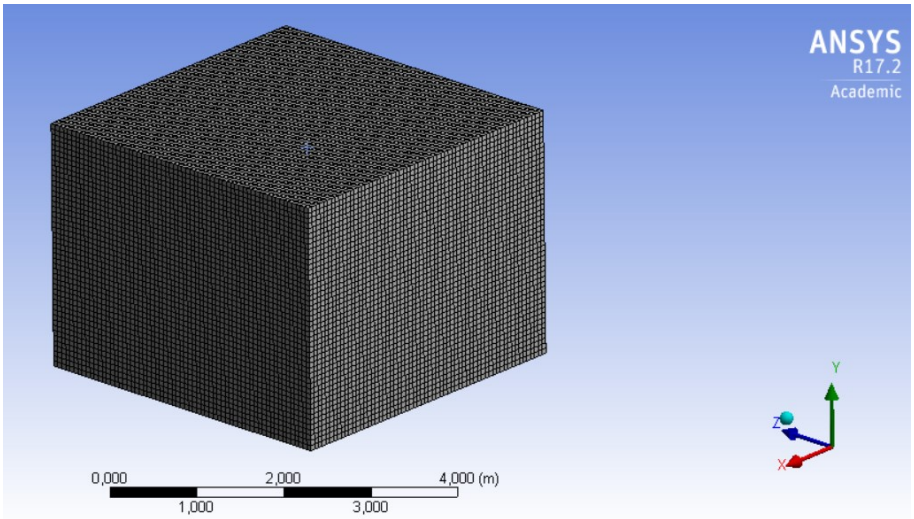

Figure 23: Numerical Solution Grid- Meshing.

The room volume is divided into 183582 elements. The minimum and maximum skewness of the elements is 0.000048896 and 0.19872 (Figure 23).

Statistics	
Nodes	193536
Elements	183582
Mesh Metric	Skewness
Min	4,8896e-005
Max	0,19872
Average	2,7172e-003
Standard Deviation	1,4525e-002

Statistics	
Nodes	193536
Elements	183582
Mesh Metric	Orthogonal Quality
Min	0,94716
Max	1,
Average	0,99965
Standard Deviation	2,8233e-003

Figure 24: Meshing Statistics

It can be seen in Figure 25 that the entire solution network consists of six-prism elements. This is an indication of the smoothness of the solution grid.

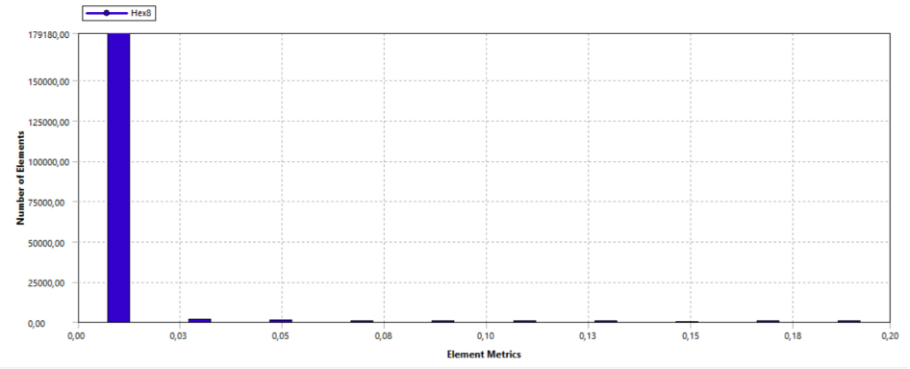

Figure 25: Element Metrics.

Mesh statistics is important to understand the mesh quality. A quick and easy inspection can be done via checking the minimum orthogonal quality statistics that should be greater than 0.1 (Figure 26) and maximum skewness that should be less than 0.95 (Figure 27).

Excellent	Very good	Good	Acceptable	Bad	Unacceptable
0-0.25	0.25-0.50	0.50-0.80	0.80-0.94	0.95-0.97	0.98-1.00

Figure 26: Skewness mesh metrics spectrum [68].

Unacceptable	Bad	Acceptable	Good	Very good	Excellent
0-0.001	0.001-0.14	0.15-0.20	0.20-0.69	0.70-0.95	0.95-1.00

Figure 27: Orthogonal quality mesh metrics spectrum [68].

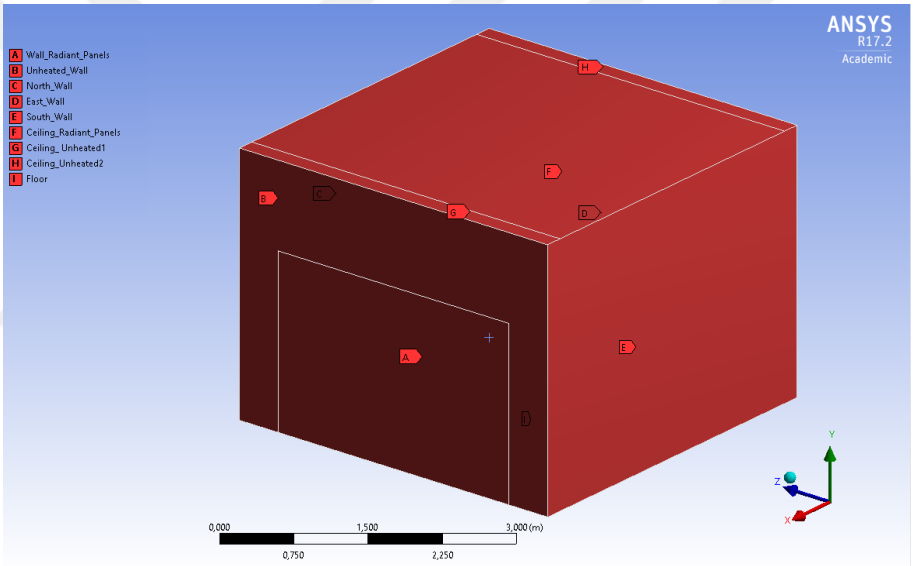

Figure 28: Named Selections.

4.3.3 Boundary Conditions and Solution Methods

Pressure-based model was chosen as solver type in solver settings. All of the analyses were carried out in consideration of the steady state. Natural convection in analysis is performed in the room model, gravity is defined as -9.81 m/s^2 in *y* direction.

The energy model has been activated, because the heat transfer among the surfaces occurs via radiation and convection. The radiation model has been

activated. The discrete ordinates (DO) model was chosen as the radiation model. *k-ε* model is chosen for the modelling of turbulence.

Multi-climate test chamber has different volumes that simulate climatic conditions. It was described in the first chapters. Boundary conditions of numerical model are defined according to the experimental work. Multi-climate test chamber was set to a winter day conditions. Test volume has surrounded with façade room that simulates the outside conditions of a winter day. The air temperature of façade room has been set to -3°C and %80 of relative humidity. Interior volume that simulates the internal partition inside a house and air temperature is set to 20°C. The floor volume is also set to an internal condition assumed that the space is occupied, and air temperature is set to 20°C. The ceiling volume was set to simulate outside conditions that has -3°C of air temperature.

Heating surface is set to a constant temperature of 303.2 K according to the experimental study. At first, the heating case was chosen as wall heating configuration to validate the simulation model. The air properties are shown in Table 10.

The Solution method has been selected as the SIMPLE. The SIMPLE scheme is the default method, and many are used to solve industrial problems [65]. As a discretization method Second Order Upwind and Body Force Weighted methods have been selected. Body Force Weighted method gives more accurate results for both natural convection and axisymmetric swirl flows [65].

Table 10: Properties of air at 293.15 K.

Density (kg/m3)	1.225
Specific Heat Cp (J/kgK)	1006.43
Thermal Conductivity (W/mK)	0.0242
Viscosity (kg/ms)	0.01789
Thermal Expansion Coefficient (1/K)	0.003367

4.3.4 Validation of Numerical Model

The average temperature values of the experimental measurements made from the surfaces were used in the numerical model. The test chamber was kept conditioned for the time of 6 hours before the measurements for achieving thermal stability. It was confirmed that it became stable, and then the measurements were done for 20 minutes. The steady-state condition of the system has increased the reliability of the measured values and reduced the standard deviation of the measurements. The standard deviation of the experimental results was found to ±0.3 °C.

When the experimental data were compared with the average surface temperature values obtained from the numerical model in which the experimental conditions were modeled, the discrepancy of the data was found to be less than 10%. It is possible to say that the numerical model made for this reason has been confirmed by experimental data. The validation of numerical model was done for both wall heating and ceiling heating cases. Each of them was validated.

4.3.4.1 Wall Heating Case

Numerical model was developed according to the boundary conditions shown in Table 13. that was taken from the experimental study for wall heating scenario.

Table 11: Boundary Conditions for Wall Heating Case, Standard Deviation is equal to ±0.3°C.

Surfaces	Boundary Conditions			
	k (W/mK)	Wall Thickness (m)	Temperature (K)	Emmissivity
Ceiling_Radiant_Panels	0.024	0.08	270.6 ±0.3	0.9
Ceiling_Unheated 1-2	0.024	0.08	270.6 ±0.3	0.9
Floor	0.024	0.04	292.9 ±0.3	0.9
North Wall	0.052	0.13	270.6 ±0.3	0.9
Wall_Radiant_Panels	0	0	303.2 ±0.3	0.8
Unheated_Wall	0.04	0.016	270.6 ±0.3	0.9
East Wall	0.032	0.04	293.1 ±0.3	0.9
South Wall	0.032	0.04	293.1 ±0.3	0.9

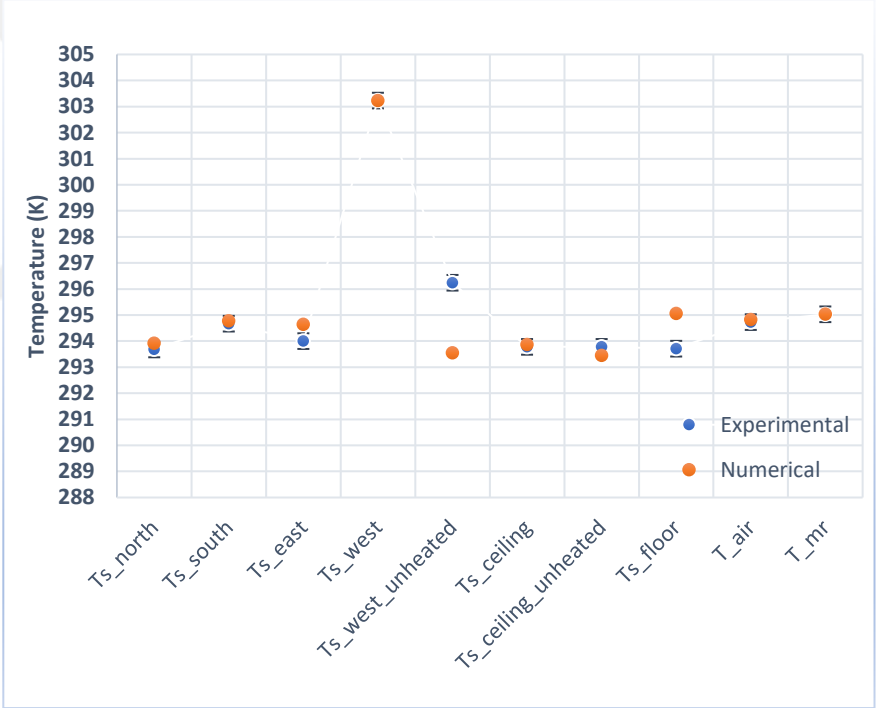

Figure 29: Experimental-Numerical Results, Standard Deviation is equal to ±0.3°C.

Validation of numerical model was successful. The data comparisons are shown in Figure 29 and Table 11.

Table 12: Experimental/Numerical Results, Standard Deviation is equal to ±0.3°C.

T_Surfaces	Experimental (K)	Numerical (K)
Ts_north	293.7 ±0.3	293.9
Ts_south	294.7 ±0.3	294.8
Ts_east	294.0 ±0.3	294.6
Ts_west	303.2 ±0.3	303.2
Ts_west_unheated	296.2 ±0.3	293.6
Ts_ceiling	293.8 ±0.3	293.9
Ts_ceiling_unheated	293.8 ±0.3	293.5
Ts_floor	293.7 ±0.3	295.1
T_air	294.7 ±0.3	294.8
T_mr	295.0 ±0.3	295.0

4.3.4.2 Ceiling Heating Case

Numerical model was developed according to the boundary conditions shown in Table 13. that was taken from the experimental study for ceiling heating scenario.

Table 13: Boundary Conditions for Ceiling Heating Case, Standard Deviation is equal to ±0.3 C

Surfaces	Boundary Conditions			
	k (W/mK)	Wall Thickness (m)	Temperature (K)	Emmissivity
Ceiling_Radiant_Panels	0	0	295.2 ±0.3	0.8
Ceiling_Unheated 1-2	0.024	0.08	270.6 ±0.3	0.9
Floor	0.024	0.04	292.9 ±0.3	0.9
North Wall	0.052	0.13	270.6 ±0.3	0.9
Wall_Radiant_Panels	0.04	0.016	270.6 ±0.3	0.8
Unheated_Wall	0.04	0.016	270.6 ±0.3	0.9
East Wall	0.032	0.04	293.1 ±0.3	0.9
South Wall	0.032	0.04	293.1 ±0.3	0.9

Validation of numerical model for ceiling case is also successful. The comparisons are shown in Figure 30 and Table 14.

Table 14: Experimental/Numerical Results (Ceiling), Standard Deviation is equal to ±0.3°C.

	Results	
T_Surfaces	**Experimental (K)**	**Numerical (K)**
Ts_north	292.8 ±0.3	292.9
Ts_south	293.8 ±0.3	294.4
Ts_east	294.0 ±0.3	294.4
Ts_west	293.1 ±0.3	292.9
Ts_west_unheated	293.1 ±0.3	293.1
Ts_ceiling	298.2 ±0.3	298.2
Ts_ceiling_unheated	296.6 ±0.3	292.9
Ts_floor	292.1 ±0.3	294.4
T_air	293.4 ±0.3	293.7
T_mrt	294.3 ±0.3	294.6

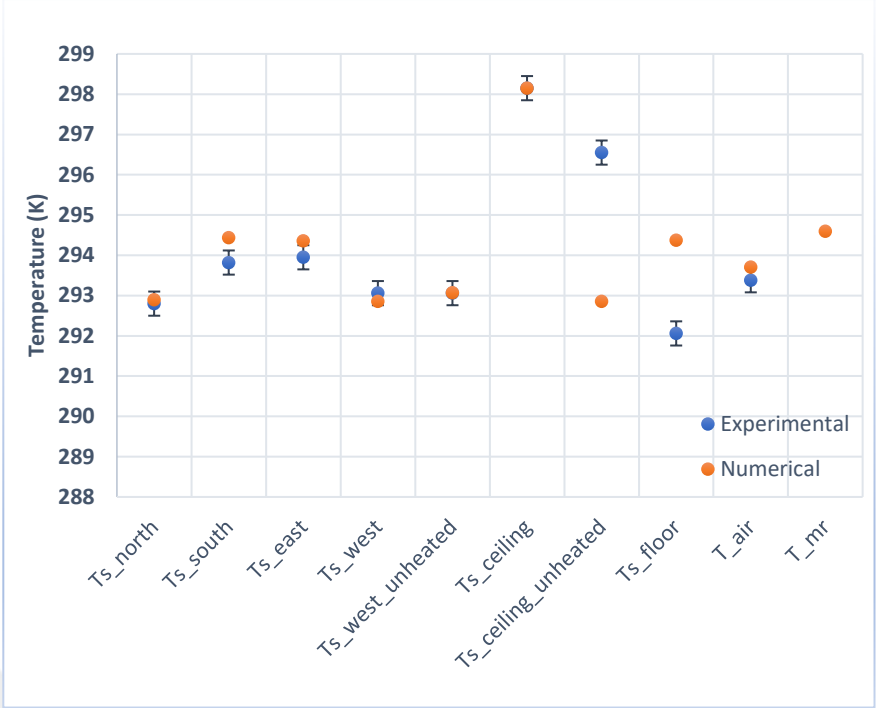

Figure 30: Experimental-Numerical Results (Ceiling), Standard Deviation is equal to ±0.3°C

4.3.4.3 Mesh Independence Test

Validated model has compared with different meshed models. The following number of elements were applied in the meshing tool of Fluent: 96900, 139707, 183582, 232356 and 384000. The mesh statistics are given below in Table 15.

Table 15: Mesh Statistics.

Mesh (-2)	**Statistics** Nodes: 103428 Elements: 96900 Mesh Metric: Skewness Min: 1,6644e-004 Max: 3,3475e-002 Average: 6,4889e-003 Standard Deviation: 5,0603e-003
Mesh (-2)	**Statistics** Nodes: 148016 Elements: 139707 Mesh Metric: Skewness Min: 4,3799e-005 Max: 3,5173e-002 Average: 3,0966e-003 Standard Deviation: 3,8476e-003
Mesh(0) Validated CFD Model	**Statistics** Nodes: 193536 Elements: 183582 Mesh Metric: Skewness Min: 4,8896e-005 Max: 0,19872 Average: 2,7172e-003 Standard Deviation: 1,4525e-002
Mesh (-2)	**Statistics** Nodes: 243984 Elements: 232356 Mesh Metric: Skewness Min: 7,2691e-005 Max: 0,29135 Average: 5,8051e-003 Standard Deviation: 2,3453e-002
Mesh (-2)	**Statistics** Nodes: 400221 Elements: 384000 Mesh Metric: Skewness Min: 1,3057e-010 Max: 1,3874e-003 Average: 1,1791e-005 Standard Deviation: 1,0483e-004

	Ts_north	Ts_south	Ts_east	Ts_west	Ts_west_unheated	Ts_ceiling	Ts_ceiling_unheated	Ts_floor	T_air	T_mr
Calibrated Model	293,9	294,8	294,6	303,2	293,6	293,9	293,5	295,1	294,8	295,0
Mesh(-1)	293,6	294,6	294,5	303,2	293,3	293,7	293,3	295,0	294,5	294,9
Mesh(-2)	293,6	294,7	294,5	303,2	293,3	293,7	293,3	295,0	294,5	294,9
Mesh(1)	293,9	294,8	294,7	303,2	293,6	294,0	293,7	295,1	294,8	295,1
Mesh(2)	294,1	295,1	294,9	303,2	293,8	294,2	293,8	295,4	295,6	295,3

Figure 31: Mesh Independency comparison.

In the results, the maximum standard deviation was obtained as ±0.8°C. The difference between the results is less than %5. The mesh tests show that the model is mesh-independent. It can be also seen in Fig. 31.

5 RESULTS AND DISCUSSION

5.1 Radiant Heating Experimental Comfort Evaluation Results

The experimental study has three different heating configurations. Since the heating application was evaluated, the multi-climate test chamber was set to a winter day conditions. Test volume has surrounded with façade room that simulates the outside conditions of a winter day. The air temperature of façade room was set to -3°C and %80 of relative humidity. Interior volume that simulates the internal partition inside a house and air temperature is set to 20°C. The floor volume was also set to an internal condition assuming that the space was occupied, and air temperature was set to 20°C. The ceiling volume was set to simulate outside conditions that has -3°C of air temperature.

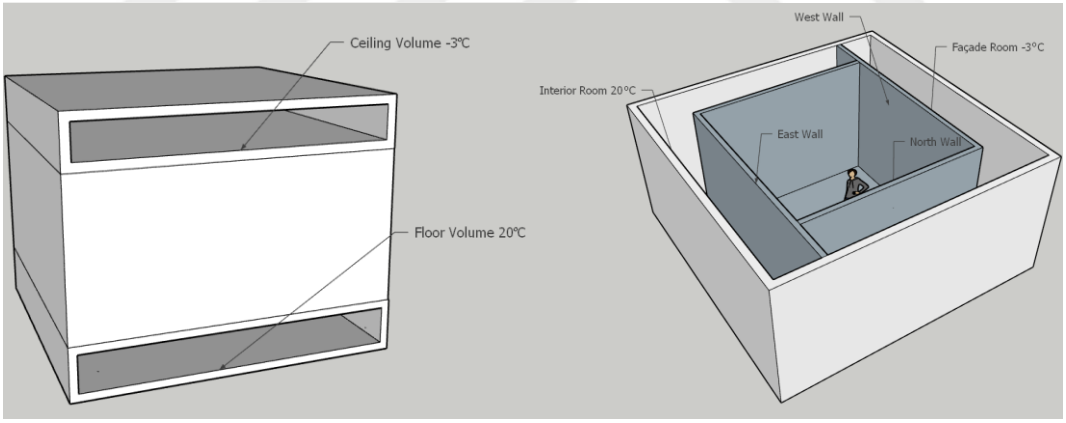

Figure 32: Boundary Conditions of Test Volume.

Boundary conditions of conditioned volumes are presented in Figure 32. The illustration of three different heating configurations is illustrated in Figure 33.

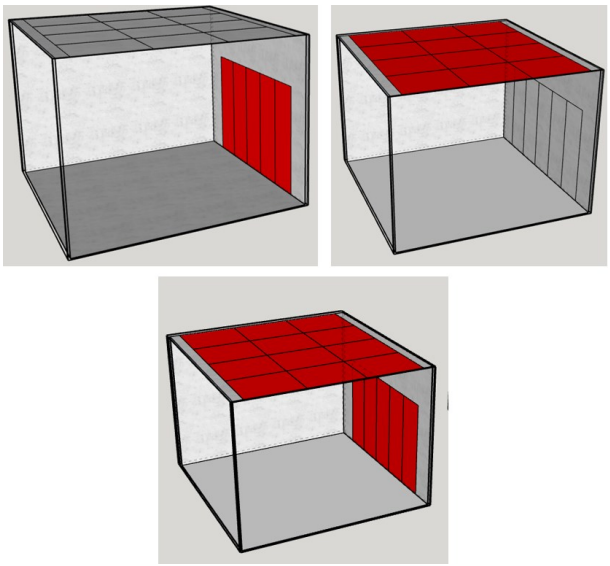

Figure 33: Experimental Study Cases: Wall Heating Case, Ceiling (12P) Heating Case, Wall and Ceiling (12P) Heating Case.

At the beginning point of the study PMV and PPV calculations were done according to the experimental results. Experimental results can be seen in Table 17. Preliminary comfort analysis was done with the parameters are shown in Table 16. The results are given in Table 18. Air velocity value was assumed to be 0.1 m/s. This thermal comfort analysis is a preliminary work to understand which cases roughly provide comfort. Later, selected cases were validated with numerical model and using numerical model, different case studies were evaluated.

Table 16: Calculation Parameters to Calculate PMV and PPD.

Parameter	**Input**
Clothing (clo)	1
Air temp. (°C)	[19.9 to 33.8 °C]
Mean radiant temp. (°C)	[20.1 to 30.5 °C]
Activity (met)	1.2
Air speed (m/s)	0.1
Relative humidity (%)	50%

Table 17: Experimental Results, Standard Deviation is equal to ±0,3°C.

(°C)	Wall					Ceiling (12 Panels)					Wall+Ceiling (12 Panels)		
	C1	C2	C3	C4	C5	C1	C2	C3	C4	C5	C1	C2	C3
Wall_Twin ±0.3	30.0	34.1	39.5	44.9	49.3	x	x	x	x	x	30.0	34.8	40.0
Wall_Twout ±0.3	29.4	33.7	38.4	43.5	47.9	x	x	x	x	x	29.6	34.3	39.2
Ceiling_Twin ±0.3	x	x	x	x	x	30.1	35.1	40.2	44.8	50.7	30.1	35.2	40.5
Ceiling_Twout ±0.3	x	x	x	x	x	29.5	34.4	39.4	43.7	49.2	29.5	34.3	39.2
Ts_north ±0.3	19.0	20.5	22.3	24.4	26.0	19.7	24.4	29.1	30.8	33.8	23.8	25.6	27.4
Ts_south ±0.3	19.9	21.5	23.2	25.3	26.8	20.7	25.3	29.7	31.4	34.4	24.6	26.4	28.4
Ts_east ±0.3	18.8	20.9	23.1	25.2	26.7	20.8	25.3	29.8	31.5	34.4	24.6	26.4	28.2
Ts_west ±0.3	26.5	30.1	34.4	38.6	41.3	19.9	24.8	29.7	31.5	34.5	28.5	32.3	36.1
Ts_west_un ±0.3	21.3	23.1	25.6	28.4	30.2	19.9	24.8	29.7	31.5	34.5	25.4	27.7	30.0
Ts_ceiling ±0.3	19.0	20.6	22.5	24.7	26.3	25.0	30.3	34.9	39.2	44.7	28.7	32.9	37.2
Ts_ceiling_un ±0.3	19.0	20.6	22.5	24.7	26.3	23.4	28.4	33.6	35.7	39.0	25.8	28.6	31.4
Ts_floor ±0.3	19.3	20.6	22.1	23.9	25.4	18.9	23.4	27.8	28.7	30.8	23.1	24.3	25.6
T_air ±0.3	19.9	21.6	23.5	26.3	27.2	20.2	24.8	29.3	30.9	33.8	24.5	26.7	28.9
T_mrt ±0.3	20.1	21.9	23.7	26.6	27.6	21.1	26.1	30.8	32.6	35.6	25.5	28.0	30.5
T_Vol_ceiling ±0.5	-2.5	-3.0	-3.1	-2.9	-2.6	-3.0	-2.6	-2.8	-2.9	-2.9	-2.5	-2.9	-2.9
T_Vol_floor ±0.5	19.8	19.7	19.7	19.8	19.7	19.7	19.7	19.6	19.7	19.7	19.8	19.8	19.8
T_Vol_outer ±0.5	-2.8	-3.0	-3.1	-2.9	-2.9	-3.0	-2.6	-2.8	-2.9	-2.9	-2.6	-2.9	-2.9
T_Vol_inner ±0.5	19.7	19.9	19.9	19.9	19.7	24.0	20.1	20.1	20.1	19.8	20.1	20.1	20.0

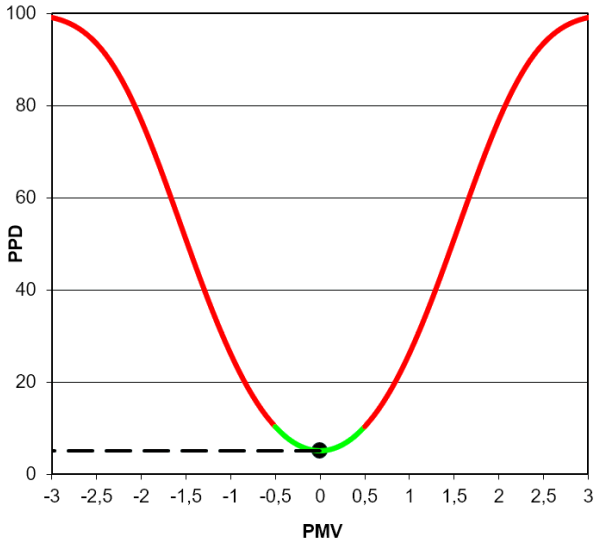

Figure 34: Neutral Conditions: PMV=0 PPD=5.

Table 18: PMV-PPD Results of Experimental Data.

	Wall					Ceiling					Wall+Ceiling		
	C1	C2	C3	C4	C5	C1	C2	C3	C4	C5	C1	C2	C3
T_air ±0.3	19.9	21.6	23.5	26.3	27.2	20.2	24.8	29.3	30.9	33.8	24.5	26.7	28.9
T_mrt ±0.3	20.1	21.9	23.7	26.6	27.6	21.1	26.1	30.8	32.6	35.6	25.5	28.0	30.5
RH	50	50	50	50	50	50	50	50	50	50	50	50	50
Air Velocity	0.1	0.1	0.1	0.1	0.1	0.1	0.1	0.1	0.1	0.1	0.1	0.1	0.1
Clothing	1	1	1	1	1	1	1	1	1	1	1	1	1
Activity	1.2	1.2	1.2	1.2	1.2	1.2	1.2	1.2	1.2	1.2	1.2	1.2	1.2
PMV	-0.3	0.0	0.5	1.1	1.3	-0.2	0.9	1.9	2.3	3.0	0.8	1.3	1.8
PPD	7.3	5.0	9.2	30.5	40.8	5.8	20.6	72.1	88.6	99.2	17.2	39.2	68.1

5.2 Radiant Heating Numerical Comfort Evaluation Results

In this chapter simulation results for the measurement point are shown. After that, results are evaluated in terms of comfort metrics Fanger's comfort model and Shukuya's human exergy balance model. Later on, air velocity streamlines, temperature contours and vertical air difference in all cases are discussed.

5.2.1 Wall Heating

After the validation of numerical model, thermal comfort assessment is done for 3 different wall temperatures. Radiant wall heating surface temperatures were set to 20°C, 25°C and 30°C in numerical model. Vertical air temperature values were taken for all cases from the numerical simulation results. PMV-PPD values were calculated and human body exergy balance calculations were done as it was explained in previous chapters. The average surface temperatures and air velocity values were taken from the simulation results. Wall heating numerical results are shown in Table 19.

Table 19: Wall Heating-Numerical Results

	Temperature (K)		
Named Sections	**Case1**	**Case2**	**Case3**
ceiling_unheated1	288.4	290.7	293.1
ceiling _radiant_panels	288.9	291.4	293.8
ceiling_unheated2	289.0	291.4	293.8
east_wall	290.2	292.4	294.6
floor	290.2	292.5	295.0
north_wall	288.9	291.4	293.9
south_wall	290.2	292.5	294.7
unheated_wall	288.8	291.1	293.5
wall_radiant Panels	293.2	298.2	303.2
T_air	289.8	292.3	294.7
T=mr	289.9	292.4	295.0
	Air Velocity (m/s)		
V_air	0.02	0.05	0.01

Numerical simulation was run for three cases. For each case the average wall surface temperatures were calculated in CFD-Post module. Air velocity and air temperature value is taken from the centre of room.

In Figure 35, In the Figure 36 and Figure 37 the temperature distributions of the surfaces of the room were examined as a result of the numerical study. The lowest temperature values were measured on the ceiling surface. The north and west wall surfaces had the slightly higher average temperature than ceiling. It is because the boundary conditions that the air temperature of façade room was set to -3°C, interior volume that simulates the internal partition inside a house and air temperature was set to 20°C, the floor volume was also set to an internal condition assumed that the space was occupied, and air temperature was set to 20°C. The ceiling volume was set to

simulate outside conditions that has -3°C of air temperature of façade walls (west and north walls) and ceiling surface that also had outside condition lower temperature distribution relatively. The highest temperature value was the surface on which the radiant heating is made. Surfaces that do not have a radiant wall panel naturally have a lower temperature.

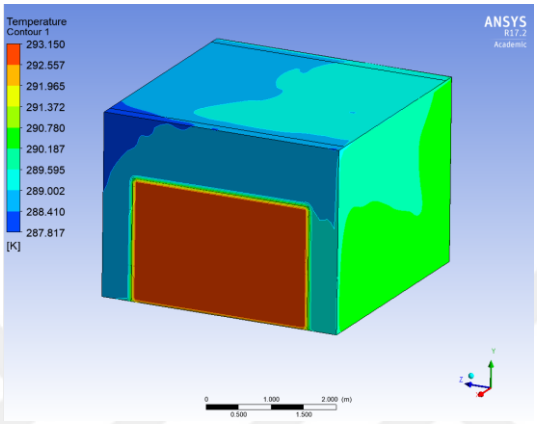

Figure 35: Temperature distribution on surfaces (Wall heating surface temperature is set to 20°C).

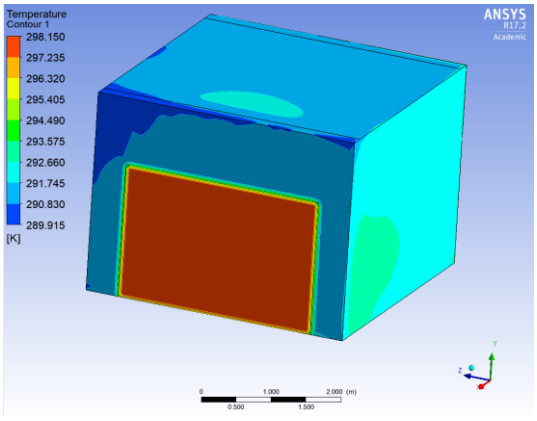

Figure 36: Temperature distribution on surfaces (Wall heating surface temperature is set to 25°C).

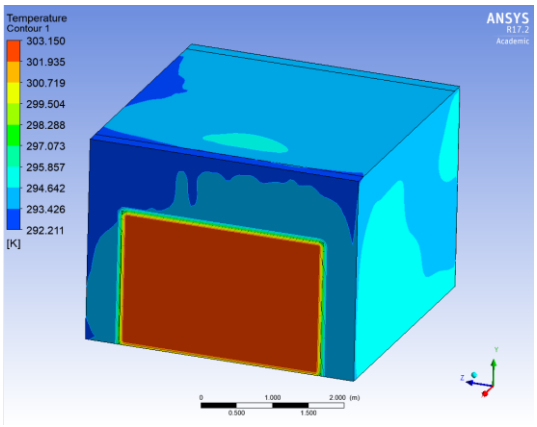

Figure 37: Temperature distribution on surfaces (Wall heating surface temperature is set to 30°C).

In the Figure 38, Figure 39 and Figure 40 volumetric temperature distribution of room air can be seen. Numerical results show that the room has quite homogeneous air distribution as it was expected. Since there is not any air-forced heating equipment inside the room local comfort parameters can be better provided and the main heat exchange inside the room occurs via radiation.

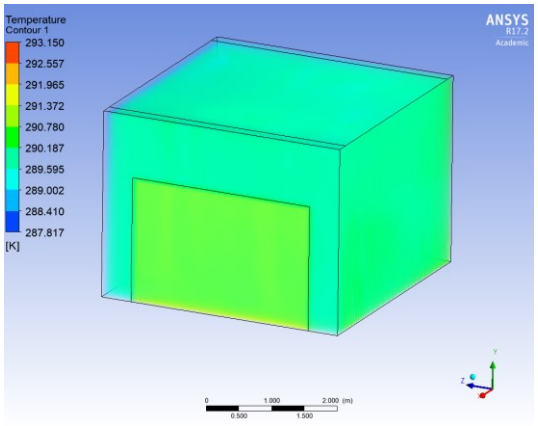

Figure 38: Volumetric Temperature distribution of room air volume (Wall heating surface temperature is set to 20°C).

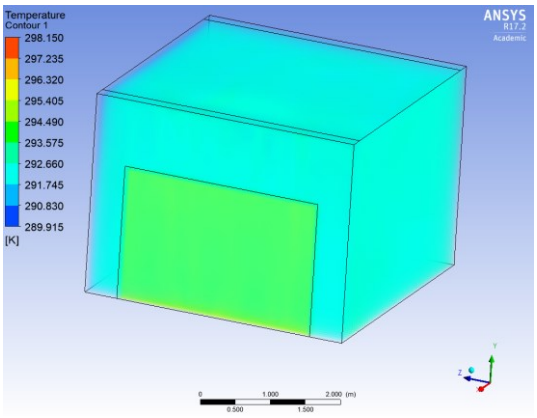

Figure 39: Temperature distribution of room air volume (Wall heating surface temperature is set to 25°C).

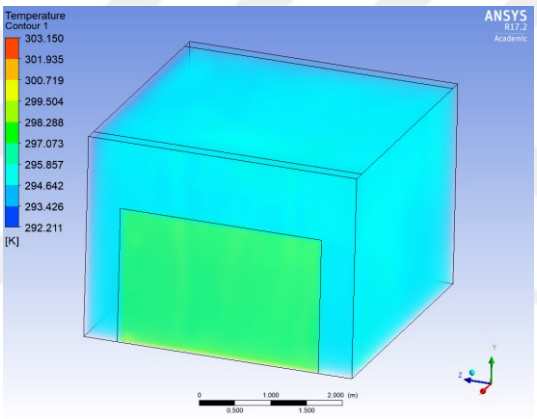

Figure 40: Temperature distribution of room air volume (Wall heating surface temperature is set to 30°C).

In the Figure 41, Figure 42, Figure 43, three different planes located at z=1, z=2, z=3 were examined to understand temperature distribution. Local temperature difference is found less than 3°C. Therefore, we can say that distribution on these planes are also homogeneous.

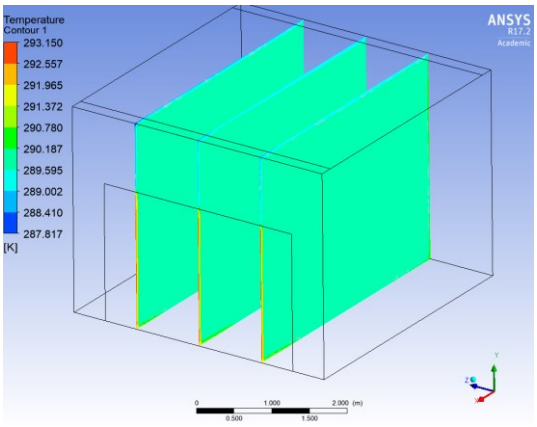

Figure 41: Temperature distribution at z=1, z=2, z=3 (Wall heating surface temperature is set to 20°C).

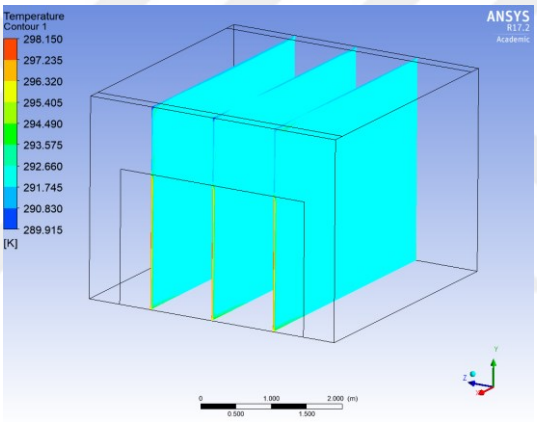

Figure 42: Temperature distribution at z=1, z=2, z=3 (Wall heating surface temperature is set to 25°C).

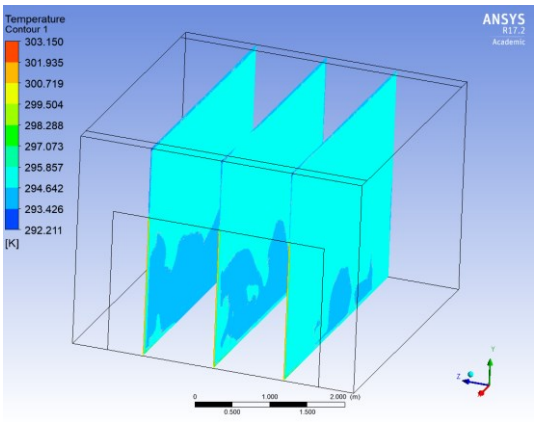

Figure 43: Temperature distribution at z=1, z=2, z=3 (Wall heating surface temperature is set to 30°C).

In Figure 44, Figure 45, Figure 46, two different planes located at y=1, y=2 were examined to understand temperature distribution on different levels of height. The temperature difference is found less than 3°C. Therefore, we can say that distribution on these planes were found quite uniform.

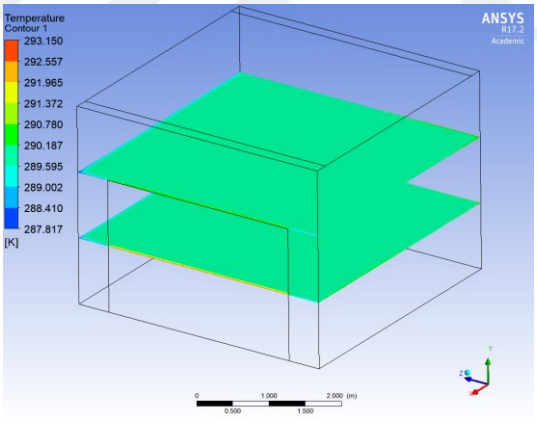

Figure 44: Temperature distribution at y=1, y=2 (Wall heating surface temperature is set to 20°C).

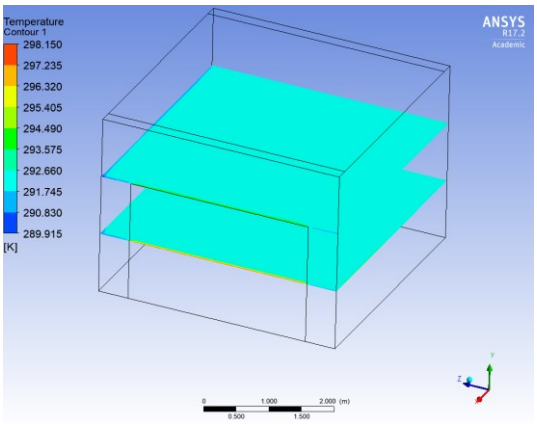

Figure 45: Temperature distribution at *y*=1, *y*=2 (Wall heating surface temperature is set to 25°C).

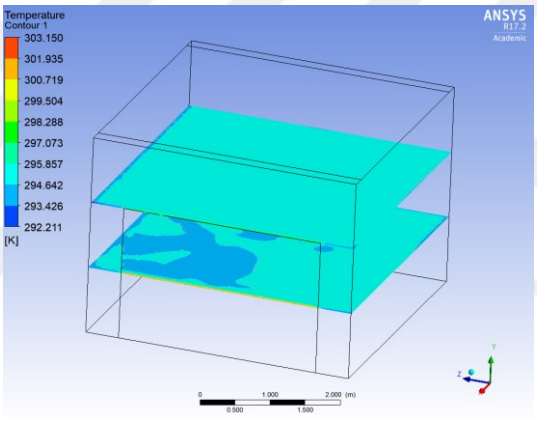

Figure 46: Temperature distribution at *y*=1, *y*=2 (Wall heating surface temperature is set to 30°C).

Figure 47, Figure 48, Figure 49 show the velocity streamlines and its distributions. Velocity values are less than 0.1 m/s which is the passive effect of radiant systems. Because of we do not have any air-forced heating system, heat exchange occurs mostly via radiation. We can see the streamlines as an effect of natural convection and velocity vectors are improved when the heating surface temperature goes higher.

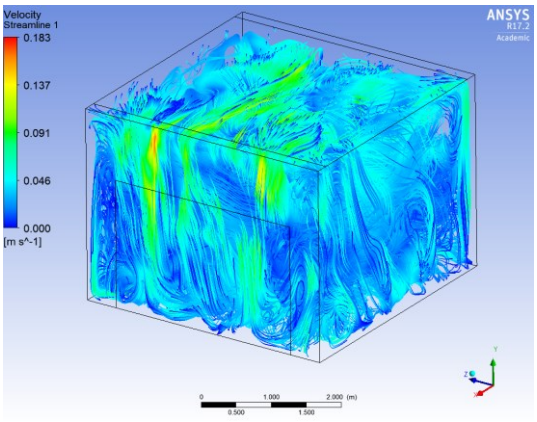

Figure 47: Velocity streamlines (Wall heating surface temperature is set to 20°C).

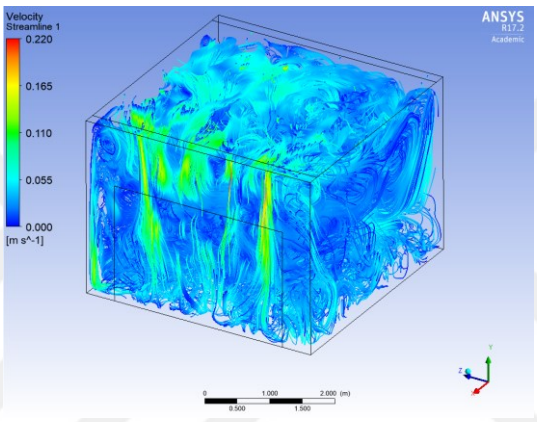

Figure 48: Velocity streamlines (Wall heating surface temperature is set to 25°C).

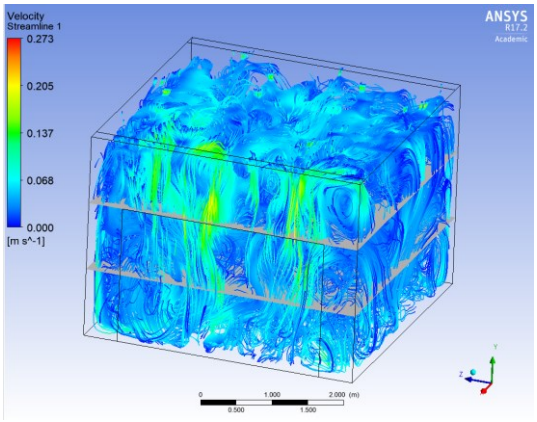

Figure 49: Velocity streamlines (Wall heating surface temperature is set to 30°C).

To sum up all simulations done for wall heating case. Numerical analysis was carried out at 3 different surface temperatures for the wall heating case. Heating surface temperatures were set to 20°C, 25°C and 30°C. Simulation results show that

the temperature inside the room is quite homogeneous. This is because of the heating occurs mostly via radiation (> 50%). There is no equipment in the room that increases air movement. Because of that, air velocity which is very important for comfort, is lower than 0.1 m/s for each case. Low air velocity which provides better comfort is one of the most characteristic features of radiant systems. It also helps to create healthy environmental quality via blocking the transportation of the dust in air.

5.2.2 Ceiling Heating

Ceiling heating scenarios were separated into two parts: first of all, heating case was simulated as 5-panel ceiling and secondly heating case was simulated for whole ceiling (12 Panels). The main aim of the first case in which 5 panels of the ceiling were active, was to compare ceiling and wall heating cases when both have the same heating surface area.

After the validation of numerical model, thermal comfort assessment is done for 3 different ceiling temperatures. Radiant surface temperature on (5P) ceiling was set to 20°C, 25°C and 30°C. For all case vertical air temperature values are taken from the numerical simulation results. PMV-PPD values and human body exergy balance calculated as it was explained in previous Chapters.

5.2.2.1 First Scenario: Ceiling Heating with 5 Panels

As it was mentioned before that the reason to simulate partial ceiling case was important to compare the wall and ceiling performance in terms of comfort. Thus, ceiling heating surface area (5 Panels) modelled as equal as the wall heating area that was 6 m^2. Vertical air temperature values were taken for all cases from the numerical simulation results. PMV-PPD values were calculated and human body exergy balance calculations were done as it was explained in previous Chapters.

The average surface temperatures and air velocity values were taken from the simulation results. Ceiling heating (5P) results are shown in Table 20.

Table 20: Ceiling Heating (5P) Numerical Results.

	Temperature (K)		
Named Sections	**Case1**	**Case2**	**Case3**
ceiling_unheated1	287,4	289,7	291,9
ceiling_radiant_panels	293,2	298,2	303,2
ceiling_unheated2	288,1	290,3	292,6
east_wall	289,4	291,7	293,9
floor	289,1	291,5	293,9
north_wall	287,4	289,7	292,0
south_wall	289,4	291,6	293,7
unheated_wall	287,6	290,1	292,5
wall_radiant Panels	287,7	290,2	292,5
T_air	299,6	293,7	290,3
T=mr	298,9	294,3	291,0
	Air Velocity (m/s)		
V_air	0.02	0.03	0.07

In the Figure 50, Figure 51 and Figure 52, the temperature distributions of the surfaces of the room were examined as a result of the numerical study. The lowest temperature values were measured on the unheated part of the ceiling. North and west wall surfaces were measured slightly higher than the unheated parts of ceiling. The temperature distribution for all cases can be seen in the Figures 50, 51, 52. The boundary conditions which are the surrounding volumes of test room have significant effect on surface temperature contours. The air temperature of façade room was set to -3°C. Interior volume that simulates the internal partition inside a house and air temperature is set to 20°C. The floor volume was also set to an internal condition assuming that the space was occupied, and air temperature was set to

20°C. The ceiling volume was set to simulate outside conditions that has -3°C of air temperature of façade walls (west and north walls) and ceiling surface that also had outside condition lower temperature distribution relatively. The highest temperature value was the surface on which the radiant heating is made. Surfaces that do not have a radiant panel naturally have a lower temperature profiles.

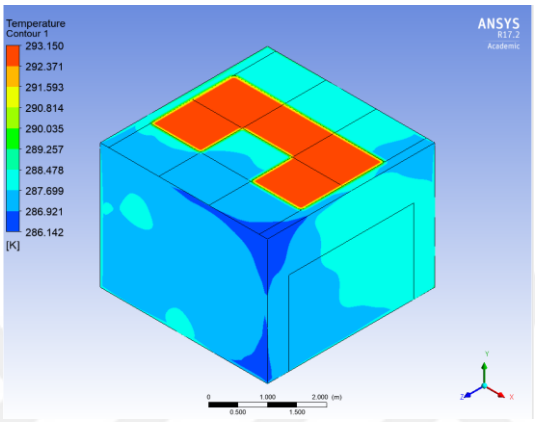

Figure 50: Temperature distribution on surfaces (5 Panel-Ceiling heating surface temperature is set to 20°C).

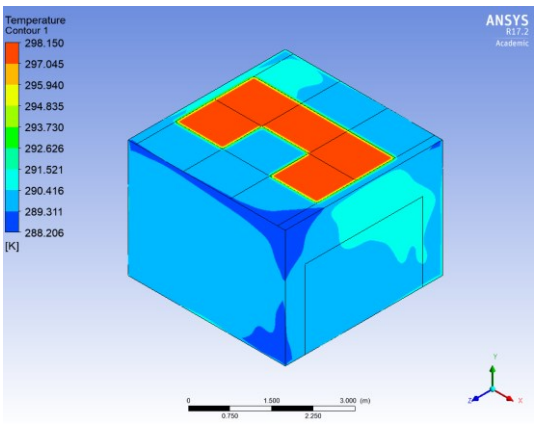

Figure 51: Temperature distribution on surfaces (5 Panel-Ceiling heating surface temperature is set to 25°C).

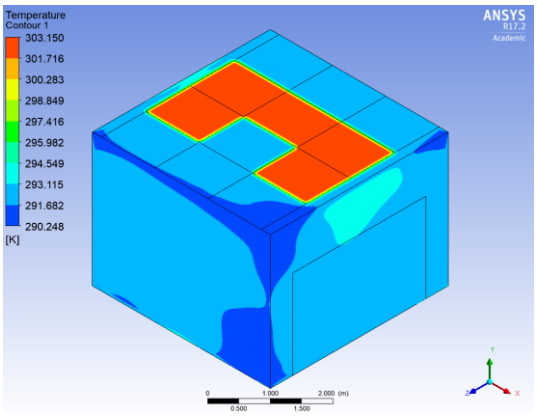

Figure 52: Temperature distribution on surfaces (5 Panel-Ceiling heating surface temperature is set to 30°C).

In Figure 53, Figure 54 and Figure 55 volumetric temperature distribution of room's air can be seen. Numerical results show that room has quite homogeneous air distribution as it was expected. Since there is not any air-forced heating equipment inside the room local comfort parameters can be better provided and the main heat exchange inside the room occurs via radiation. When we compare the wall heating and ceiling heating cases (5P), it is considered that wall heating case has more homogenous volumetric contour even the heating surface area of both cases were equal.

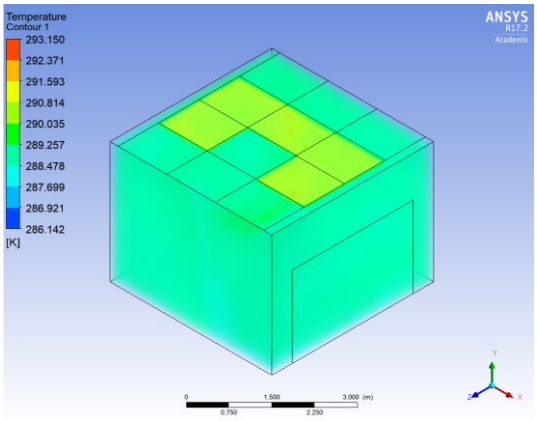

Figure 53: Temperature distribution of room air volume (5 Panel-Ceiling heating surface temperature is set to 20°C).

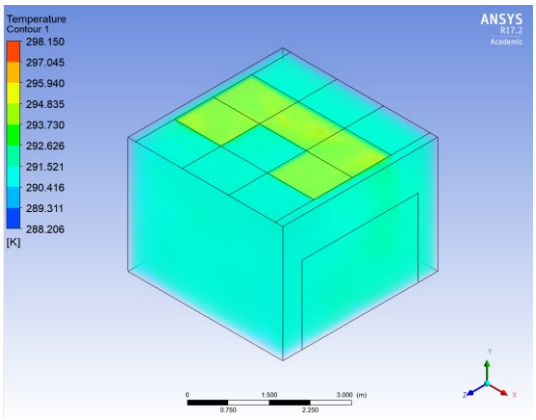

Figure 54: Temperature distribution of room air volume (5 Panel-Ceiling heating surface temperature is set to 25°C).

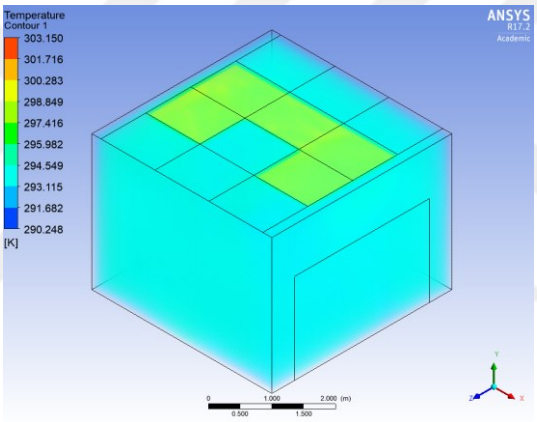

Figure 55: Temperature distribution of room air volume (5 Panel-Ceiling heating surface temperature is set to 30°C).

In Figure 56, Figure 57, Figure 58, three different planes located at z=1, z=2, z=3 were examined to understand temperature distribution. Local temperature difference is found less than 3°C. Therefore, we can say that distribution on these planes are also homogeneous

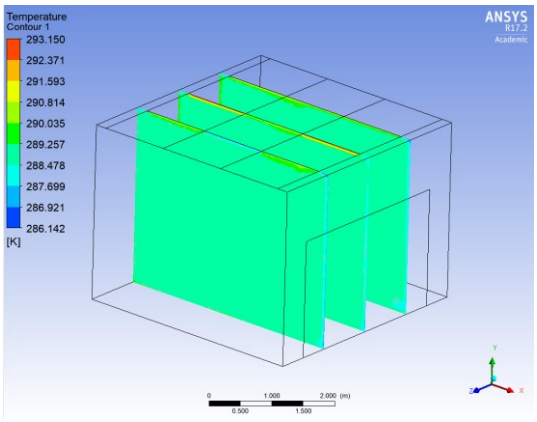

Figure 56: Temperature distribution at z=1, z=2, z=3 (5 Panel-Ceiling heating surface temperature is set to 20°C).

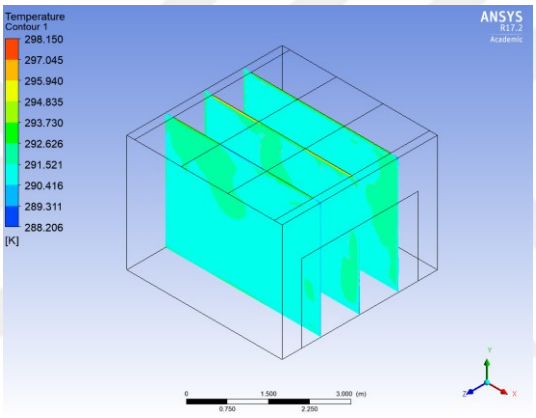

Figure 57: Temperature distribution at z=1, z=2, z=3 (5 Panel-Ceiling heating surface temperature is set to 25°C).

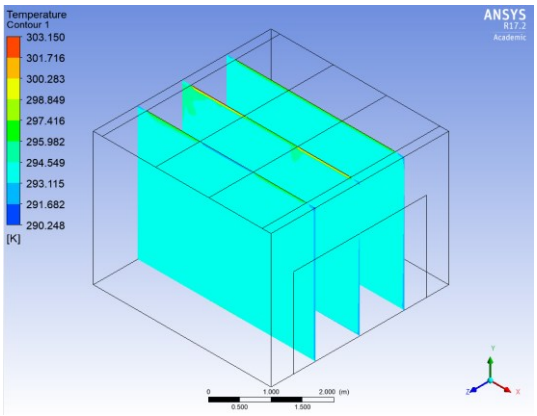

Figure 58: Temperature distribution at z=1, z=2, z=3 (5 Panel-Ceiling heating surface temperature is set to 30°C).

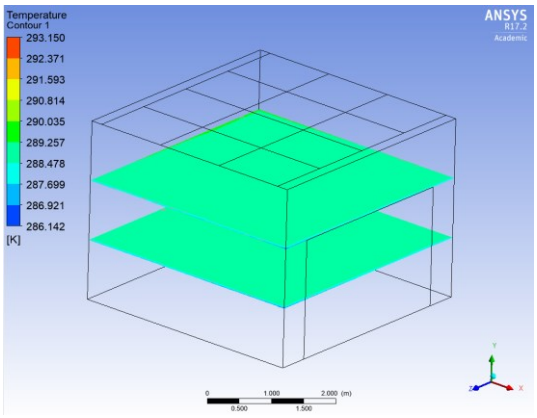

Figure 59: Temperature distribution at y=1, y=2 (5 Panel-Ceiling heating surface temperature is set to 20°C).

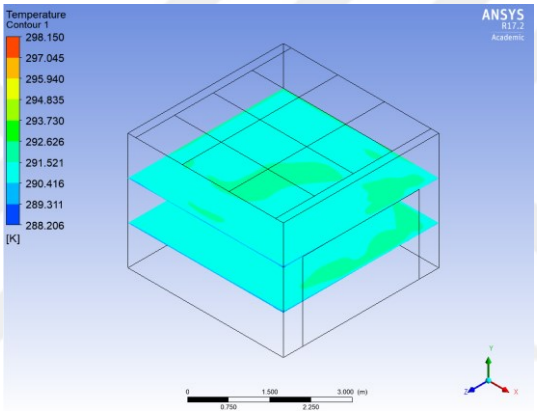

Figure 60: Temperature distribution at y=1, y=2 (5 Panel-Ceiling heating surface temperature is set to 25°C).

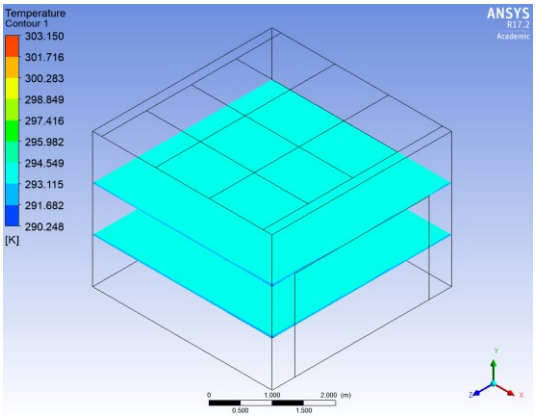

Figure 61: Temperature distribution at y=1, y=2 (5 Panel-Ceiling heating surface temperature is set to 30°C).

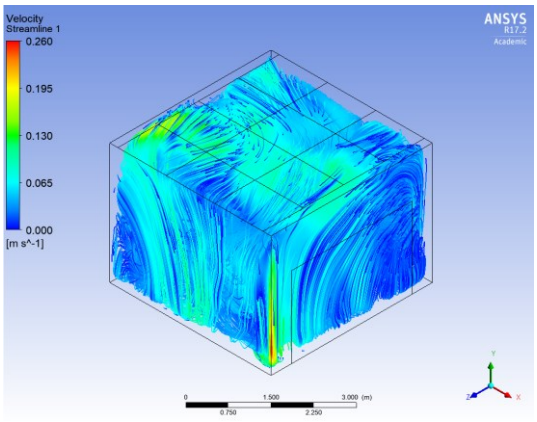

Figure 62: Velocity streamlines (5 Panel-Ceiling heating surface temperature is set to 20°C)

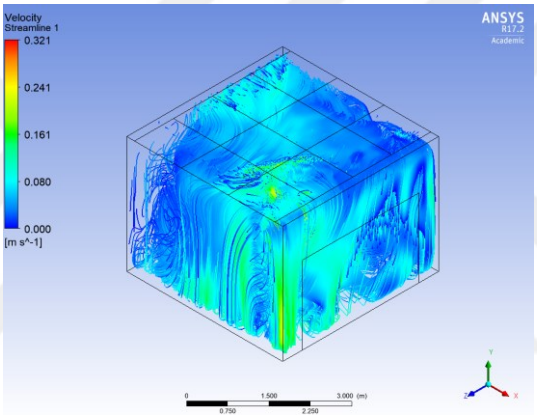

Figure 63: Velocity streamlines (5 Panel-Ceiling heating surface temperature is set to 25°C).

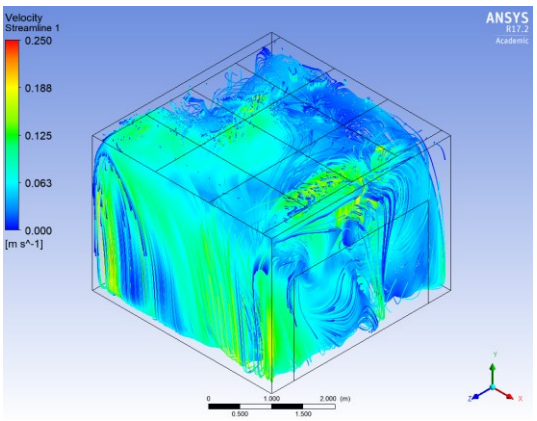

Figure 64: Velocity streamlines (5 Panel-Ceiling heating surface temperature is set to 30°C).

To sum up all simulations done for ceiling heating (5P) case. Numerical analysis was carried out at 3 different surface temperatures for the wall heating case. Heating surface temperatures were set to 20°C, 25°C and 30°C. Simulation results show that the temperature inside the room is quite homogeneous. This is because of the heating occurs mostly via radiation (> 50%). There is no equipment in the room that increases air movement. Because of that air velocity which is very important for comfort is lower than 0.1 m/s for each case. However, when it is compared with the wall heating case, the air velocity amounts in 5P ceiling heating case are slightly higher than wall heating.

5.2.2.2 Second Scenario: Ceiling Heating with 12 Panels

Ceiling heating scenarios were separated into two parts: first of all, heating case was simulated as 5-panel ceiling and secondly heating case was simulated for whole ceiling (12 Panels). In this part the ceiling heating case for 12 panels configuration is evaluated.

By using the validated numerical model, radiant surface temperature on (12P) ceiling was set to 20°C, 25°C and 30°C. For all cases, vertical air temperature values are taken from the numerical simulation results. PMV-PPD values and human body exergy balance were calculated as it was explained in previous Chapters.

In Figure 65, Figure 66 and Figure 67, the temperature distributions of the surfaces of the room were examined as a result of the numerical study. The lowest temperature values were measured on the north and west wall surfaces. The temperature distribution for all cases can be seen in Figures. The boundary conditions which are the surrounding volumes of test room have significant effect on surface temperature contours. The air temperature of façade room was set to -

3°C. Interior volume that simulates the internal partition inside a house and air temperature is set to 20°C. The floor volume was also set to an internal condition assuming that the space was occupied, and air temperature was set to 20°C. The ceiling volume was set to simulate outside conditions that has -3°C of air temperature of façade walls (west and north walls) and ceiling surface that also had outside condition lower temperature distribution relatively. The highest temperature value was on the ceiling surface. Surfaces that do not have a radiant panel naturally have a lower temperature profiles. It is considered that the surface area of radiant heater plays a significant role on temperature distribution.

The surface temperatures and air velocity values are shown in Table 21.

Table 21: Ceiling Heating(12P)-Numerical Results.

	Temperature (K)		
Named Sections	**Case1**	**Case2**	**Case3**
ceiling_unheated1	289.3	292.6	297.0
ceiling_radiant_panels	293.2	298.2	303.2
ceiling_unheated2	289.9	293.1	297.4
east_wall	291.2	294.4	298.4
floor	291.0	294.4	298.6
north_wall	289.5	292.9	297.2
south_wall	291.2	292.4	298.5
unheated_wall	289.6	293.1	297.4
wall_radiant Panels	289.5	292.9	297.1
T_air	290.3	293.7	299.6
T=mr	291.0	294.3	298.9
	Air Velocity (m/s)		
V_air	0.04	0.06	0.09

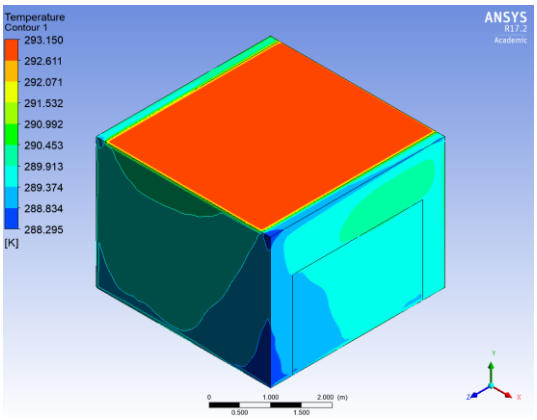

Figure 65: Temperature gradient on surfaces (Ceiling heating-12P surface temperature is set to 20°C).

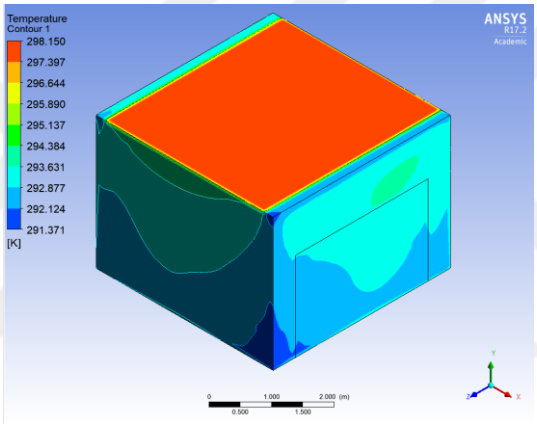

Figure 66: Temperature distribution on surfaces (Ceiling heating-12P surface temperature is set to 25°C).

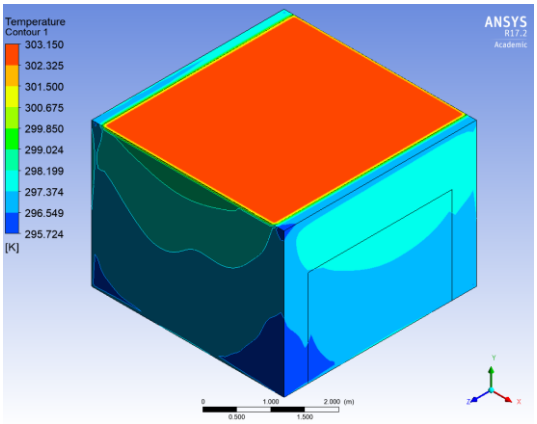

Figure 67: Temperature distribution on surfaces (Ceiling heating-12P surface temperature is set to 30°C).

In Figure 68, Figure 69 and Figure 70 volumetric temperature distribution of room's air can be seen. Numerical results show that room has quite homogeneous air distribution as it was expected with the increased surface area. Since there is not any air forced heating equipment inside the room, the local comfort parameters can be better provided and the main heat exchange inside the room occurs via radiation. When we compare the wall heating and ceiling heating cases 5-Panels and 12-Panels, it is considered that 12-Panels heating case has more homogenous volumetric contour.

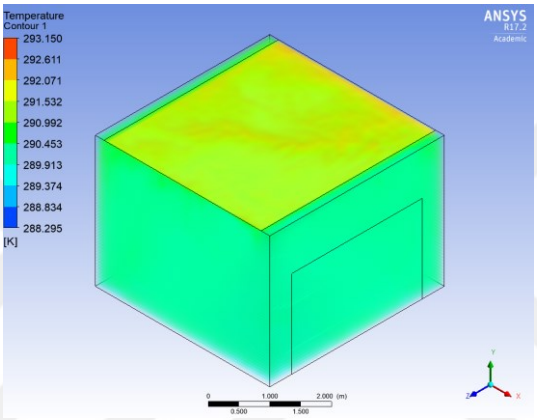

Figure 68: Temperature distribution of room air volume (Ceiling heating-12P surface temperature is set to 20°C).

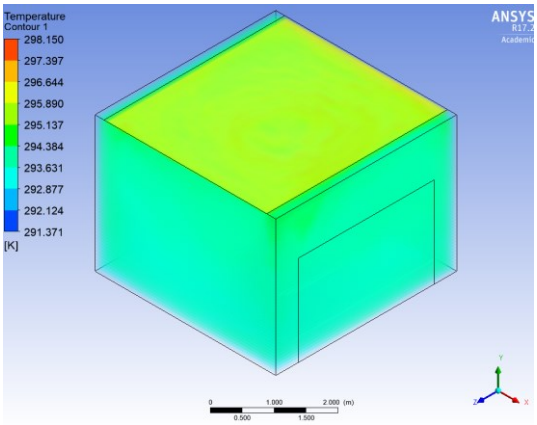

Figure 69: Temperature distribution of room air volume (Ceiling heating-12P surface temperature is set to 25°C).

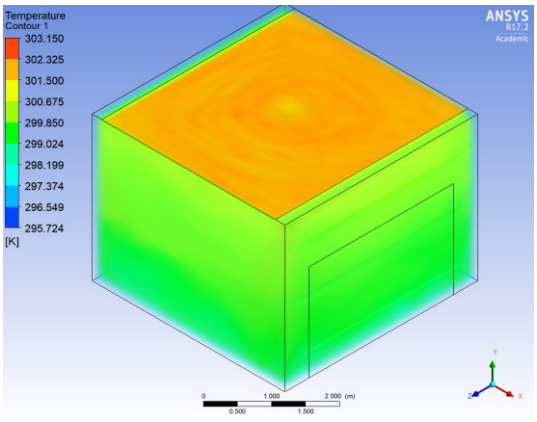

Figure 70: Temperature distribution of room air volume (Ceiling heating-12P surface temperature is set to 30°C).

In Figure 71, Figure 72, Figure 73, three different planes located at z=1, z=2, z=3 were examined to understand temperature distribution. Local temperature difference is found less than 3°C. Therefore, we can say that distribution on these planes are also homogeneous.

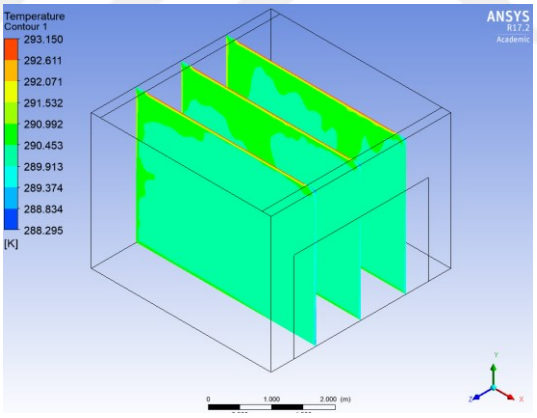

Figure 71: Temperature distribution at z=1, z=2, z=3 (Ceiling heating-12P surface temperature is set to 20°C)

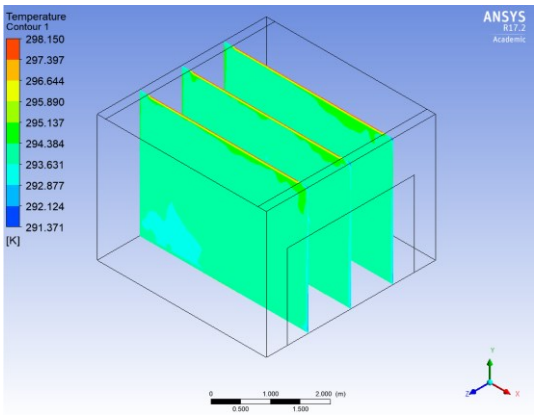

Figure 72: Temperature distribution at z=1, z=2, z=3 (Ceiling heating-12P surface temperature is set to 25°C).

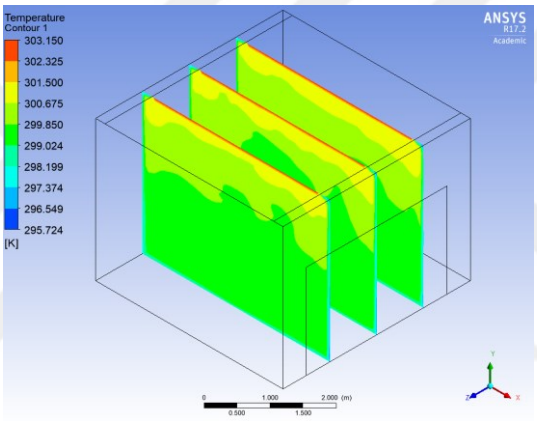

Figure 73: Temperature distribution at z=1, z=2, z=3 (Ceiling heating-12P surface temperature is set to 30°C).

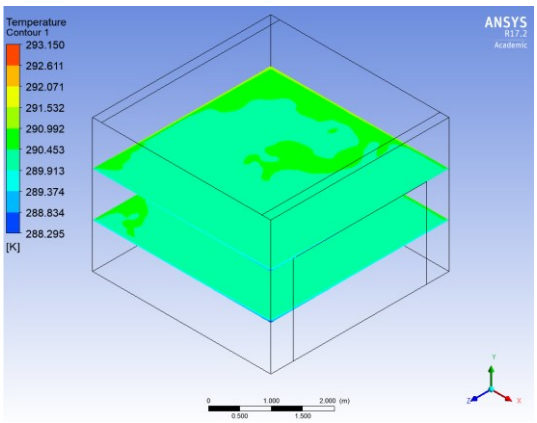

Figure 74: Temperature distribution at y=1, y=2 (Ceiling heating-12P surface temperature is set to 20°C).

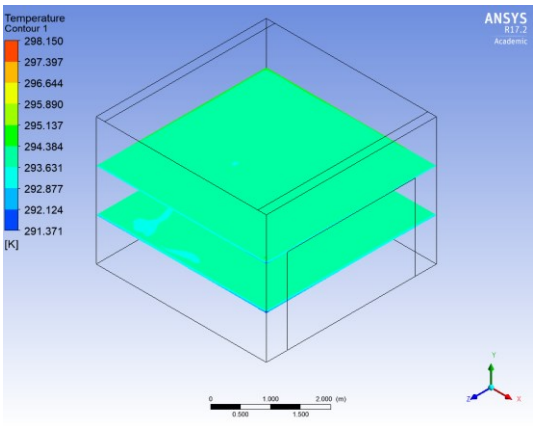

Figure 75: Temperature distribution at y=1, y=2 (Ceiling heating-12P surface temperature is set to 25°C).

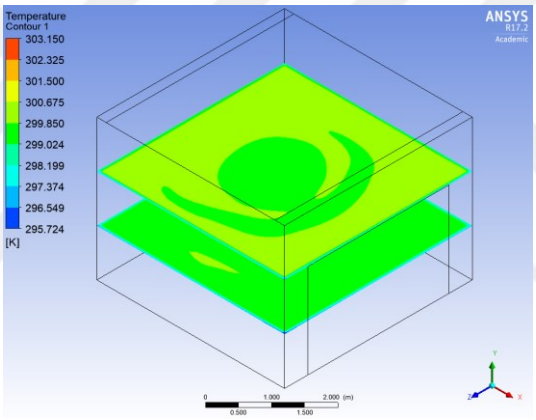

Figure 76: Temperature distribution at y=1, y=2 (Ceiling heating-12P surface temperature is set to 30°C).

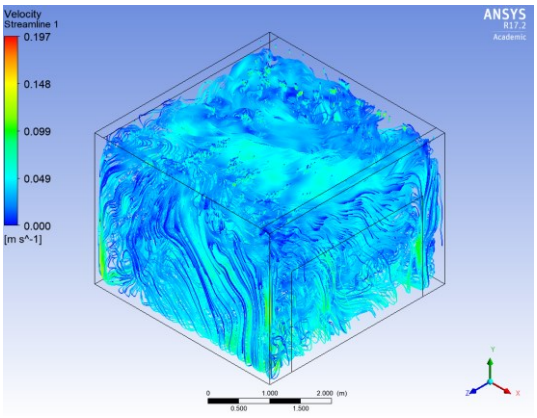

Figure 77: Velocity streamlines (Ceiling heating-12P surface temperature is set to 20°C).

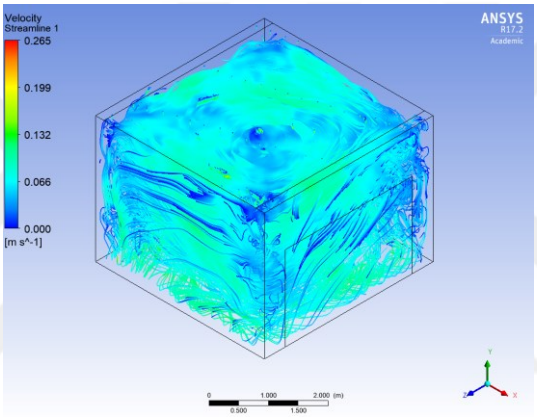

Figure 78: Velocity streamlines (Ceiling heating-12P surface temperature is set to 25°C).

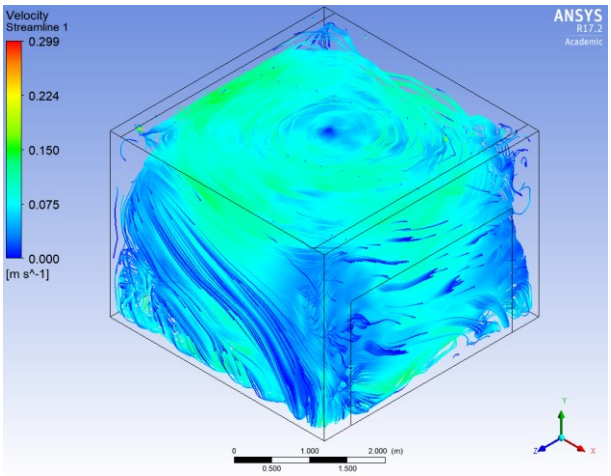

Figure 79: Velocity streamlines (Ceiling heating-12P surface temperature is set to 30°C.

To sum up all simulations done for ceiling heating (12P) case: Numerical analysis was carried out at 3 different surface temperatures for the wall heating case. Heating surface temperatures were set to 20°C, 25°C and 30°C. Simulation results show that the temperature inside the room is quite homogeneous. This is because of the heating occurs mostly via radiation (> 50%). There is no equipment in the room that increases air movement. So the air velocity which is very important for comfort is lower than 0.1 m/s for each case.

5.2.3 Wall and Ceiling (12P) Heating

The aim of this study is to evaluate the comfort of radiant systems in terms of different heating locations. Here we analyzed ceiling and wall heating configuration when both surfaces were heated. Wall panels and whole ceiling panels (12 Panels) were activated for heating.

By using the validated numerical model, analyses were done for 3 different wall-ceiling temperatures. Radiant surface temperatures were set to 20°C, 22°C and 24°C. These set values were selected according to the experimental results to avoid over-heating of the room. For all case vertical air temperature values are taken from the numerical simulation results. PMV-PPD values were calculated and human body exergy balance calculation was also done as it was explained in previous Chapters.

In Figure 80, Figure 81 and Figure 82, the temperature distributions of the surfaces of the room were examined as a result of the numerical study. The lowest temperature values were measured on the north and west wall surfaces. The temperature distribution for all cases can be seen in Figures. The boundary conditions which are the surrounding volumes of test room have significant effect on surface temperature contours. The air temperature of façade room was set to -

3°C. Interior volume that simulates the internal partition inside a house and air temperature is set to 20°C. The floor volume was also set to an internal condition assuming that the space was occupied, and air temperature was set to 20°C. The ceiling volume was set to simulate outside conditions that has -3°C of air temperature of façade walls (west and north walls) and ceiling surface that also had outside condition lower temperature distribution relatively. The highest temperature values were on the heated surfaces. In this case according to the surface area, the most homogeneous temperature distribution was provided with lower surface temperatures. It is considered that the surface area of radiant heater plays a significant role on temperature distribution.

Table 22: Wall and Ceiling Heating-Numerical Results.

	Temperature (K)		
Named Sections	**Case1**	**Case2**	**Case3**
ceiling_unheated1	290.3	291.8	293.5
ceiling_radiant_panels	293.2	295.2	297.2
ceiling_unheated2	291.0	292.6	294.2
east_wall	292.1	292.6	295.2
floor	292.1	293.7	295.4
north_wall	290.5	292.1	293.8
south_wall	292.2	293.7	295.3
unheated_wall	290.5	292.1	293.8
wall_radiant Panels	293.2	295.2	297.2
T_air	292.5	294.3	296.3
T=mr	292.0	293.5	295.4
	Air Velocity (m/s)		
V_air	0.01	0.02	0.07

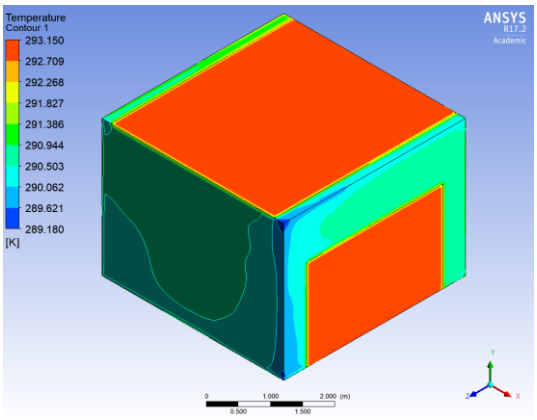

Figure 80: Temperature distribution on surfaces (Ceiling and Wall heating surface temperatures are set to 20°C).

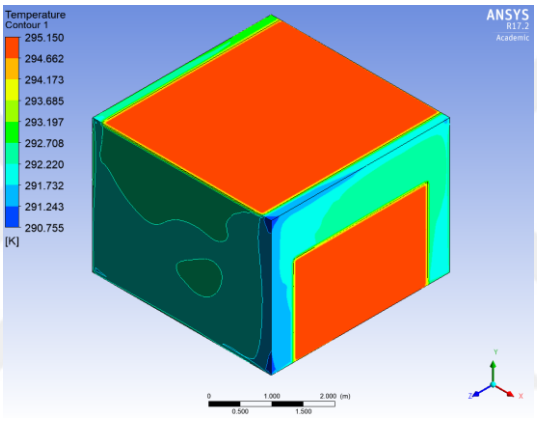

Figure 81: Temperature distribution on surfaces (Ceiling and Wall heating surface temperatures are set to 22°C).

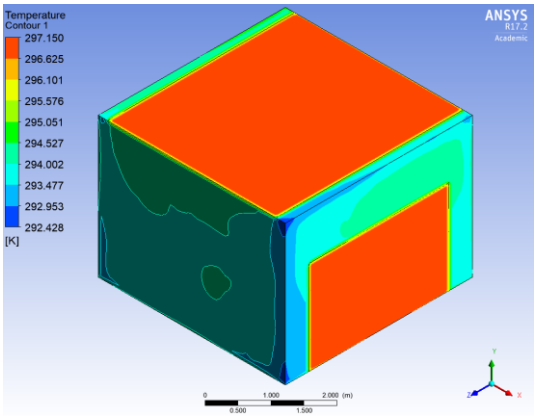

Figure 82: Temperature distribution on surfaces (Ceiling and Wall heating surface temperatures are set to 24°C).

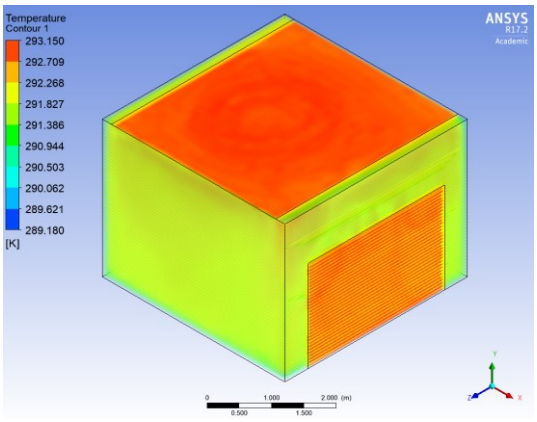

Figure 83: Temperature distribution of room air volume (Ceiling and Wall heating surface temperatures are set to 20°C).

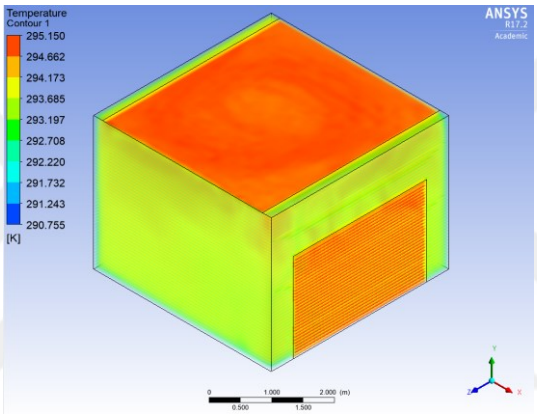

Figure 84: Temperature distribution of room air volume (Ceiling and Wall heating surface temperatures are set to 22°C).

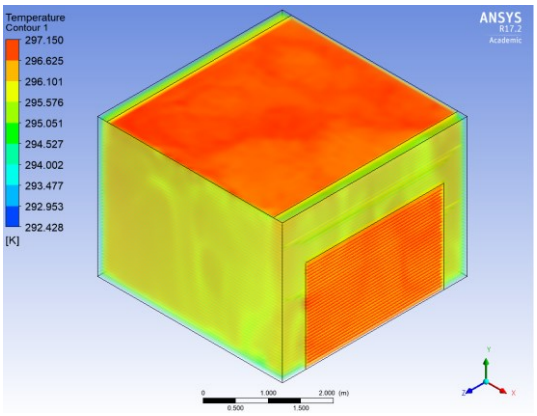

Figure 85: Temperature distribution of room air volume (Ceiling and Wall heating surface temperatures are set to 24°C).

In Figure 86, Figure 87, Figure 88, three different planes located at z=1, z=2, z=3 were examined to understand temperature distribution. Local temperature difference is found less than 3°C. Therefore, we can say that distribution on these planes are also homogeneous.

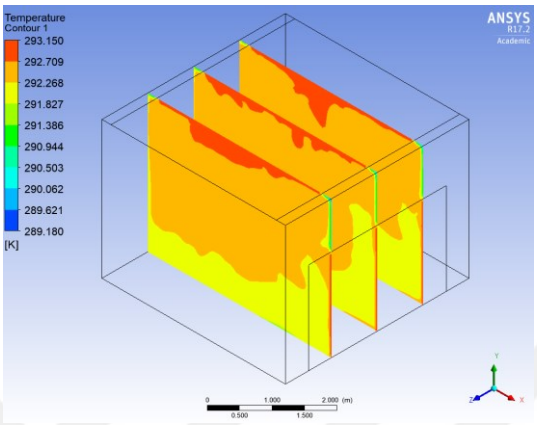

Figure 86: Temperature distribution at z=1, z=2, z=3 (Ceiling and Wall heating surface temperatures are set to 20°C).

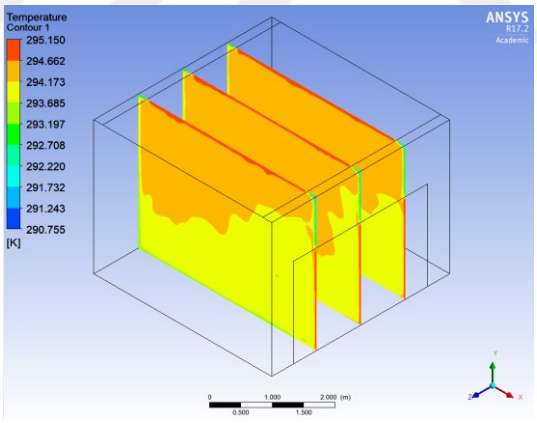

Figure 87: Temperature distribution at z=1, z=2, z=3 (Ceiling and Wall heating surface temperatures are set to 22°C).

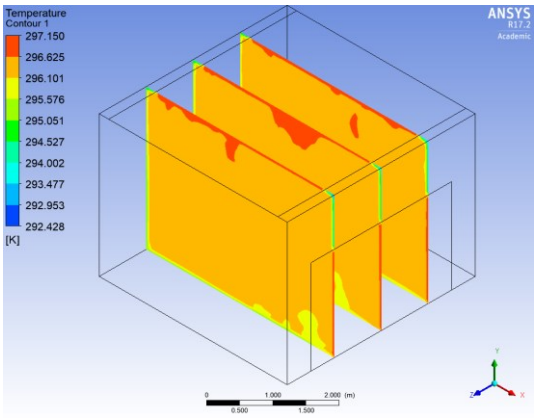

Figure 88: Temperature distribution at z=1, z=2, z=3 (Ceiling and Wall heating surface temperatures are set to 24°C).

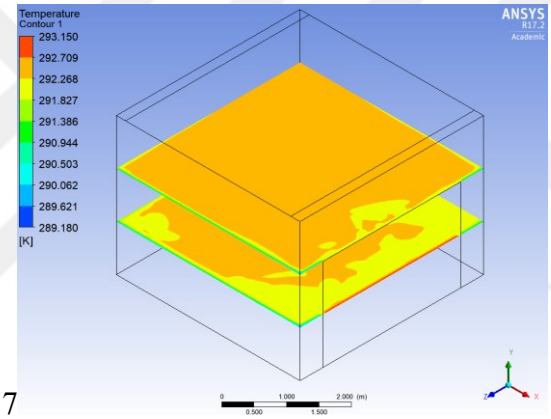

7

Figure 89: Temperature distribution at *y*=1, *y*=2 (Ceiling and Wall heating surface temperatures are set to 20°C).

In Figure 89, Figure 90, Figure 91, two different planes located at y=1, y=2 were examined to understand temperature distribution. Local temperature difference is found less than 3°C. Therefore, we can say that distribution on these planes are also homogeneous.

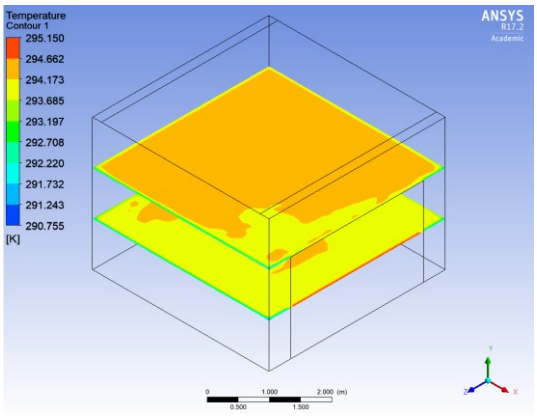

Figure 90: Temperature distribution at y=1, y=2 (Ceiling and Wall heating surface temperatures are set to 22°C).

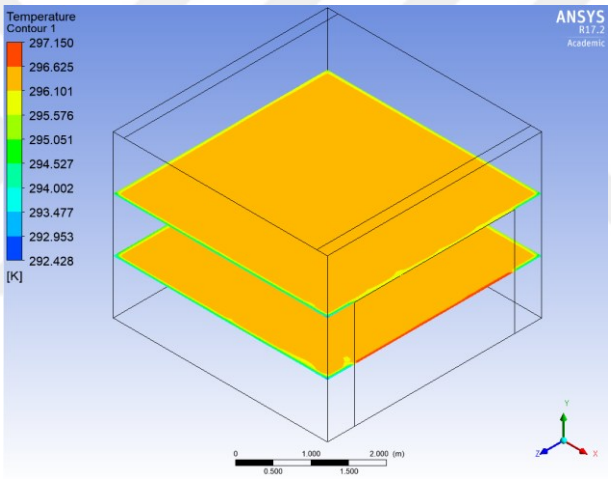

Figure 91: Temperature distribution at y=1, y=2 (Ceiling and Wall heating surface temperatures are set to 24°C).

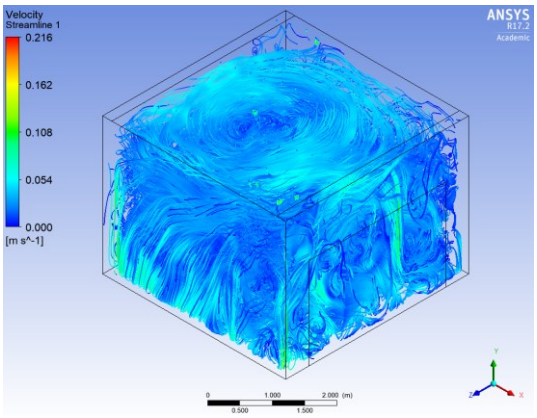

Figure 92: Velocity streamlines (Ceiling and Wall heating surface temperatures are set to 20°C).

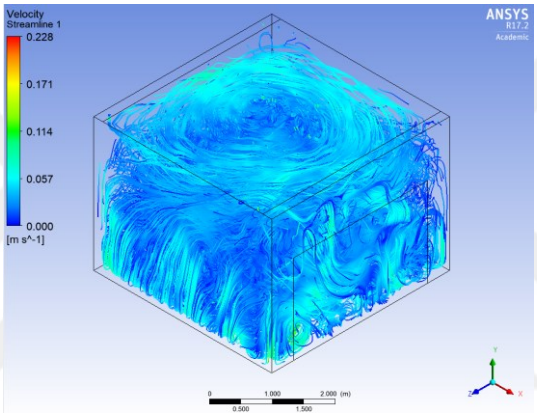

Figure 93: Velocity streamlines (Ceiling and Wall heating surface temperatures are set to 22°C).

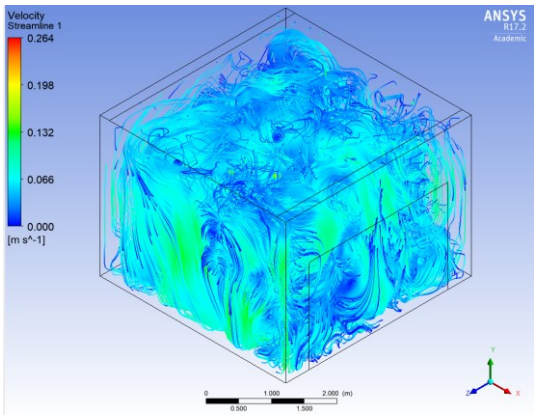

Figure 94: Velocity streamlines (Ceiling and Wall heating surface temperatures are set to 24°C).

To sum up all simulations done for wall heating case: Numerical analysis was carried out at 3 different surface temperatures for the wall heating case. Heating surface temperatures were set to 20°C, 22°C and 24°C. Simulation results show that the temperature inside the room is quite homogeneous. This is because of the heating occurs mostly via radiation (> 50%). There is no equipment in the room that increases air movement. Because of that, the air velocity which is very important for comfort is lower than 0.1 m/s for each case. Low air velocity which provides better comfort is one of the most characteristic features of radiant systems. It also helps to create healthy environmental quality via blocking the transportation of the dust in air.

5.3 Thermal Comfort Assessment

In PMV approach, Fanger has combined psychological theory with statistical data and has developed a mathematical model that predicts thermal sensation. According to Fanger, PMV indicator, which is used to determine comfort conditions for six comfort variables such as clothing, ambient air temperature, average radiant temperature, air velocity, the metabolic activity rate and relative humidity. These metrics are classified as personal parameters which are clothing and metabolic rate and environmental parameters which are air temperature, mean radiant temperature, relative humidity and air velocity.

5.3.1 PMV and PPD

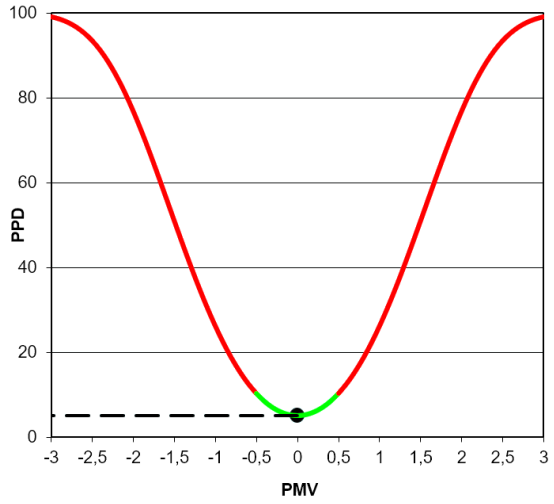

Figure 95: Neutral Conditions: PMV=0, PPD=5.

Table 23: Calculation parameters: of PMV and PPD according to the numerical study.

Parameter	Input
Clothing (clo)	Constant (1)
Air temp. (°C)	Numerical Result
Mean radiant temp. (°C)	Numerical Result
Activity (met)	1.2
Air speed (m/s)	Numerical Result
Relative humidity (%)	Constant (50%)

5.3.1.1 Wall Heating

According to the standards [6, 7] Predicted Mean Vote (PMV) values should be between -0.5 and +0.5 for a comfortable environment. In this part of the thesis the PMV-PPD values were calculated by using the numerical results according to the guidance of the standards [6, 7]. Validated numerical model was used for comfort simulations. Thermal comfort assessment was done for 3 different wall temperatures. Radiant wall heating surface temperatures were set to 20°C, 25°C and 30°C in numerical model.

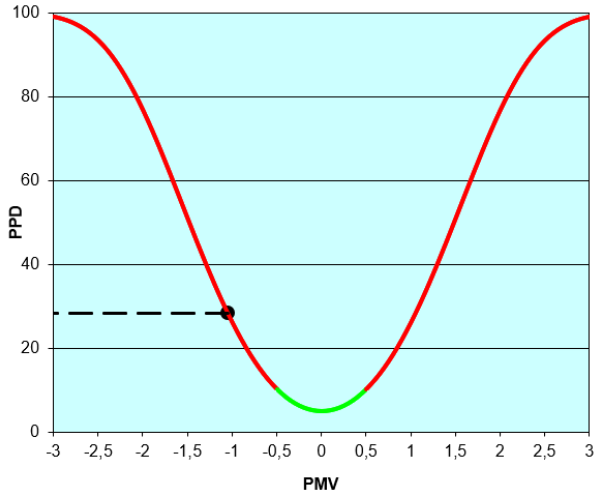

Figure 96: Wall Heating Case1: PMV=-1.1 PPD=28.3, Feeling: “Slightly Cool”.

In the case of wall heating, general comfort assessment was done for each case. In Case 1, occupants feel “Slightly Cool”. In the first case, where the surface temperature is set to 20 °C or 293.15 K, PMV and PPD values are found as -1.1 and %28.3 which does not provide comfort, according to the related standards mentioned before.

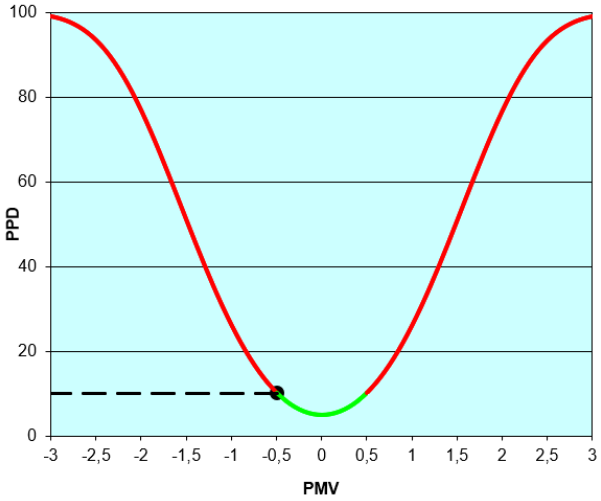

Figure 97: Wall Heating Case2: PMV=-0.5 PPD=10, “Neutral”.

In Case 2, occupants feel “Neutral”. In the second case, where the surface temperature is set to 25 °C or 298.15 K, PMV and PPD values are found as -0.5 and %10 that shows comfort is provided in the occupied space.

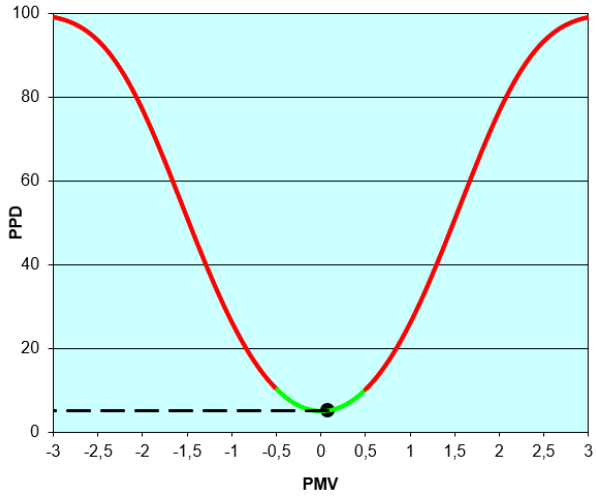

Figure 98: Wall Heating Case3: PMV=0.1 PPD=5.1, "Neutral".

In Case 3, occupants feel "Neutral". In the third case, where the surface temperature is set to 30 °C or 303.15 K, PMV and PPD values are found as 0.1 and %5.1 that shows comfort is provided in the occupied space. PMV value is almost 0, that shows this has the best comfort value for wall heating scenarios.

5.3.1.2 Ceiling Heating (5-Panels)

Ceiling heating scenarios were separated into two parts: first of all, heating case was simulated as 5-panel ceiling and secondly heating case was simulated for whole ceiling (12 Panels). In this part, the ceiling heating case for 5-panels configuration is evaluated. By using the validated numerical model, radiant surface temperature on (5P) ceiling was set to 20°C, 25°C and 30°C. In the case of ceiling heating with 5-panels, general comfort assessment was done for three cases. PMV-PPD values were calculated as it was explained in previous Chapters.

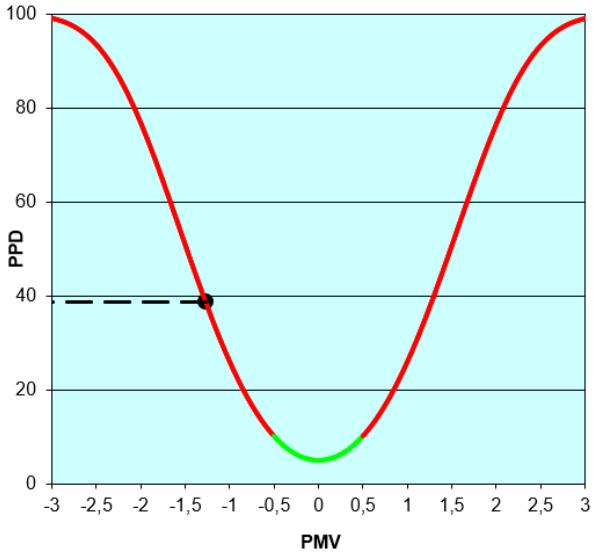

Figure 99: Ceiling Heating(5P) Case1: PMV=-1.3 PPD=38.7, “Slightly Cool”.

In Case 1: occupants feel “Slightly Cool”, where the surface temperature is set to 20 °C or 293.15 K, PMV and PPD values are found as =-1.3 and 38.7 that does not provide comfort. According to the related standards mentioned before, PMV values should be between -0.5 and +0.5 for a comfortable environment.

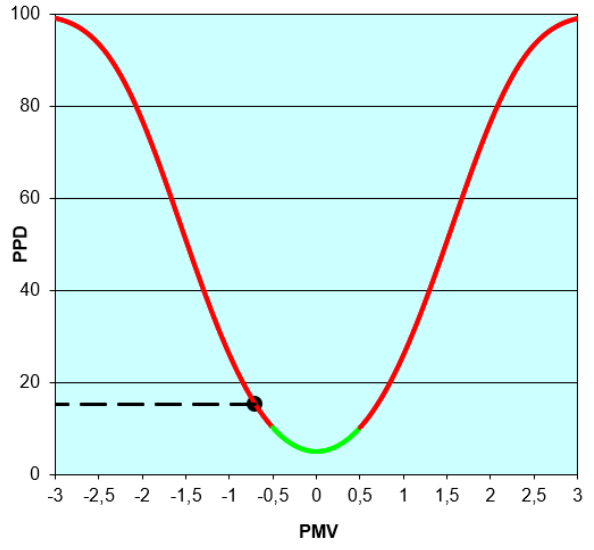

Figure 100: Ceiling Heating(5P) Case2: PMV=-0.7 PPD=15.3, “Slightly Cold”.

In Case 2: occupants feel “Slightly Cold”, where the surface temperature is set to 25 °C or 298.15 K, PMV and PPD values are found as 0.7 and %15.3 that shows comfort is not provided in the occupied space.

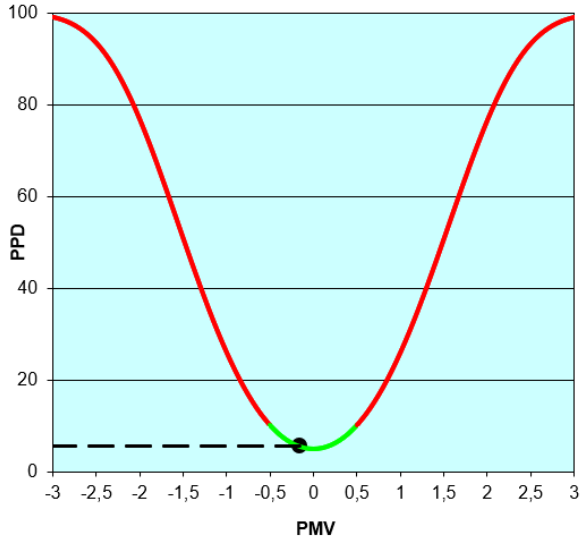

Figure 101: Ceiling Heating (5P) Case3: PMV=-0.2 PPD=5.5, “Neutral”.

In Case 3: occupants feel “Neutral” where the surface temperature is set to 30 °C or 303.15 K, PMV and PPD values are found as -0.2 PPD and %5.5 that shows comfort is provided in the occupied space. PMV value is close to 0, that shows this case has the best comfort value among other ceiling heating with 6 panels scenarios.

5.3.1.3 Ceiling Heating (12-Panels)

Ceiling heating scenarios were separated into two parts: first of all, heating case was simulated as 5-panel ceiling and secondly heating case was simulated for whole ceiling (12-Panels). In this part the ceiling heating case for 12 panels configuration is evaluated.

By using the validated numerical model, radiant surface temperature on (12P) ceiling was set to 20°C, 25°C and 30°C. PMV-PPD values were calculated by using numerical results. In the case of ceiling heating with 12 panels, general comfort assessment was done for each case.

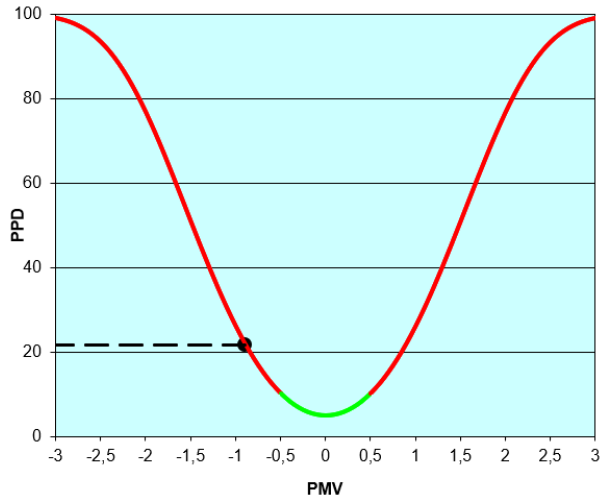

Figure 102: Ceiling Heating(12P) Case1: PMV=-0.9 PPD=21.7, “Slightly Cool”.

In Case 1: occupants feel “Slightly Cool”. In the first case, where the surface temperature is set to 20 °C or 293.15 K, PMV and PPD values are found as 0.9 and %21.7 that does not provide comfort. According to the related standards mentioned before, PMV values should be between -0.5 and +0.5 for a comfortable environment.

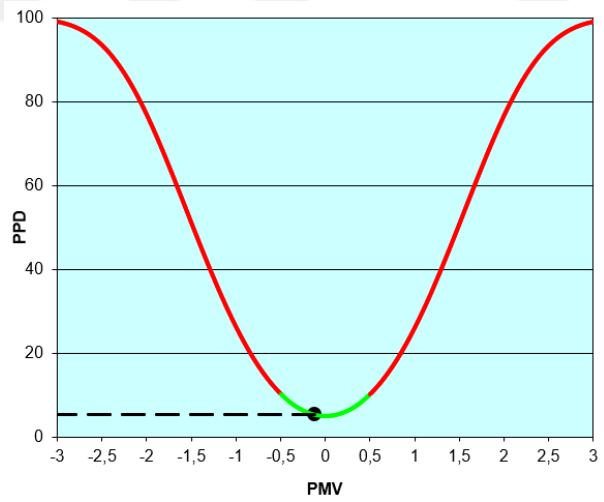

Figure 103: Ceiling Heating(12P) Case2: PMV=-0.1 PPD=5.4, “Neutral”.

In Case 2: occupants feel “Neutral”. In the second case, where the surface temperature is set to 25 °C or 298.15 K, PMV and PPD values are found as -0.1 and % 5.4 that shows comfort is provided in the occupied space. PMV value is close to 0, that shows this case has the best comfort value among other ceiling heating (12P) scenarios.

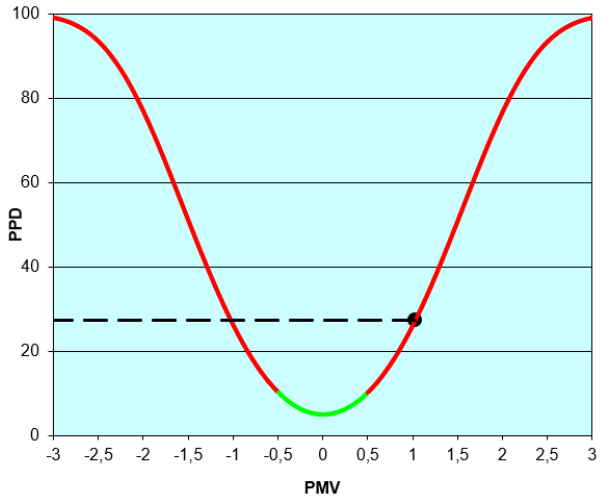

Figure 104: Ceiling Heating Case3: PMV=1.1 PPD=29.6, "Slightly Hot".

In Case 3: occupants feel "Slightly Hot" where the surface temperature is set to 30 °C or 303.15 K, PMV and PPD values are found as 1.1 and % 29.6 that shows comfort is provided in the occupied space.

5.3.1.4 Wall and Ceiling(12P) Heating

The aim of this study is to evaluate the comfort of radiant systems in terms of different heating locations. Here we analysed ceiling and wall heating configuration when both surfaces were heated. Wall panels and whole ceiling panels (12-Panels) were activated for heating.

By using the validated numerical model, analyses were done for 3 different wall-ceiling temperatures. Radiant surface temperatures were set to 20°C, 22°C and 24°C. These set values were selected according to the experimental results to avoid over heating of the room. PMV-PPD values were calculated by using numerical results.

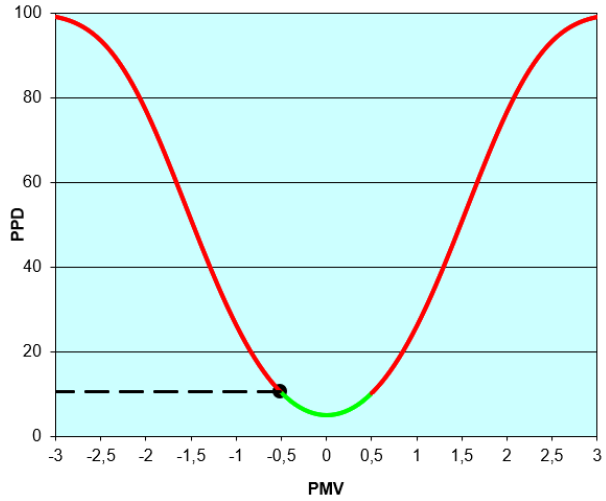

Figure 105: Wall and Ceiling(12) Heating Case1: PMV=-0.5 PPD=10.2, “Neutral”.

In Case 1: occupants feel “Neutral”, where the surface temperature is set to 20 °C or 293.15 K, PMV and PPD values are found as -0.5 and 10.2 that provides comfort. According to the related standards mentioned before, PMV values should be between -0.5 and +0.5 for a comfortable environment.

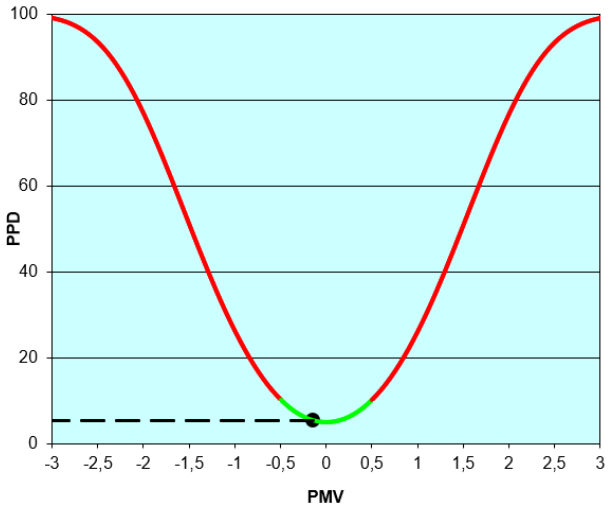

Figure 106: Wall and Ceiling Heating Case2: PMV=-0.1 PPD=5.4, “Neutral”.

In Case 2: occupants feel “Neutral” where the surface temperature is set to 22 °C or 295.15 K, PMV and PPD values are found as -0.1 and % 5.4 that shows comfort

is provided in the occupied space. PMV value is close to 0, that shows this case has the best comfort value among other wall and ceiling (12P) scenarios.

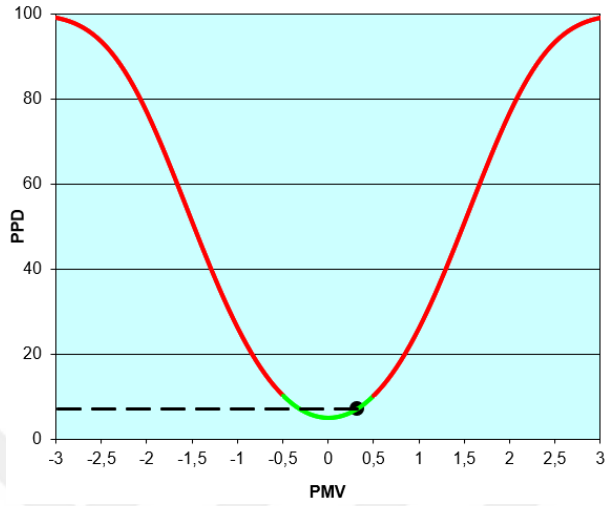

Figure 107: Wall and Ceiling Heating Case3: PMV=0.3 PPD=7.1, "Neutral".

In Case 3: occupants feel "Neutral" where the surface temperature is set to 24 °C or 297.15 K, PMV and PPD values are found as 0.3 and % 7.1 that shows comfort is provided in the occupied space.

5.3.2 Vertical Air Temperature Profile

Simulation results are shown in this chapter. The surface temperatures are read from the CFD model. Average Surface temperature amounts are read from the CFD model. In addition to that the air temperature is taken from different points shown in Figure 108.

In Figures 109, 110, 111, 112, vertical air temperature profiles are given. It is clear that air distribution was quite homogeneous as it was seen in different sections with some temperature contours. Local temperature difference was found less than 3°C

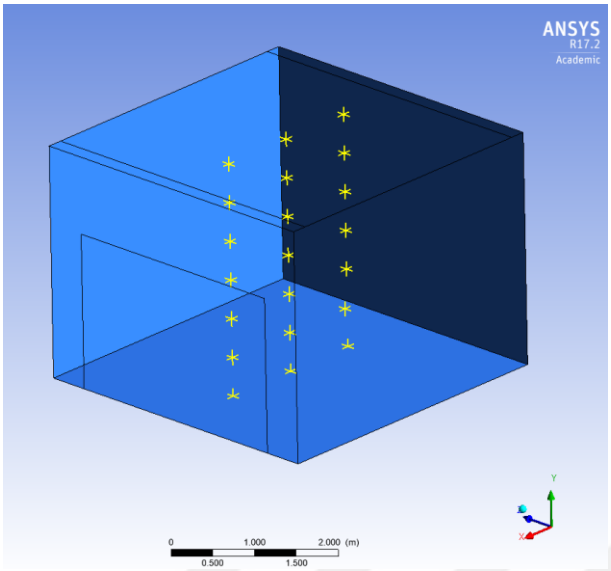

Figure 108: Vertical Air Temperature Measurement Points

5.3.2.1 Wall Heating

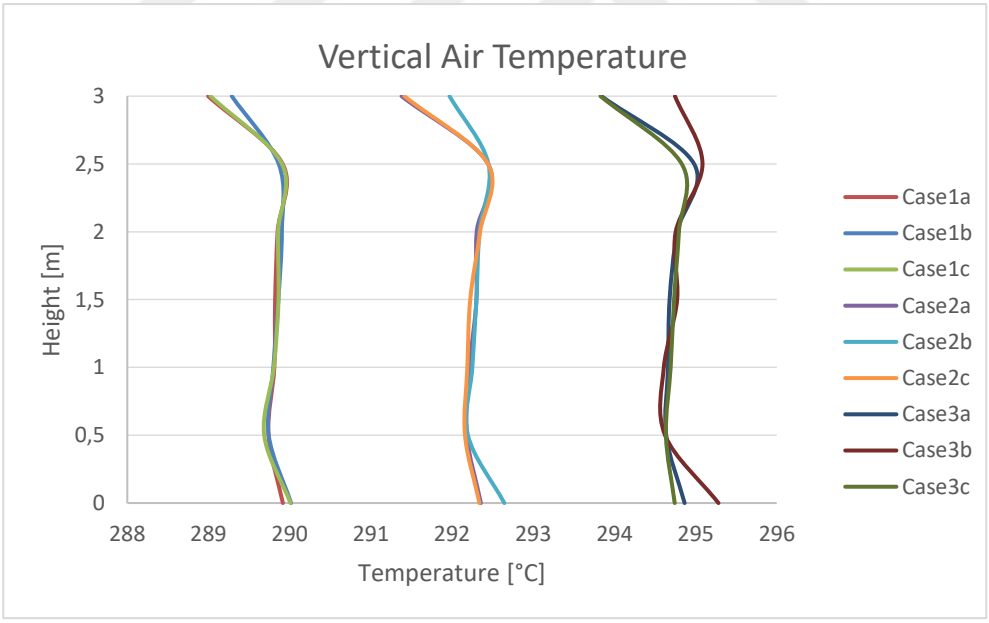

Figure 109: Vertical Air Temperature (Wall Heating)

5.3.2.2 Ceiling Heating (5 Panels)

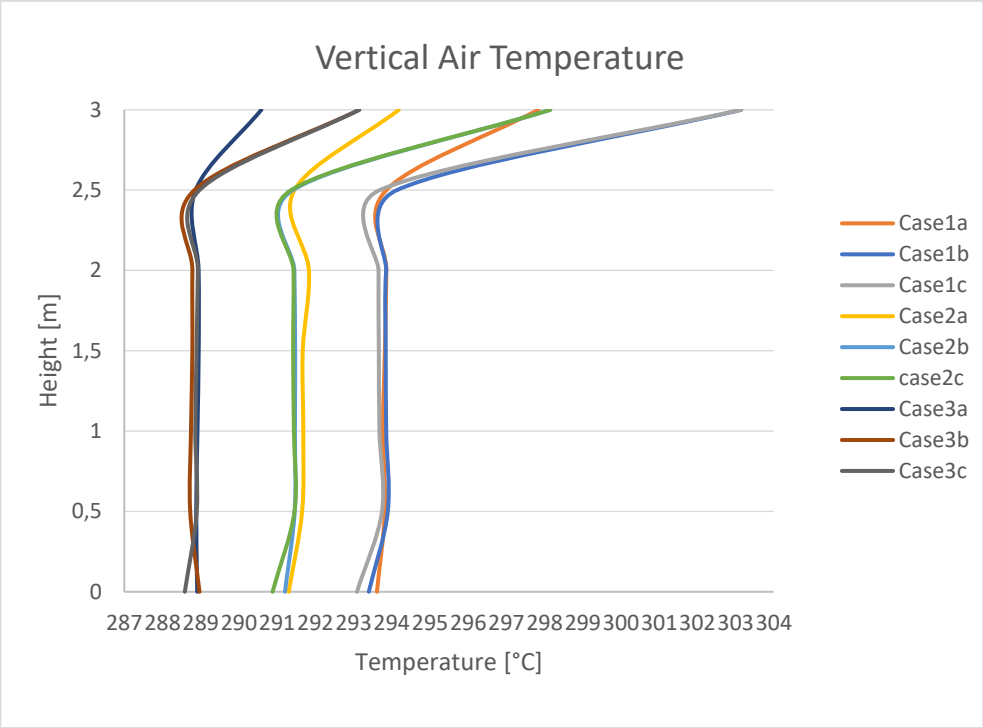

Figure 110: Vertical Air Temperature (Ceiling Heating 5 Panels)

5.3.2.3 Ceiling Heating (12 Panels)

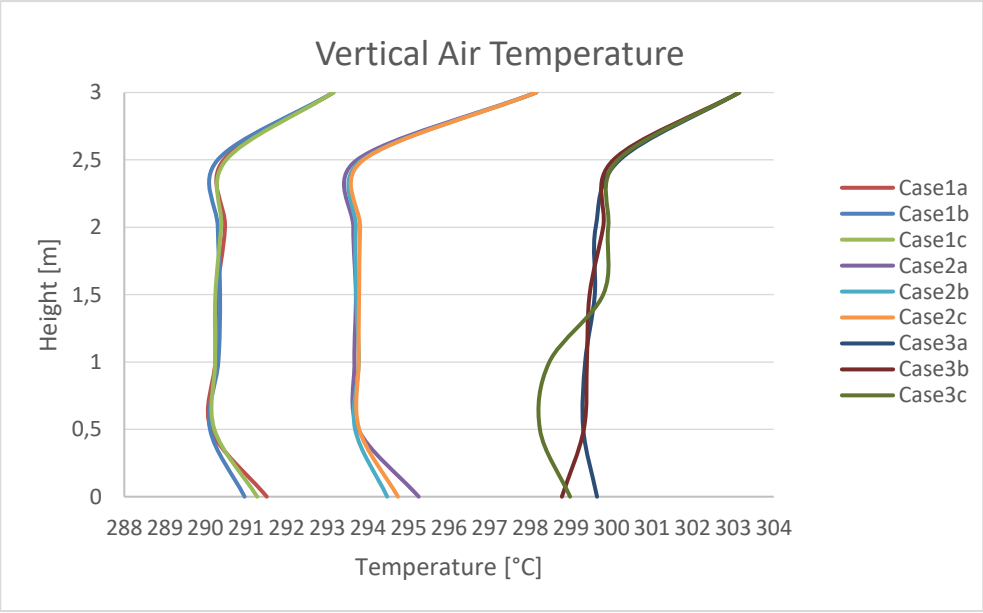

Figure 111: Vertical Air Temperature (Ceiling Heating 12 Panels)

5.3.2.4 Wall and Ceiling (12P) Heating

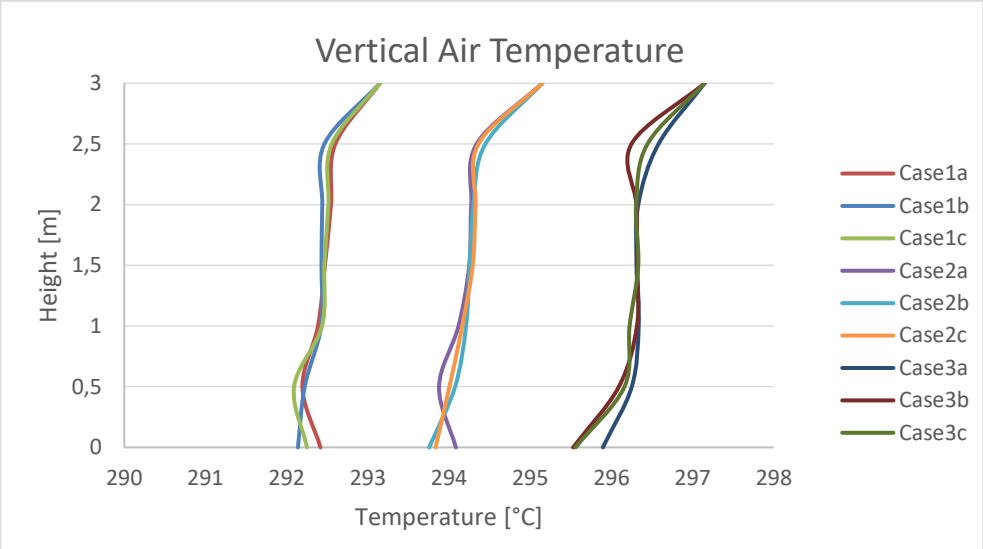

Figure 112: Vertical Air Temperature (Wall and Ceiling Heating 12 Panels)

5.3.3 Human Body Exergy Balance

In this part of thesis, the following guidelines are used for the calculation of human body exergy balance. The six variables shown in Table 27: metabolic energy generation rate; amount of clothing in clo unit; surrounding air temperature; surrounding air relative humidity; mean radiant temperature; air velocity. As it was described in previous chapters, exergy calculation input parameters are given again in Table 27.

The mathematical formulae of the respective terms in the exergy balance equation are given in Appendix A. It consists of human body exergy balance terms that should be calculated during the exergy analysis. Every term in Table A are expressed for the infinitesimal period of time, and for one square-meter of human-body surface. The symbols used in these the formulae from the top to the bottom are described in the Table B in Appendix A. This calculation procedure is taken from Annex 49 guidebook [49].

According to the equations are given in Appendix A the exergy balance calculations in this thesis are done by using R statistical code. The comfort research library called “comf v0.1.7” is used for the calculations. Input parameters are taken from the experimental measurements.

Table 24: Human Body Exergy Balance Calculation Parameters According to the Numerical Study

Input Variables-Outdoor	
Outdoor Air Temperature	-3.0 °C
Relative Humidity of Outdoor Air	80% (Kept Constant)
Input Variables-Indoor	
Room Air Temperature(°C)	Numerical Results
Mean Radiant Temperature (°C)	Numerical Results
Relative Humidity of Room Air (%)	50% (Kept Constant)
Air Speed (m/s)	Numerical Results
Human Body	
Clothing (clo)	1 (Kept Constant)
Activity (met)	1.2 (Kept Constant)

Human body exergy calculation carried out according to the numerical results are given in Table 25 below.

Table 25: Human Body Exergy Balance Calculation Results

	WALL			CEILING (5P)			CEILING (12P)			W&C (12P)		
The exergy input components	C1	C2	C3	C1	C2	C3	C1	C2	C3	C1	C2	C3
Warm Exergy input through metabolism	9.0	9.0	9.0	9.0	9.0	9.0	9.0	9.0	9.0	9.0	9.0	9.0
Warm Exergy input through inhaled humid air	0.1	0.1	0.1	0.1	0.1	0.1	0.1	0.1	0.1	0.1	0.1	0.1
Wet Exergy input through inhaled dry air	0.0	0.0	0.0	0.0	0.0	0.0	0.0	0.0	0.1	0.0	0.0	0.1
Warm Exergy input through water lung	0.0	0.0	0.0	0.0	0.0	0.0	0.0	0.0	0.0	0.0	0.0	0.0
Wet Exergy input through water lung	0.1	0.1	0.1	0.1	0.1	0.1	0.1	0.1	0.1	0.1	0.1	0.1
Warm Exergy input through water from sweat	0.0	0.1	0.1	0.0	0.1	0.1	0.1	0.1	0.1	0.1	0.1	0.1
Wet Exergy input through water from sweat	-0.2	-0.3	-0.5	-0.2	-0.3	-0.4	-0.3	-0.4	-0.9	-0.3	-0.4	-0.6
Warm Exergy input through radiation	3.3	4.1	5.1	2.9	3.8	4.7	3.6	4.8	6.8	4.0	4.5	5.3
Total exergy input	12.2	13.0	14.0	11.9	12.7	13.5	12.6	13.7	15.4	12.9	13.4	14.1
Exergy stored in core	-0.1	-0.1	-0.1	-0.1	-0.1	-0.1	-0.1	-0.1	0.0	-0.1	-0.1	-0.1
Exergy stored in shell	-0.8	-0.4	-0.1	-1.0	-0.6	-0.3	-0.7	-0.3	0.0	-0.5	-0.3	-0.1
Warm Exergy output through exhaled humid air	0.3	0.3	0.3	0.3	0.3	0.3	0.3	0.3	0.3	0.3	0.3	0.3
Wet Exergy output through exhaled dry air	0.8	0.8	0.8	0.8	0.8	0.8	0.8	0.8	0.8	0.8	0.8	0.8
Warm Exergy output through water vapour from sweat	0.0	0.0	0.0	0.0	0.0	0.0	0.0	0.0	0.0	0.0	0.0	0.0
Wet Exergy output through water vapour from sweat	0.2	0.3	0.5	0.2	0.3	0.4	0.2	0.4	1.1	0.3	0.4	0.6
Warm Exergy output through radiation	5.6	6.4	7.3	5.3	6.1	6.9	5.8	7.0	8.7	6.4	6.9	7.6
Warm Exergy output through convection	2.4	2.3	2.2	2.4	2.3	2.2	2.5	2.3	1.5	2.2	2.0	1.9
Total exergy output	8.4	9.6	10.9	7.9	9.1	10.3	8.9	10.5	12.5	9.4	10.2	11.0
Total exergy consumption	**3.8**	**3.4**	**3.1**	**4.0**	**3.6**	**3.2**	**3.7**	**3.2**	**2.9**	**3.4**	**3.2**	**3.0**
Calculated skin temperature	31.8	32.8	33.7	31.4	32.4	33.3	32.1	33.4	34.7	32.7	33.4	34.0
Calculated core temperature	36.8	36.9	36.9	36.8	36.8	36.9	36.8	36.9	36.9	36.8	36.9	36.9
Calculated skin wettedness	0.1	0.1	0.1	0.1	0.1	0.1	0.1	0.1	0.2	0.1	0.1	0.1
PMV	-0.3	0.0	0.5	-1.3	-0.7	-0.2	-0.9	-0.1	1.1	0.8	1.3	1.8
PPD	7.3	5.0	9.2	38.7	15.3	5.5	21.7	5.4	29.6	17.2	39.2	68.1

6 CONCLUSION

In this thesis, both experimental and numerical studies have been carried out to determine different radiant heating scenarios. An experimental chamber was used for this purpose. Numerical studies were conducted for different cases. Experimental tests were used to validate the numerical model. Comfort analysis were made for different heating scenarios accordingly. Thermal comfort in the room was investigated for different panel heating surface configurations. Thermal comfort values were calculated according to ISO 7730 [6] and ASHRAE 55 [7] standards which are based on the first law of thermodynamics. In addition to that, a recent comfort evaluation method, the human body exergy concept, has been used for the comfort evaluation. Human body exergy balance is based on the second law of thermodynamics. This method was also used for this study to evaluate human thermal comfort by using exergy analysis. Exergy analysis allows taking environmental conditions into consideration for thermal comfort and it clearly shows how the human exergy consumption is connected to environmental conditions. The results indicate that under steady-state conditions there is a relation between exergy consumption of the human body and the expected level of thermal comfort, expressed as a PMV value. Exergy-based analysis gives more information about the environmental impact on expected thermal sensation than energy-based types of analysis.

All the numerical analysis studies were conducted using the Academic version of ANSYS 17.1. Numerical solutions were made in Fluent, a widely used computational fluid dynamics module. The Discrete Ordinates model (since there is no scattering inside the room) was used for radiative heat transfer. Before choosing the radiation model, the numerical solution of discrete ordinates model and

analytical calculation method were compared on a simple example problem. A small sized, room geometry ($0.5m^3$) used for the calculation, was explained in Chapter 4.2.4. The error analysis show that the deviation rate was less than %1 and therefore DO model was validated before the numerical study. The natural convection was modelled using the Boussinesq approach, and the standard k-ε model which is a common numerical solution and gives good results in the flow near the wall was picked to model turbulence. This gives us to analyze air velocity streamlines caused by the natural convection. Even radiative heat transfer dominates the convection-based heat transfer; the turbulence model is still needed for the cases that surface temperature differences are higher. Numerical solution results were compared with different mesh numbers and mesh independence was observed. The temperature field and the velocity field were visually inspected using CFD-Post software as the final processor program. It was expected that the air velocity values to be lower than air-forced conditioning system and the results yielded in that way.

Experimental tests were done in a multi-climate test chamber that consists of 5 zones including façade volume, inner zone volume, floor volume, ceiling volume and test volume. Setup was developed for winter conditions. Based on the studied cases and the boundary conditions, steady-state requirements were reached within 5–6 h in terms of stability of supply-water temperature and water flow rates Surface temperature of the panels and unheated surfaces, indoor and surrounding volumes air temperatures were almost continuous, only then each run was begun. In the test results the standard deviation was calculated as ±0,3°C.

For the comfort calculations, activity level was selected as 1.2 met and the clothing was selected as 1 clo. These average values were taken from literature. These data were used as input to thermal comfort assessment. Experimental and

numerical analysis of radiant heating system show that the radiant systems have advantage on homogeneous air temperature distribution, low air velocity. It does not cause unfavorable high temperature differences in the vertical direction that can be encountered in forced convection-based systems.

Radiant panels have been investigated to provide and maintain thermal comfort at different surface set temperatures. In the given set values, temperature distribution in the vertical and horizontal direction, mean radiant temperature and air velocity values in the room were examined. It has been observed that the exergy consumption values in the radiant heating system are close to the lowest values stated in the literature. Also, the temperature distribution in the room is considerably homogeneous compared to all conventional systems. This demonstrates that radiant systems using low-ex energy sources provide efficient, environmentally-friendly comfort solutions.

Radiant systems provide comfort by using low quality of energy, too. Exergy consumption rate of human body changes from 2.89 to 4.04 W/m^2. In parallel with this calculation, PMV values ranges from -1.3 to 1.9. The best thermal comfort performance in terms of comfort and exergy consumption, wall heating has better performance. In terms of vertical air temperature distribution all cases provide homogeneous air temperature gradient except ceiling heating with 5 panels case which has more than 3 °C of temperature difference from ceiling to floor. The temperature difference between 0 m to 2.5 m in all other cases were smaller than 3 °C. Therefore, it is also clear that the radiant system provides local comfort as well. Another conclusion is when the heating surface area is larger, the heating surface temperature requirement as well as the air velocity decreases.

For comfort evaluation it is considered that just only one approach is not enough. For instance, human body consumes less exergy when thermal comfort is provided. However sometimes even comfort is not provided, exergy consumption may be low. It can be seen in ceiling heating (12 Panel) Case-3. It cannot be the only evaluation method for thermal comfort. It helps to understand comfort under the light of second law of thermodynamics.

Future work suggestions can be as follows:

- Numerical and experimental analyses were done according to a general room geometry and characteristics. The room that was evaluated did not have any windows or openings. Also, there was no air infiltration to the room. However, in a real room environment, these parameters should be taken into consideration. In addition to the cooling effect of windows, there is also the solar radiation effect that should be evaluated in terms of comfort by using energy and exergy balance approaches.
- The hybrid usage of radiant systems and air-forced system can be evaluated in terms of thermal comfort for future studies.
- Location-based demand-responsive heating is a novel topic for future comfort studies. In the future, location-based heating and cooling strategies should be developed considering the occupant's needs. This approach will lead to the extension of the current advanced control strategies into multi-zone controls of heating and cooling systems. For the localization of heating surface issue, this research will put light to the future human adaptive thermal comfort solutions which can be also named as location-based intelligent heating or cooling strategies. As energy consumption in commercial and residential buildings exceed 40% of the total energy used in

most countries, HVAC (Heating Ventilation and Air Conditioning) systems typically consume more than 50% of the building energy use. And it is shown in the literature that [78] indicates the optimal control of HVAC system can achieve energy savings of up to 45%. Therefore, optimized control of conditioning systems can potentially reduce significant amount of energy consumption globally. The localization of the radiant heating systems and usage of them according to the demand needed by occupants can be a challenging topic for HVAC industry since demand response is becoming an important mean to reduce peak energy consumption and balance energy demand and supply.

- The coupling of Computational Fluid Dynamics and Building Energy Simulation (BES) techniques can let researches to evaluate dynamic behavior of radiant heating systems.

APPENDIX A

Here in Appendix A., human body exergy balance calculation procedure is given according to the ANNEX 49 [49].

1) Assume six variables shown in Table 4 in Chapter 2.3.3: metabolic energy generation rate; amount of clothing in clo unit; surrounding air temperature; surrounding air relative humidity; mean radiant temperature; air current.

2) Calculate the body-core temperature, the bodyshell (skin) temperature, the clothing-surface temperature, and the skin-wettedness. These values can be determined by following the procedure given by Gagge et al [69, 70, 71].

3) Calculate the sweat-secretion rate using the skin wettedness.

4) Substitute the results of three calculated temperatures and the sweat-secretion rate into the terms given in the equation below and calculate their values except the term of exergy consumption.

5) Substitute the values of exergy obtained from the above calculation into exergy balance equation and then calculate the value of exergy consumption.

The mathematical formulae of the respective terms in the exergy balance equation are given in Table A. Every term in Table A is expressed for the infinitesimal period of time, and for one square-meter of human-body surface. The symbols used in these formulae from the top to the bottom is described in the Table B.

Furthermore, detailed explanations can be found in Annex 49 guidebook for the calculation of human body exergy balance [49]:

Table A: Formulae of Exergy Balance Equation [49]

Warm exergy generated by metabolism
$M\left(1-\frac{T_o}{T_{cr}}\right)dt$
Warm/cool and wet/dry exergies of the inhaled humid air
$V_{in}\left[\left\{c_{pa}\left(\frac{\mathfrak{R}_a}{RT_{ra}}\right)(P-p_{vr})+c_{pv}\left(\frac{\mathfrak{R}_w}{RT_{ra}}\right)p_{vr}\right\}\left\{(T_{ra}-T_o)-T_o\ln\frac{T_{ra}}{T_o}\right\}+\frac{T_o}{T_{ra}}\left\{(P-p_{vr})\ln\frac{P-p_{vr}}{P-p_o}+p_{vr}\ln\frac{p_{vr}}{p_{vo}}\right\}\right]dt$
Warm and wet exergies of the liquid water generated in the core by metabolism
$V_{w-core}\rho_w\left[c_{pw}\left\{(T_{cr}-T_o)-T_o\ln\frac{T_{cr}}{T_o}\right\}+\frac{R}{\mathfrak{R}_w}T_o\ln\frac{p_{vs}(T_o)}{p_{vo}}\right]dt$
Warm/cool and wet/dry exergies of the sum of liquid water generated in the shell by metabolism and dry air to let the liquid water disperse
$V_{w-shell}\rho_w\left[c_{pw}\left\{(T_{sk}-T_o)-T_o\ln\frac{T_{sk}}{T_o}\right\}+\frac{R}{\mathfrak{R}_w}T_o\left\{\ln\frac{p_{vs}(T_o)}{p_{vo}}+\frac{P-p_{vr}}{p_{vr}}\ln\frac{P-p_{vr}}{P-p_{vo}}\right\}\right]dt$
Warm/cool radiant exergy absorbed by the whole of skin and clothing surfaces
$f_{eff}f_{cl}\sum_{j=1}^{N}a_{pj}\varepsilon_{cl}h_{rb}\frac{(T_j-T_o)^2}{(T_j+T_o)}dt$
Exergy consumption rate, which is only for thermoregulation
$\delta S_g T_o$
Warm exergy stored in the core and the shell
$Q_{core}\left(1-\frac{T_o}{T_{cr}}\right)dT_{cr}+Q_{shell}\left(1-\frac{T_o}{T_{sk}}\right)dT_{sk}$
Warm and wet exergies of the exhaled humid air
$V_{out}\left[\left\{c_{pa}\left(\frac{\mathfrak{R}_a}{RT_{cr}}\right)(P-p_{vs}(T_{cr}))+c_{pv}\left(\frac{\mathfrak{R}_w}{RT_{cr}}\right)p_{vs}(T_{cr})\right\}\left\{(T_{cr}-T_o)-T_o\ln\frac{T_{cr}}{T_o}\right\}+\frac{T_o}{T_{cr}}\left\{(P-p_{vs}(T_{cr}))\ln\frac{P-p_{vs}(T_{cr})}{P-p_{vo}}+p_{vs}(T_{cr})\ln\frac{p_{vs}(T_{cr})}{p_{vo}}\right\}\right]dt$
Warm/cool exergy of the water vapor originating from the sweat and wet/dry exergy of the humid air containing the evaporated sweat
$V_{w-shell}\rho_w\left[c_{pv}\left\{(T_{cl}-T_o)-T_o\ln\frac{T_{cl}}{T_o}\right\}+\frac{R}{\mathfrak{R}_w}T_o\left\{\ln\frac{p_{vr}}{p_{vo}}+\frac{P-p_{vr}}{p_{vr}}\ln\frac{P-p_{vr}}{P-p_{vo}}\right\}\right]dt$
Warm/cool radiant exergy discharged from the whole of skin and clothing surfaces
$f_{eff}f_{cl}\varepsilon_{cl}h_{rb}\frac{(T_{cl}-T_o)^2}{(T_{cl}+T_o)}dt$
Warm/cool exergy transferred by convection from the whole of skin and clothing surfaces into the surrounding air
$f_{cl}h_{ccl}(T_{cl}-T_m)\left(1-\frac{T_o}{T_{cl}}\right)dt$

Table B: Mathematical symbols used in Table A

M	metabolic energy generation rate [W/m2]
T_o	outdoor air temperature as environmental temperature for exergy calculation [K]
T_{cr}	body-core temperature [K]
t	time [s] and is its infinitesimal increment dt
V_{in}	volumetric rate of inhaled air [(m^3/s)/m^2]
c_{pa}	specific heat capacity of dry air [J/(kgK)]
$\mathfrak{M}_a$	molar mass of dry air [g/mol]
R	gas constant [J/(mol K)]
T_{ra}	room air temperature [K]
P	atmospheric air pressure [Pa]
p_{vr}	water-vapor pressure in the room space [Pa]
c_{pv}	specific heat capacity of water vapor [J/(kgK)]
$\mathfrak{M}_w$	molar mass of water molecules [g/mol]
p_{vo}	water-vapor pressure of the outdoor air [Pa]
V_{w-core}	volumetric rate of liquid water generated in the body core [(m^3/s)/m^2]
ρ_w	density of liquid water [kg/m^3]
c_{pw}	specific heat capacity of liquid water [J/(kgK)]
$p_{vs}(T_o)$	saturated water-vapor pressure at outdoor air temperature [Pa]
$V_{w-shell}$	the volumetric rate of liquid water generated in the body shell as sweat [(m^3/s)/m^2]
T_{sk}	skin temperature [K]
f_{eff}	the ratio of the effective area of human body for radiant-heat exchange to the surface area of the human body with clothing
f_{cl}	the ratio of human body area with clothing to the naked human body area
a_{pj}	absorption coefficient between the human body surface
ε_{cl}	emittance of clothing surface [dimensionless]
h_{rb}	radiative heat-transfer coefficient of a black surface [W/(m^{2}K)]
T_j	temperature of surface [K] j
δS_g	amount of entropy generation during the infinitesimal period [(Onnes/s)/m^2]
Q_{core}	heat capacity of body core [J/(m^{2}K)]
dT_{cr}	infinitesimal increment of body-core temperature [K]
Q_{shell}	heat capacity of body shell [J/(m^{2}K)]
dT_{sk}	infinitesimal increment of skin temperature [K]
V_{out}	volumetric rate of exhaled air [(m^3/s)/m^2]
$p_{vs}(T_{cr})$	saturated water-vapor pressure at body-core temperature [K]
T_{cl}	clothing surface temperature [K]
h_{ccl}	average convective heat transfer coefficient over clothed body-surface [W/(m^{2}K)]

BIBLIOGRAPHY

[1] P. O. Fanger (1970). Thermal Comfort, Analysis and Application in Environment Engineering. Danish Technical Press, Copenhagen.

[2] T. Catalina, J. Virgone and F. Kuznik, "Evaluation of thermal comfort using combined CFD and experimentation study in a test room equipped with a cooling ceiling", Building and Environment, vol. 44, no. 8, pp. 1740-1750, 2009.

[3] M. Bojić, D. Cvetković, V. Marjanović, M. Blagojević and Z. Djordjević, "Performances of low temperature radiant heating systems", Energy and Buildings, vol. 61, pp. 233-238, 2013.

[4] A. Omer, "Energy, environment and sustainable development", Renewable and Sustainable Energy Reviews, vol. 12, no. 9, pp. 2265-2300, 2008.

[5] B. Olesen, “Radiant floor cooling systems”, ASHRAE J. 50 vol. 9, p. 16–22, 2008.

[6] ISO 7730:2005: “Ergonomics of the thermal environment-Analytical determination and interpretation of thermal comfort using calculation of the PMV and PPD indices and local thermal comfort criteria”, International Standardization Organization, Geneva (2005)

[7] ANSI/ASHRAE Standard 55-2013: “Thermal Environmental Conditions for Human Occupancy”, ASH1RAE standard, ISSN 1041-2336

[8] ASHRAE, “ASHRAE Handbook-HVAC Systems and Equipment”, American Society of Heating Refrigerating and Air-Conditioning Engineers. Inc., Atlanta, 2012.

[9] H. Salt, "Preliminary design considerations for a rockbed/floor space-heating system", Building and Environment, vol. 20, no. 4, pp. 221-231, 1985.

[10] T. Weber and G. Jóhannesson, "An optimized RC-network for thermally activated building components", Building and Environment, vol. 40, no. 1, pp. 1-14, 2005.

[11] H. Feustel and C. Stetiu, "Hydronic radiant cooling-preliminary assessment", Energy and Buildings, vol. 22, no. 3, pp. 193-205, 1995.

[12] M. De Carli, M. Scarpa, R. Tomasi and A. Zarrella, "DIGITHON: A numerical model for the thermal balance of rooms equipped with radiant systems", Building and Environment, vol. 57, pp. 126-144.

[13] J. Babiak, B.W. Olesen, D. Petrás, “Low temperature heating and high temperature cooling”, REHVA guidebook no. 7, 2009.

[14] H. Feustel and C. Stetiu, "Hydronic radiant cooling — preliminary assessment", Energy and Buildings, vol. 22, no. 3, pp. 193-205, 1995.

[15] T. Catalina, J. Virgone and F. Kuznik, "Evaluation of thermal comfort using combined CFD and experimentation study in a test room equipped with a cooling ceiling", Building and Environment, vol. 44, no. 8, pp. 1740-1750, 2009.

[16] L. Zhang and J. Niu, "Indoor humidity behaviors associated with decoupled cooling in hot and humid climates", Building and Environment, vol. 38, no. 1, pp. 99-107, 2003.

[17] X. Hao, G. Zhang, Y. Chen, S. Zou and D. Moschandreas, "A combined system of chilled ceiling, displacement ventilation and desiccant dehumidification", Building and Environment, vol. 42, no. 9, pp. 3298-3308, 2007.

[18] B.W. Olesen, “Radiant floor heating in theory and practice”, ASHRAE Journal, 44(7): pp.19-26.

[19] M. Yeo, I. Yang and K. Kim, "Historical changes and recent energy saving potential of residential heating in Korea", Energy and Buildings, vol. 35, no. 7, pp. 715-727, 2003.

[20] Z. Zhuang, Y. Li, B. Chen and J. Guo, "Chinese kang as a domestic heating system in rural northern China—A review", Energy and Buildings, vol. 41, no. 1, pp. 111-119, 2009.

[21] N. Bansal and India, "Characteristic parameters of a hypocaust construction", Building and Environment, vol. 34, no. 3, pp. 305-318, 1998.

[22] A. Athienitis, "Investigation of thermal performance of a passive solar building with floor radiant heating", Solar Energy, vol. 61, no. 5, pp. 337-345, 1997.

[23] J. Ren, L. Zhu, Y. Wang, C. Wang and W. Xiong, "Very low temperature radiant heating/cooling indoor end system for efficient use of renewable energies", Solar Energy, vol. 84, no. 6, pp. 1072-1083, 2010.

[24] Robert B., Olesen B. W., Kwang W.K., “History of radiant heating & cooling systems: part 1.”, ASHRAE Journal, 2010; 52: pp. 40–47

[25] Almughrabi N., Prijotomo J., Faqih M., “Suleymaniye Mosque: Space Construction and Technical Challenges”, International Journal of Education and Research Vol. 3 No. 6, 2015

[26] W. Chu, M. Kim, K. Lee, B. Bhandari, G. Lee, H. Yoon, H. Kim, J. Park, E. Bilegt, J. Lee, J. Song, G. Park, P. Bhandari, C. Lee, C. Song and S. Ahn, "Design and performance evaluation of Korean traditional heating system—Ondol: Case study of Nepal", Energy and Buildings, vol. 138, pp. 406-414, 2017.

[27] J. An, S. Kim, H. Kim and J. Seo, "Emission behavior of formaldehyde and TVOC from engineered flooring in under heating and air circulation systems", Building and Environment, vol. 45, no. 8, pp. 1826-1833, 2010.

[28] D. Kim, "The natural environment control system of Korean traditional architecture: Comparison with Korean contemporary architecture", Building and Environment, vol. 41, no. 12, pp. 1905-1912, 2006.

[29] M. Tye-Gingras and L. Gosselin, "Comfort and energy consumption of hydronic heating radiant ceilings and walls based on CFD analysis", Building and Environment, vol. 54, pp. 1-13, 2012.

[30] K. Rhee and K. Kim, "A 50-year review of basic and applied research in radiant heating and cooling systems for the built environment", Building and Environment, vol. 91, pp. 166-190, 2015.

[31] Y. A. Çengel, “A. Heat Transfer: A Practical Approach 2nd Edition.”, McGraw-Hill, 1998

[32] EN 15251:” Criteria for the Indoor Environment Including Thermal, Indoor Air Quality, Light and Noise.”, European Committee for Standardization, Brussels, Belgium, 2007.

[33] J. Nicol, and M. Wilson, “A critique of European Standard EN 15251: strengths, weaknesses and lessons for future standards.”, Building Research & Information, 39(2), pp.183-193, 2010.

[34] M. Humphreys, “Quantifying occupant comfort: are combined indices of the indoor environment practicable.”, Building Research & Information, 33(4), pp.317-325, 2005.

[35] B. W. Olesen, M. Schøler, and P. O. Fanger, “Discomfort caused by vertical air temperature differences.”, Indoor Clim., pp. 561-579, 1978.

[36] P. Fanger, A. Melikov, H. Hanzawa and J. Ring, “Air turbulence and sensation of draught”, Energy and Buildings, 12(1), pp.21-39, 1988.

[37] J. Toftum, A. Melikov, A. Tynel, M. Bruzda, and P. Fanger, (2003). Human Response to Air Movement-Evaluation of ASHRAE's Draft Criteria (RP-843). HVAC&R Research, 9(2), pp.187-202.

[38] ISO 10551:1995: “Ergonomics of the Thermal Environment – Assessment of the Influence of the Thermal Environment Using Subjective Judgement Scales”, International Standards Organization, Geneva, Switzerland, 1995.

[39] T. Imanari, T. Omori, K. Bogaki, “Thermal comfort and energy consumption of the radiant ceiling panel system: Comparison with the conventional all-air system. “, Energy and Buildings, Volume 30, Issue 2, pp.167-175, 1999.

[40] L. Zagreus, C. Huizenga, E. Arens, and D Lehrer, “Listening to the occupants: A Web-based indoor environmental quality survey.”, Indoor Air, 14(s8), pp. 65-74, 2004.

[41] M. Prek, “Thermodynamical analysis of human thermal comfort.”, Second ASME-ZSIS International Thermal Science Seminar (ITSS II), pp. 732–743., 2004.

[42] M. Prek, "Exergy analysis of thermal comfort", International Journal of Exergy, vol. 1, no. 3, p. 303, 2004.

[43] Z. Rant, “Energy value and pricing”, Journal of Mechanical Engineering 1, pp. 4-7, 1995.

[44] D. Schmidt, “Low exergy systems for high-performance buildings and communities.”, Energy and Buildings, no. 41, pp. 331–336., 2009.

[45] A. H. Masanori Shukuya, “Introduction to the Concept of Exergy—for a Better Understanding of Low-Temperature-Heating and High-Temperature-Cooling Systems,”, VTT Building Technology, Espoo, Finland. VTT—Research notes 2158, pp. 1–41, 2002.

[46] ECBCS Annex 37, “Low Exergy Systems for Heating and Cooling in Buildings”, International Energy Agency, 2003.

[47] S. Dietrich, “Design of Low Exergy Buildings—Method and a Pre-Design Tool”, no. 3, pp. 1–47, 2004.

[48] M Shukuya, M. Saito, K. Isawa, T. Iwamatsu, H. Asada, “Human body exergy balance and thermal comfort”, Working Report of The International Energy Agency, Energy Conservation in Buildings and Community Systems, Annex 49. Fraunhofer, 2010

[49] ECBCS Annex 49, “Low Exergy Systems for High-performance Built Environments and Communities”, International Energy Agency, 2005.

[50]. I., Oshida, “Solar Energy”, NHK Shuppan, pp. 179, 1981.

[51] M. Shukuya, “Exergy concept and its application to the built environment. Building and Environment, 44(7), pp. 1545-1550, 2009.

[52] M. Schweiker and M Shukuya, “User Behavior in Relation to His Short- and Long-term thermal background”, Proceedings of Second PALENC Conference and 28th AIVC Conference in the 21st Century, pp. 913-918.

[53] K. Tokunaga and M. Shukuya, “An Experimental Study on Sweat Secretion and Its Evaporation Effect in a Variety of Thermal Environment in Summer”, Proceedings of 1st International Exergy, Life Cycle Assessment, and Sustainability Workshop & Symposium.

[54] H. Asada, F. Hideaki, T. Ohkuma, M. Shukuya, “Development of exergy calculation tool for the whole of human body, indoor environment and heating systems”, Summaries of technical papers of Annual Meeting Architectural Institute of Japan D-2, pp. 585-6, 2008.

[55] R Development Core Team, “R: a language and environment for statistical computing”, [Online]. Available: http://www.R-project.org, 2008.

[56] TS 825: “Thermal insulation requirements for buildings”, Turkish Standards, 2008.

[57] A. Koca, and Ş. Atayılmaz, “Experimental investigation of heat transfer and dehumidifying performance of novel condensing panel”. Energy and Buildings, 129, pp.120-137, 2016.

[58] A. Koca, Z. Gemici, Y. Topacoglu, G. Cetin, R.C. Acet, B. Kanbur, “Experimental investigation of heat transfer coefficients between hydronic radiant heated wall and room”, Energy and Buildings, 82, pp.211-221, 2014.

[59] B.W. Olesen, F. Bonnefoi, E. Michel, M. De Carli, “Heat exchange coefficient between floor surface and space by floor cooling−theory or a question of definition”, ASHRAE Transactions: Symposia, vol. DA-00-8-2, p. 684–694, 2000.

[60] ANSI/ASHRAE Standard 138-2005: “Method of Testing for Rating Ceiling Panels for Sensible Heating and Cooling”, American Society of Heating, Refrigerating and Air-Conditioning Engineers, Inc., 2005.

[61] EN 14240:2004: “Ventilation for Buildings Chilled Ceilings Testing and Rating”, British Standards, 2004.

[62] F. Kuznik, G. Rusaouën, and J. Brau, “Experimental and numerical study of a full scale ventilated enclosure: Comparison of four two equations closure turbulence models”, Building and Environment, 42(3), pp.1043-1053, 2007.

[63] F. M. White, Fluid Mechanics, New York: McGraw-Hill, 2003.

[64] F. P. Incropera, P. D. Dewitt, “Fundamentals of Heat and Mass Transfer”, John Wiley and Sons, 2002.

[65] ANSYS Inc, “ANSYS FLUENT 12.0 User's Guide”, ANSYS, Inc., 2009.

[66] B. Spalding and E. Launder, “Lectures in Mathematical Models of Turbulence”, Academic Press, London, England, 1972.

[67] J. R. Howell, M. P. Menguc, R. Siegel, “Thermal Radiation Heat Transfer, 6th Edition”, Taylor and Francis, 2015.

[68] M. Ozen, “Meshing Workshop”, 13th November 2014. [Online]. Available: https://www.ozeninc.com/wp-content/uploads/2014/11/MESHING_WORKSHOP_2014.pdf.

[69] A. P. Gagge, A. P. Fobelets, L. G. Berglund, “A standard predictive index of human response to the thermal environment”, ASHRAE Transactions Vol.92, Part 2B, No.1, pp. 709-731, 1986.

[70] A. P. Gagge, J. A. Stolwijk, Y. Nishi, “An Effective Temperature Scale Based on a Simple Model of Human Physiological Regulatory Response”, ASHRAE Transactions Vol.77(1), pp. 247-262, 1971.

[71] A. P. Gagge, Y. Nishi, R. R. Gonzalez, “Standard Effective Temperature – A Single Temperature Index of Temperature Sensation and Thermal Discomfort”, Proceedings of the CIB Commission W45 Symposium, London, pp. 229-250, 1972.

[72] M. Bojić, D. Cvetković, V. Marjanović, M. Blagojević and Z. Djordjević, “Performances of low temperature radiant heating systems”, Energy and Buildings, 61, pp.233-238, 2013.

[73] P.O. Fanger, B.W. Olesen, G. Langkilde, and L. Banhidi, “Comfort limits for heated ceilings”, ASHRAE Transactions 86(2): pp. 141-156, 1980.

[74] ISO 7726:1998: “Ergonomics of the Thermal Environment – Instruments for Measuring Physical Quantities”, International Standards Organization, Geneva, Switzerland, 2001.

[75] C. Huizenga, Z. Hui and E. Arens, "A model of human physiology and comfort for assessing complex thermal environments", Building and Environment, vol. 36, no. 6, pp. 691-699, 2001.

[76] M. Ala-Juusela, “Heating and Cooling with Focus on Increased Energy Efficiency and Improved Comfort. Guidebook to IEA ECBS Annex 37”, VTT Building and Transport, Espoo, Finland. VTT—Research notes 2256, 2004.

[77] K. Isawa, T. Komizo, M. Shukuya, “The relationship between human-body exergy consumption rate and a combination of indoor air temperature and mean radiant temperature”, Transactions of Architectural Institute of Japan No.570, pp. 29-35, 2003.

[78] M. Shukuya, “Exergy, entropy, exergy and space heating systems”, Proceedings of Healthy Buildings (3th International Conference), Budapest, Hungary, 22–25 August, vol. I, pp. 369–374, 1994.

[79] V. M. Zavala, S.T. Celinski, P. Dickinson, Techno-Economic Evaluation of a Next-Generation Building Energy Management System. Technical Report ANL/MCS-TM-313, Argonne National Laboratory, 2011

VITA

Ruşen Can Acet received the BSc degree in Mechanical Engineering from Ege University, in 2011 and has completed his MSc in Mechanical Engineering at Özyeğin University under the supervision of Prof. Dr. M. Pınar Mengüç. His research area is mainly related with energy field, consisting of following topics: energy efficiency in buildings, low temperature heating-cooling systems, indoor environmental quality, human thermal comfort. In parallel with his MSc study at Ozyegin University, he has been working as an R&D Engineer at Environment and Energy Research Department of Mir Araştırma Geliştirme A.Ş, a project-based research company conducting interdisciplinary research activities in national / international projects.